NTNU
Norwegian University of
Science and Technology

The possibility of using reinforcement bars of aluminium in concrete structures

Åsne Takle Eide
Elisabeth Male Kolberg
Eva-Marie Østbye

Master of Science in Civil and Environmental Engineering
Submission date: June 2018
Supervisor: Jan Arve Øverli, KT

Norwegian University of Science and Technology
Department of Structural Engineering

Department of Structural Engineering
Faculty of Engineering
NTNU- Norwegian University of Science and Technology

ACCESSIBILITY

Open

MASTER THESIS 2018

SUBJECT AREA:	DATE:	NO. OF PAGES:
Structural Engineering	11th June	Report: 124 Appendix: 59

TITLE:

The possibility of using reinforcement bars of aluminium in concrete structures

Muligheten for bruk av armeringsstenger av aluminium i betongkonstruksjoner

BY:

Åsne Takle Eide
Elisabeth Male Kolberg
Eva-Marie Østbye

SUMMARY:
In this study, the possibility of using aluminium as reinforcement in concrete structures is investigated, with use of a low pH concrete. The thesis is assigned by NTNU, and is a part of the science project DARE2C, a project that SINTEF is researching together with NTNU and several other companies from the construction and innovation industry. It is believed that using aluminium as reinforcement will have a favourable impact to the concrete durability, and contribute to more maintenance-free constructions.

A laboratory study is performed, which includes production and testing of six reinforced concrete beams, where the beams are reinforced differently with a variation of material and cross-sectional shapes. Five of the beams are reinforced with alloyed aluminium, while the last beam is reinforced with steel reinforcement. The steel reinforcement is ribbed, while the aluminium reinforcement has smooth surface. The concrete prescription and the alloyed aluminium reinforcement are adjusted to chemically function together. The beam design is performed in accordance with the Eurocode, with some adjustments due to usage of aluminium reinforcement.

Calculations are performed prior to the laboratory testing. In connection with the beam production, cylinders were produced to verify the concrete properties. The tests from laboratory resulted in shear failure for the reference beam with steel reinforcement, while the remaining five beams with aluminium reinforcement obtained anchorage failure. The bond between the concrete and aluminium bars was poor due to the smooth surface of the reinforcement. Thus, the calculated values differed from the laboratory test results.

The deflections were larger in the laboratory than calculated for all beams. Control calculations performed after the laboratory testing for the steel reinforced beam, show that the deflection from the laboratory is valid. For the aluminium reinforced beams, the large deflections can be explained due to poor bond strength. Calculations of the actual bond strength are carried out for the steel reinforced beam and for one of the aluminium reinforced beam. The calculations show that the bond strength of the aluminium reinforced beam was lower than the given requirements, while it was higher for the steel reinforced beam.

RESPONSIBLE TEACHER: Professor Jan Arve Øverli

SUPERVISOR: Professor Jan Arve Øverli

CARRIED OUT AT: Department of Structural Engineering, NTNU

Preface

This study is performed as a Master's Thesis in the course TKT4920 Structural Design during the spring of 2018, with a total duration of 20 weeks. The thesis is a part of the 2 years MSc in Civil and Environmental Engineering, and is written at the Department of Structural Engineering at the Norwegian University of Science and Technology (NTNU). All of the members have completed a bachelor's degree in Civil Engineering, with specialization in Structural Engineering.

Main supervisor of the study has been professor Jan Arve Øverli at NTNU.

The master thesis is a practical laboratory assignment where the study of using aluminium as reinforcement in concrete structures is carried out, which is done in collaboration with the DARE2C-project.

Along the way, modifications of the test setup were performed based on output results from laboratory testing. Therefore, it was necessary to carry out new calculations, and additional theory had to be considered.

The laboratory work was unfortunately postponed three weeks, and the results differed from the expectations. Still, it has been a very interesting process working on this subject, hence during this study, both our practical and theoretical knowledge have grown.

Trondheim, June 11th 2018

Åsne Takle Eide	Elisabeth Male Kolberg	Eva-Marie Østbye

Acknowledgements

We would like to thank the following persons for helping us with our master thesis:

Jan Arve Øverli our main supervisor, for the great following up during the study with good conversations, guidance and feedback on the way. He helped us get in touch with several people from e.g. SINTEF, Hydro and NTNU. He was also very easy to cooperate with based on his availability, which was a safety net for us.

Steinar Seehuus and Ove Loftaas from NTNU, for showing great interest in our work and invaluable help in the laboratory. They helped us organize the laboratory details. They also shared some of their knowledge with us through helpful conversations and ideas along the way.

Bjørn Strickert Schjølberg from NTNU, for helping us with the test setup and performing the 4-point bending test of the beams in the NTNU laboratory.

Harald Justnes, Gunrid Kjellmark, Erik Johansen and Roger Leistad from SINTEF, for great collaboration. They have helped us with the concrete receipt, testing of material properties, knowledge within their special field and assistance in laboratory.

Hans Sigurd Amundsen chemical engineering and biotechnology master student from NTNU, for collaborating across field of study. He has together with his supervisors Hans Jørgen Roven (NTNU), Oddvin Reiso (Hydro) and Trond Furu (Hydro), which we also would like to thank, shown great interest in our subject and contributed with the alloyed aluminium reinforcement. He also organized and executed the aluminium production together with staff from Hydro, SINTEF and NTNU.

At last we want to thank all others involved in the DARE2C-project.

Summary

In this study, the possibility of using aluminium as reinforcement in concrete structures is investigated, with use of a low pH concrete. The thesis is assigned by NTNU, and is a part of the science project DARE2C, a project that SINTEF is researching together with NTNU and several other companies from the construction and innovation industry. It is believed that using aluminium as reinforcement will have a favourable impact to the concrete durability, and contribute to more maintenance-free constructions.

A laboratory study is performed, which includes production and testing of six reinforced concrete beams, where the beams are reinforced differently with a variation of material and cross-sectional shapes. Five of the beams are reinforced with alloyed aluminium, while the last beam is reinforced with steel reinforcement. The steel reinforcement is ribbed, while the aluminium reinforcement has smooth surface. The concrete prescription and the alloyed aluminium reinforcement are adjusted to chemically function together. The beam design is performed in accordance with the Eurocode, with some adjustments due to usage of aluminium reinforcement.

Calculations are performed prior to the laboratory testing. In connection with the beam production, cylinders were produced to verify the concrete properties. The tests from laboratory resulted in shear failure for the reference beam with steel reinforcement, while the remaining five beams with aluminium reinforcement obtained anchorage failure. The bond between the concrete and aluminium bars was poor due to the smooth surface of the reinforcement. Thus, the calculated values differed from the laboratory test results.

The deflections were larger in the laboratory than calculated for all beams. Control calculations performed after the laboratory testing for the steel reinforced beam, show that the deflection from the laboratory is valid. For the aluminium reinforced beams, the large deflections can be explained due to poor bond strength. Calculations of the actual bond strength are carried out for the steel reinforced beam and for one of the aluminium reinforced beam. The calculations show that the bond strength of the aluminium reinforced beam was lower than the given requirements, while it was higher for the steel reinforced beam.

Sammendrag

I denne oppgaven undersøkes muligheten til å benytte armeringsstenger av aluminium i betongkonstruksjoner, med en betongresept som gir lavere pH. Oppgaven er tildelt av NTNU, og er en del av forskningsprosjektet DARE2C, et prosjekt som SINTEF har sammen med NTNU og flere andre relevante aktører fra bygge- og innovasjonsbransjen. Forskere mener at anvendelse av aluminiumsarmering vil slå positivt ut på betongens bestandighet, og bidra til mer vedlikeholdsfrie konstruksjoner.

Et laboratoriestudie med produksjon og testing av seks armerte betongbjelker er gjennomført, der betongbjelkene har armeringsjern av ulikt materiale og tversnittsform. Fem av bjelkene er armert med armeringsjern av alminiumslegering, mens den siste bjelken har stålarmering. Stålarmeringen har riller, mens aluminiumarmeringen har glatt overflate. Betongresepten og ameringen av aluminiumslegering er tilpasset for kjemisk å fungere sammen. Bjelkene er dimensjonert i henhold til Norsk Standard, der antagelser i forbindelse med aluminiumsarmeringen er gjort.

Beregninger er foretatt i forkant av laboratoriearbeidet. I forbindelse med produksjon av bjelkene ble det også støpt sylindere for å kontrollere betongens egenskaper. Testene fra laboratoriet resulterte i skjærbrudd for referansebjelken med stålarmering, og forankringsbrudd for de fem resterende bjelkene med aluminiumsarmering. Heften mellom betongen og aluminiumsarmeringen var dårling grunnet glatt overflate på armeringen, som videre medførte at forhåndsberegnede verdier ikke stemte overens med resultater fra testene utført i laboratoriet.

Nedbøyningen var større i laboratoriet enn beregnet, for alle bjelkene. Kontrollberegninger utført i etterkant av testingen for bjelken med stålarmering, viser at nedbøyningen fra laboratoriet er gyldig. For bjelkene med aluminiumsarmering kan de store nedbøyningene forklares av den lave heftfastheten. Beregninger av den faktiske heftfastheten er utført for bjelken med stålarmering, og for én av bjelkene med aluminiumsarmering. Beregningene viser at heftfastheten til bjelken med aluminiumsarmering var lavere enn de gitte kravene, mens den var høyere for bjelken med stålarmering.

Table of Contents

Nomenclature

Latin upper case letters

A_{al}	Cross-sectional area of aluminium reinforcement
A_c	Cross-sectional area of concrete
$A_{c.eff}$	Effective tension area of concrete
A_r	Cross-sectional area of reinforcement
A_s	Cross-sectional area of steel reinforcement
A_{sb}	Cross-sectional area of balanced reinforcement
A_{sl}	Area of the tensile reinforcement
$A_{s,min}$	Minimum cross-sectional area of reinforcement
$C_{Rd,c}$	Factor
D	Diameter
E_{Al}	Design value of modulus of elasticity of reinforcing aluminium
E_{cm}	Secant modulus of elasticity of reinforced concrete
E_r	Design value of modulus of elasticity of reinforcement
E_s	Design value of modulus of elasticity of reinforcing steel
F	Maximum load at failure for small specimens
I_c	Contribution from the concrete to the moment of inertia for the cracked cross section
I_{c1}	Contribution from the concrete to the moment of inertia for the uncracked cross section
I_{r1}	Contribution from the reinforcement to the moment of inertia for the uncracked cross section
L	Length
L_m	Distance between point loads
L_s	Distance between support and point load

M	Bending moment
M_{Ed}	Design value of the applied internal bending moment
M_{crack}	Crack moment
M_{Rd}	Bending moment capacity
O_r	Circumference of reinforcement
P	External load
P_{crack}	Crack load
P_{cr}	Critical load
T_c	Compression resultant of the stresses in the concrete compression zone
S	Force in the tensile reinforcement
$S_{r.max}$	Maximum final crack spacing
V	Shear force
V_{Ed}	Design value of the applied shear force
V_{ol}	Volume of the container
$V_{Rd,c}$	Shear capacity without shear reinforcement
$V_{Rd,max}$	Shear force
$V_{Rd,s}$	Shear capacity without shear reinforcement

Latin lower case letters

a_{cs}	Effective shear span with respect to the control section
a_v	Mechanical shear span
b	Overall width of the cross-sectional
b_w	Smallest width of the cross-sectionals in the tensile area
c	Concrete cover
d	Effective depth of a cross-sectional; diameter of small specimen
d_{dg}	Largest aggregate size
f_{bd}	Ultimate bond stress
f_c	Compressive strength of concrete
f_{cd}	Design value of concrete compressive strength
f_{ck}	Characteristic compressive cylinder strength of concrete
f_{cm}	Mean value of concrete cylinder compressive strength
f_{ct}	Tensile splitting strength
f_{ctm}	Mean value of axial tensile strength of concrete
f_r	Tensile reinforcement strength
f_{td}	Design value of concrete tensile strength
f_{ym}	Mean value of yield strength of reinforcement
h	Height
k	Factor
k_{1-4}	Factors
l_{bd}	Design anchor length
$l_{b,min}$	Minimum anchor length
$l_{b,rqd}$	Required anchor length
m_a	Mass of container
m_r	Mass of small specimen received condition
m_st	Apparent mass of the stirrup
m_w	Apparent mass of the immersed specimen
m_1	Mass of container
m_1	Mass of container filled with compacted concrete
v_{min}	Smallest shear resistance
z	Inner lever arm of internal forces

Greek lower case letters

α	Compression zone factor
α_b	Balanced reinforced compression zone factor
α_v	Distance from edge of a support
α_{1-5}	Influencing factors
β	Ratio
δ	Deflection of beam
ε_{Al}	Compressive strain in the aluminium
ε_c	Compressive strain in the concrete
ε_{cu}	Ultimate compressive strain in the concrete
ε_r	Strain of reinforcement
ε_s	Strain of steel reinforcement
ε_{yd}	Design yield strain of reinforcement
κ	Curvature
λ	Effective hight of the compression zone
ν	Strength reduction factor for concrete cracked in shear
η	Effective strength; ratio
ρ_c	Concrete density
ρ_l	Reinforcement ratio for bonded longitudinal reinforcement in the tensile zone
ρ_w	Water density
ϕ	Diameter of a reinforcing bar

Chapter 1

Introduction

1.1 Background

Today, concrete is the most used construction materials within the construction industry worldwide. As a construction material, concrete is known for its ability to withstand large compressive loads, while it's more vulnerable when exposed to tensile loading. Thus, concrete structures are usually reinforced to improve its tensile capacity.

The reinforcement material that dominates today's marked is steel rods, normally with a diameter in the range of 8-32 mm. Corrosion of steel reinforcement initiated by carbonation or chloride ingress is today the main degradation mechanism of reinforced concrete. A concrete reinforcement material that doesn't corrode is in demand. At the same time, since the gross volume of concrete produced annually in the world is 10^{10} m^3 (Justnes, 2017), the reinforcement material must be composed of common chemical elements.

There is an on-going project called DARE2C, where the main purpose is to develop a new type of reinforced concrete that is more durable and environmentally-friendly than existing concrete qualities. In this project, a new concept for low pH concrete that allows reinforcement with aluminium is described. (Justnes, 2017)

1.2 Scope and Aim

The overall aim of this study is to investigate the possibility of using aluminium as reinforcement in concrete structures. The study is performed as a research for the DARE2C project. To evaluate the accuracy and suitability, both aluminium and steel reinforced concrete beams are produced and tested in laboratory, based on beforehand calculations. More specifically, we wanted to:

- Research the behaviour of aluminium reinforcement in concrete structures.
- Investigate if regulations for steel reinforced concrete, as e.g. Eurocode, are valid for aluminium reinforcement as well.

1.3 Thesis Structure

It was necessary to set boundaries by limiting the amount of theory, calculations and laboratory work. The DARE2C science project has a lot of potential and opportunities, hence clear restrictions were set at an early stage to define the assignment. The thesis consist of in total 10 chapters and below the main part of each chapter is presented to give an overview.

- Chapter 1 introduces the background material including general facts about concrete, and presents the scope and aim of this master thesis.
- Chapter 2 contains the background theory of the DARE2C-project, including previous laboratory research. In addition, theory of the materials used in this thesis is introduced. At last the most common failure types are presented with basic illustrations and descriptions of how the failure types arise.
- Chapter 3 presents the selection of structural design including beam layout and reinforcement types. Further on, several calculations for both the ultimate limit state and the serviceability state are executed, in conjunction with the chosen structural design. The theory behind the calculations are also described.
- Chapter 4 contains the practical information about how the task has been solved. This includes the production and testing of beams and small specimens. It also presents standard testing routines of the material properties of both fresh and hardened concrete, in addition to the equipment and the test setup used in the laboratory.

- Chapter 5 presents modifications performed correlated to calculations and the beam setup of each beam, based on results from laboratory testing. The modified calculations are presented in the same order as in chapter 3.
- Chapter 6 presents the results from laboratory testing of small specimens and beams. The explanation of the beam setup modifications is also presented here.
- Chapter 7 presents the discussion part, where results are analyzed. Calculated values are compared with laboratory results, and some of the beam results are compared with each other. Overall, this chapter gives a greater understanding of the laboratory outcomes.
- Chapter 8 contains the final conclusion, which sums up the most important topics from the discussion and answers the objectives of this thesis.
- Chapter 9 points out the sources of error that can have impacted the thesis. This includes the possibility of human or machine made errors in conjunction with theory approaches, assumptions or execution of calculations and laboratory work.
- Chapter 10 presents the possibilities of further studies for this master thesis by introducing potential improvements. Further studies for the DARE2C-project are also presented.

As shown in the chapter overview above, modifications were done related to the beam setup. To improve the overall understanding, the beam calculations are divided into two separate chapters:

– The first part, presented in chapter 3, is based on the original beam design and setup, and was performed prior to laboratory beam testing.

– The second part, presented in chapter 5, is based on modifications performed in conjunction with the outcome from laboratory beam testing.

Chapter 2

Theoretical background

Aluminium is the second most commonly used metal after steel (Xing and Ozbulut, 2016), and is a very common element in earth's crust. The problem of using aluminium as reinforcement is that it will be degraded by the high pH of natural concrete, and develop hydrogen gas. Therefore, aluminium can only function in a sufficiently low pH concrete. (Justnes, 2017)

It is desirable to use a more environmentally-friendly cement in the concrete than pure Portland cement. In recent years, the production of cement has been identified as the third largest emitters of carbon dioxide (CO_2), contributing to 5 to 8% of the total anthropogenic emissions. Four main methods are currently in place to obtain this challenge: i) switching from fossil fuels to alternative fuels, ii) increase efficiencies in factories, iii) implementation of supplementary cementitious materials (SCMs) replacing cement clinker and iv) carbon capture and storage. Replacing the clinker partially by SCMs is the most promising method on a short term, because a significant reduction in the CO_2 emission could be expected. The amount of raw material needed per unit cement is also reduced when replacing cement with SCMs, and the cement production volume of a cement plant will increase. (Justnes, 2017)

2.1 DARE2C

"Durable Aluminium Reinforced Environmentally-friendly Concrete Construction - DARE2C" is a project led by the Norwegian aluminium producer Hydro with the cement producer Norcem, supported by HTC, the contractor Veidekke and the research institutions SINTEF and NTNU as partners. (Justnes, 2017)

The main purpose of this project is, as mentioned, to develop a new type of reinforced concrete that is more durable and environmentally-friendly than existing concrete qualities. This will be reached by:

1. Replacing today's steel based reinforcement with aluminium, preferable recycled aluminium
2. Replacing some of the cement clinker in the concrete with calcined clay and possibly "red-mud", which is a rest product from alumina production

The aim is to replace about 50% of the clinker with less CO_2-intensive cement constituents, such as red-mud and calcined clay. These SCMs are pozzolans that will make the concrete less alkaline, i.e. lower the pH in the concrete, which is necessary when using aluminium as reinforcement in concrete. This allows higher w/c-ratio, giving more permeable concrete. (Justnes, 2017)

High permeability is not a problem for aluminium reinforced concrete as aluminium is resilient to atmospheric CO_2 and also chlorides when alloyed with 5% magnesium. High permeability is in fact beneficial for the concrete to carbonate fast, and faster carbonation binds CO_2 and further reduce the overall CO_2 emission. The reason why aluminium is resilient to CO_2 and chlorides is because it forms a dense oxide layer (Al_2O_3) on the surface when the metal gets in contact with air. This layer will prevent the aluminium from further oxidation (or corrosion), (Justnes, 2017) however this oxide layer is only stable for pH values higher than pH 4 and lower than pH 9. (Xing and Ozbulut, 2016) Alloying with magnesium may give an even more stable oxide layer of spinel ($MgAl_2O_4$) rather than just pure aluminiumoxide (Al_2O_3). (Prof. Dr. Justnes, H., Chief Scientist, private communication, 2018)

It is desirable to use red-mud together with calcined clay, but this is not possible yet because of stability requirements. Therefore, only calcined clay will be used as SCM for this study.

As a proof of the DARE2C concept, SINTEF tested two different paste mixes with w/c=0,60:

a) 100% ordinary Portland cement

b) 50% ordinary Portland cement and 50% calcined marl

These pastes were poured separately into two plastic cups where each of them had an aluminium plate inserted. After a few moments it was observed that hydrogen gas started to bubble vigorously along the plate for paste a), while only a few small bubbles were observed for paste b). After the pastes had hardened they were split, and the reference paste with pure Portland cement showed many cavities

next to the aluminium plate. The paste with calcined marl had only a few small gas voids on the interface (maybe just entrained air from the mixing), and thermal analysis showed no sign of calcium hydroxide which can attack the aluminium metal neither at 28 days nor after 2 years. These observations together with the studies on blended cement give confidence in the DARE2C concept. (Justnes, 2017)

2.2 Concrete

Concrete is a versatile material and is the most used building material worldwide. The advantages of using concrete are many. The raw materials are found throughout the world, it can be cast in any shape and dimension, and it has good fire resistance, high strength and good durability. The concrete got its real breakthrough when it was reinforced with steel rods. (Sørensen, 2013)

Ordinary concrete is a composition of water (15-20 %), cement (10-20 %) and aggregates (60-70 %), in addition to any admixtures and additives in smaller amounts. The aggregate consist of sand, gravel and coarse aggregate. Particles with diameter smaller than 8 mm are called gravel, and the particles smaller than 4 mm are defined as sand. Coarse aggregate is the particles that is larger than 8 mm. (Sørensen, 2013)

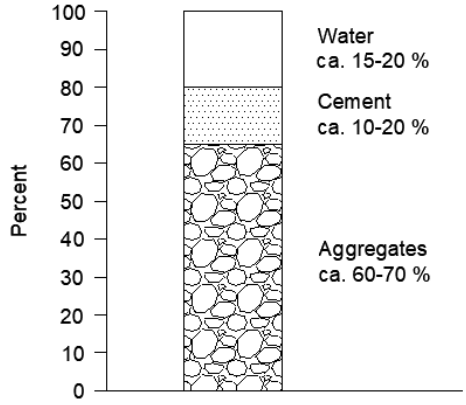

Figure 2.1: Approximately volume distribution of the materials in concrete

Cement, which is the binding material, is a very alkaline material with pH 13. The pH value in the concrete adjusts by the mass ratio between water and cement, the

w/c-ratio, and the composition of the cement and SCMs. As mentioned in Chapter 2.1, the pH-value in ordinary concrete can be reduced by using SCMs, which gives an opportunity to use aluminium as reinforcement in concrete structures.

In this study, calcined clay is used as SCM, and the full composition of the concrete is showed in the prescription in Chapter 4.1.1.

The material properties for the concrete change when replacing parts of the cement with calcined clay. For the fastening period, a high w/c-ratio makes the concrete more porous the carbonating process speed up. In general, the replacement of this large amount of cement by pozzolan reduce the early fastening strength. On the other hand, laboratory studies showed that it was possible to accomplish 10 MPa after one day with 50 % replacement and a w/c-ratio of 0.55, which gave the same strength as ordinary concrete after 28 days. This means therefore that the concrete strength easily increase by decreasing the w/c-ratio. (Prof. Dr. Justnes, H., Chief Scientist, private communication, 2018)

The durability of this concrete is close to maintenance-free as long as the reinforcement can handle the perhaps too high pH values at the beginning. Aluminium alloyed with 5 % Magnesium is used in the boat industry, and is durable against seawater. Therefore the reinforcement will not corrode in the concrete carbonation process, and is resistance against chlorides. (Prof. Dr. Justnes, H., Chief Scientist, private communication, 2018)

2.3 Reinforcement

Regular steel reinforcement is hot rolled, and the bars are in most cases deformed. This means that the bar is supplied with heavy ridges on its surface to assist in binding the reinforcement to the concrete mechanically. This is essential for the bond properties, which must be good for the concrete and reinforcement to collaborate.

Pure aluminium is not common to use in construction industry based on its low strength, hence aluminium is usually alloyed with other metals to obtain desirable properties such as strength and stiffness. (Xing and Ozbulut, 2016) Another disadvantage of pure aluminium is the large temperature coefficient compared with concrete, steel and other metals. Temperature variations could cause structural problems based on different expansions/contractions of each material, where growth of cracks in aluminium reinforced concrete would be one of them. Thus, aluminium alloyed with other metals would reduce this temperature coefficient. (Justnes, 2017)

Aluminium often replaces steel based on its light weight, which is approximately one third of steel's, and its high resistance against corrosion. In addition, the aluminium density and Young's Modulus are also about one third of steel's. (Karlsson, 2014)

Table 2.1: Comparison of material properties for aluminium and steel

Material	Young's Modulus, E [GPa]	Density, ρ [kg/l]	Ultimate tensile strength, f_t [MPa]
Aluminium	70	2.70	110
Steel	210	7.87	400

In this study, aluminium reinforcement alloyed with 5 % magnesium, Al-5Mg, and ordinary steel reinforcement, are used. The focus will be on the aluminium alloyed reinforcement, with steel reinforcement as a reference. The alloy has been determined from experiments made in the SINTEF chemistry-lab, "paste-lab", where the development of hydrogen gas caused by the reaction between the alloy and the paste have been observed.

2.4 Failure types for beams

Traditionally, concrete structures are reinforced to prevent and avoid development of large and concentrated cracks. Reinforcement helps to distribute cracks evenly along the entire structure. This study presents only beams reinforced in the longitudinal direction, without any shear reinforcement.

Three of the most common failure types for beams are bending moment, shear and anchoring failure. In this subsection these failure modes are briefly described.

Moment failure

Bending moment failure of beams arise when external loads is applied in the compression zone. This results in bending cracks (vertical cracks) throughout the longitudinal tensile strength zone, as shown in Figure 2.2. At a specific load, the bending moment ends up crushing the concrete in the compression zone. Further, the cracks along the tensile zone expand and the beam break at the middle region because the moment acting on the beam surpass the moment capacity of the beam.

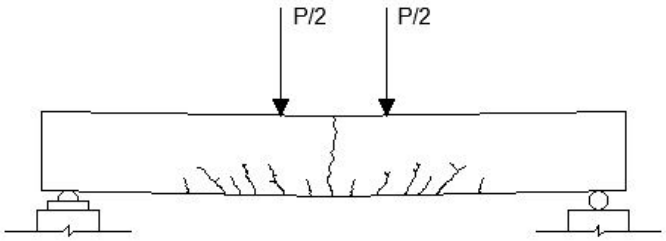

Figure 2.2: Moment failure of a beam.

Shear failure

Shear failure arise when compression stresses, from external loads, exceed the shear capacity. By exceeding the shear capacity of the structure, shear cracks occur from the load application point and diagonal down towards the closest support, as shown in Figure 2.3. When designing the shear capacity of a structure, both tensile and compressive shear must be taken into account.

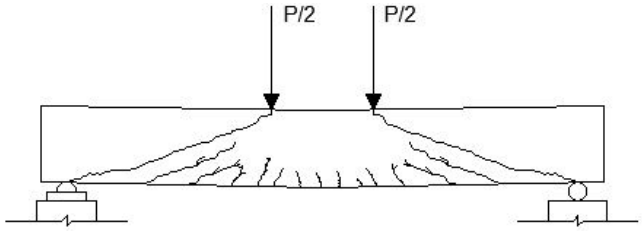

Figure 2.3: Shear failure of a beam

Anchorage failure

Friction, adhesion and mechanical cogging cause the bond strength between ribbed reinforcement bars and concrete (Sørensen, 2013). Failure according to anchorage arise when the bond strength is either poor or absent.

The reinforcement bars in the tensile zone are exposed to a tensile force pulling the bars towards the centre whenever the structure is loaded (Sørensen, 2013). Compared with bending moment failure, where a lot of small cracks occur in the longitudinal direction in the tension zone, this type of failure develops larger and more concentrated cracks at the centre region, as shown in Figure 2.4. The reason for the large crack development is the poor bond strength of the reinforcement,

which leads to a slip at the ends, indicated as a displacement with a Δ symbol in Figure 2.4. Since the reinforcement is slipping at the ends, it cannot withstand the crack development at the centre for an increasing force. The cracks in the middle region of the beam would therefore increase, instead of new cracks developing.

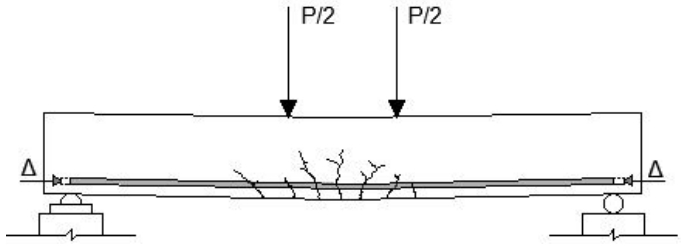

Figure 2.4: Anchor failure of a beam

Figure 2.4 shows only one of many scenarios for an anchorage failure type. The reinforcement must be anchored properly at the ends to avoid the lack of bond strength. To obtain the bond strength throughout the structure, ribbed reinforcement bars are often used. At the ends of structural concrete building components, it's common to curve the reinforcement or connect the reinforcement to end plates (by welding), to obtain the anchoring effect. Shorter reinforcement bars can also be used as anchoring by placing them with spacing orthogonally, and fasten by tying or welding them together with the main reinforcement.

If the reinforcement bars have a smooth surface, this would lower the bond strength between the bars and the concrete compared to ribbed bars, because it has less friction resistance.

Chapter 3

Beam design

This chapter contains the calculations for the selected beam layouts, both for the ultimate limit state (ULS) and the serviceability limit state (SLS). The calculations are in accordance with NS-EN 1992-1-1 *Design of concrete structures* (EC2). These formulas are originally based on concrete with steel reinforcement, but it is assumed that they can be used for aluminium reinforcement as well. The previous concrete standard NS-EN 3473 and the book *Betongkonstruksjoner* by Svein Ivar Sørensen has also been used in this chapter.

In order to control the beam capacities against failure, calculations have been carried out in the ULS. In this state, the capacities are calculated on the basis of the strain properties for the materials and dimensioning strengths. For this task, it is interesting to look at the real behavior for the beams at loading, and all safety factors are therefore set equal to 1,0. The considered ULS controls are moment and shear capacity, and the chosen beam layouts are based on these calculations. Calculations on the anchorage and the relation between loading and compression zone height have also been performed.

For the SLS it must be proved that the structure satisfies the requirements related to its use and purpose for the entire service life. Requirements for this state must also ensure the durability of the structure. Crack spacing and deflection calculations are the controls carried out for this state.

For the calculations, Microsoft Office Excel has been used. This software is user-friendly and gives a well arranged setup. Especially for the ULS calculations, this have been beneficial since we could easily change the inputs to get the desired outputs. The calculations done in Excel are controlled by hand. Additionally, calculations were performed in Mathcad. All calculations are shown in the Appendix.

3.1 Basis of beam design

Since aluminium is used as reinforcement, parts of the cement is replaced with calcined clay. The access to calcined clay was limited to approximately 50 kg, which results in approximately 300 liters of concrete. It was desirable to make multiple beams to increase the accuracy and reliability of the results, and with the opportunity to compare multiple cases. The size of each beam was limited to just below 50 liters, which resulted in 6 beams and 24 cylinders. The capacity of the mixing machine was 200 liters, hence it was decided to cast the concrete in two batches.

The limited volume of each beam also limits the length. The length of the beam was chosen to 1,1 m while the distance between the supports was chosen to 1,0 m. The design of the beam cross section is based on the theory that the beam was going to behave as a beam, and not a plate. This limits the height to a third of the span length, which in this case limits the height to approximately 1000 mm / 3 $\approx$ 333 mm. To avoid shear failure it was possible to reduce the height further.

All the beams are assumed simply supported with two external point loads (4-point bending test), with a point of attack symmetrically on the beams. The placing of the external loads will affect whether the beams will fail in bending moment or in shear. The boundary conditions provide a system that is in static equilibrium, which means that the number of unknowns are less than equations of equilibrium. For such a simple static model, calculation by hand is preferred.

It was desirable that the beams should obtain bending moment failure, as the 4-point bending test gives a constant moment and zero shear force in the moment zone between the two external loads. In this way, it is easier to compare the laboratory results with the hand calculations since the whole load is taken up as a moment here. To obtain just this type of failure, adjustments of the input values as cross section dimensions, reinforcement amounts and distances in the static system are necessary. By achieving as low utilization for the shear force as possible, it increases the possibility that the beams would fail according to bending moment. At the same time it was desired to obtain certain values for the failure load, strain and compression zone height. All desired values could not be obtained at the same time, so some values had to be compromised on behalf of others.

Material properties used in the beam design are based on mean values for the expected concrete strength of 30 MPa after 28 days of hardening, given in EC2, Table 3.1. Mean values are also used for the steel reinforcement, while the values used for the aluminium reinforcement are expected values based on the chosen aluminium alloy, Al-5Mg.

3.2 Beam layout

Choices made in this chapter are based on the premises described in chapter 3.1. The statical system of the beams are shown in Figure 3.1.

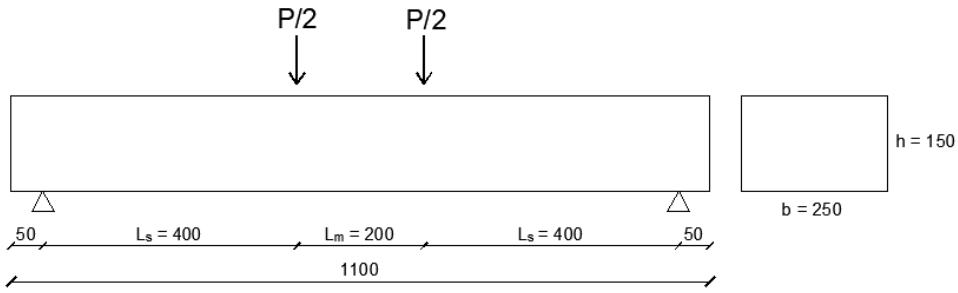

Figure 3.1: Statical system of the beams

The beam dimensions are set to a width of 250 mm and a height of 150 mm. The focus in this task is to obtain bending moment failure for six beams. These beams have the following reinforcement:

- Circular steel rods - 1 beam
- T-shaped aluminium rods - 2 beams
- Circular aluminium rods - 3 beams

One beam with circular steel rods, two beams with T-shaped aluminium rods and three beams with circular aluminium rods will be tested. Although steel reinforcement has been tested numerous times before, it has not been tested with the selected concrete. Therefore it is desirable to see if it behaves as assumed, and moreover the comparison of steel and aluminium reinforcement will be more relevant.

Since aluminium rods are a reinforcement type that is not in use today, the rods need to be produced from scratch. This gives the opportunity to choose whichever profile for the aluminium rods. As circular steel rods are dominating the market today, it's interesting to choose an alternative cross section for the aluminium rods in addition to the circular aluminium rods. The choice fell on T-profiles turned upside down, to achieve a larger effective height, with cross-sectional dimensions as shown in Figure 3.2. This profile has a larger surface area than the circular profiles, which gives an opportunity to achieve better bond if the surface has ridges.

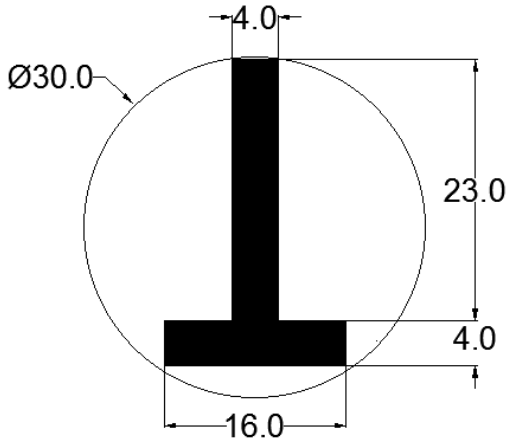

Figure 3.2: T-shaped aluminium rod

The extrusion machine used to produce the aluminium rods gave a limitation for the profiles to be within an outer diameter of 30 mm. The dimensions are chosen to aim for approximately the same amount of reinforcement area as the circular aluminium rods (in total per beam), see Table 3.1.

Table 3.1: Calculation of reinforcement amount

Reinforcement type	Area of rod [mm^2]	Number of rods	Sum area [mm^2]	Failure load [kN]
Circular steel rods	113	2	226	60,7
T-shaped aluminium rods	156	3	468	62,7
Circular aluminium rods	78,5	6	471	66,1

The chosen reinforcement amounts given in Table 3.1, are based on the statical system from Figure 3.1 and the expected concrete strength of 30 MPa. To obtain a bending moment failure, a relatively small amount of reinforcement is used. 6ø10 were chosen for the beams with circular aluminium rods and 3 rods were chosen for the beams with T-profiles. The reference beam with circular steel reinforcement didn't have the same reinforcement amount as the beams with aluminium rods. This was because it would give an over-reinforced cross section which was not desired. Instead, a reinforcement amount which resulted in a failure load close to the failure load obtained for the other beams was chosen, regardless of failure type. 2ø12 was then chosen for the reference beam with steel reinforcement. Figure 3.3 shows the cross section for the beam with steel reinforcement while Figure 3.4 shows the different cross sections for the beams with aluminium reinforcement.

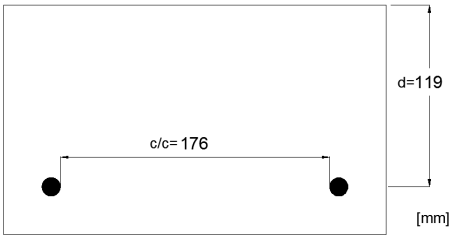

Figure 3.3: Cross section with steel reinforcement: 2ø12

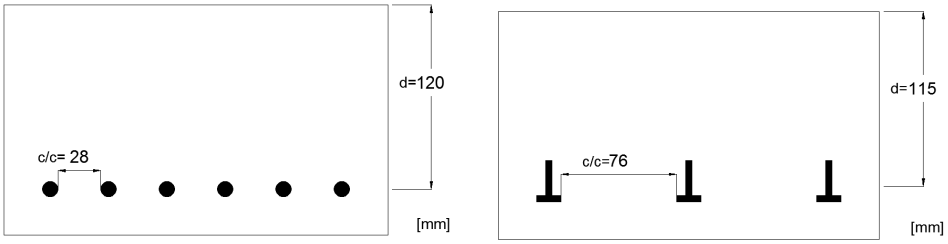

(a) 6ø10 **(b)** 3 T-profiles

Figure 3.4: Cross sections with aluminium reinforcement

The beams are named based on their batch number (B1/B2), reinforcement shape and amount (2ø12/6ø10/3T), and reinforcement material (STEEL/ALU). Table 3.2 shows an overview of the beam identification.

Table 3.2: Identification of beams

Batch number	Reinforcement shape and amount	Reinforcement material	Identification
1	6ø10	Aluminium	B1-6ø10-ALU1
	6ø10	Aluminium	B1-6ø10-ALU2
	6ø10	Aluminium	B1-6ø10-ALU3
2	2ø12	Steel	B2-2ø12-STEEL
	3 T-profiles	Aluminium	B2-3T-ALU1
	3 T-profiles	Aluminium	B2-3T-ALU2

In addition, all of the beams have transversal rods fastened at the bottom of the longitudinal reinforcement in each end, to ensure sufficient anchorage.

When considering bond between the concrete and the reinforcement, the ideal case is that the reinforcement has some kind of ridges on the surface. This was not possible for the aluminium rods at this point. The aluminium rods have therefore smooth surfaces while the steel rods are ribbed. Since the aluminium rods have smooth surfaces, the bond may not be sufficient along the reinforcement. It is still assumed full bond between the concrete and the reinforcement.

3.3 Moment capacity

Rules for calculating the moment capacity are given in EC2, 6.1.

When determining the ultimate moment resistance of reinforced concrete cross section in accordance with EC2, following assumptions need to be satisfied:

- Full bond between the concrete and reinforcement.
- Plane sections remain plane.
- Stress and strain relation given in EC2, 3.1.7.
- The tensile strength of the concrete is ignored.

Furthermore, it needs to be defined when failure occurs, i.e. certain failure criteria must be chosen:

- Compressive failure when $\varepsilon_c = \varepsilon_{cu}$; ε_{cu2} or ε_{cu3} depending on chosen stress-strain diagram from EC2, fig. 3.3 or 3.4
- Failure in the reinforcement when $\varepsilon_s = \varepsilon_{ud}$

For common reinforcement amounts, the final failure is assumed to occur when the compressive failure criterion for the concrete is exceeded.

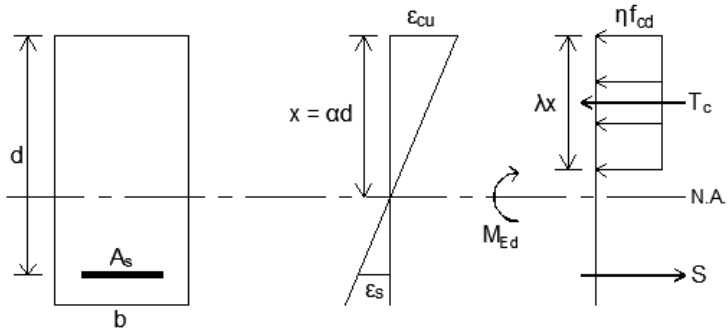

Figure 3.5: Calculation model for moment capacity

Figure 3.5 shows the simplified calculation model for moment capacity, with a rectangular compression stress block. EC2, 3.1.7(3) allows this simplification when the compression zone αd, is completely utilized. As seen from the figure, the strains vary linearly in the compression zone, from $\varepsilon_c = 0$ at the neutral axis to $\varepsilon_c = \varepsilon_{cu}$ on the top of the cross section.

The moment capacity in the compression zone is expressed by the moment that occurs due to the internal forces:

$$M_{Rd} = \lambda \cdot \eta \cdot \alpha \cdot (1 - 0.5 \cdot \alpha) \cdot f_{ck} \cdot b \cdot d^2 \tag{3.1}$$

The factor λ defines the effective height of the compression zone, while the factor η defines the effective strength. For the given strength class, these factors are set to:

$$\left.\begin{array}{l} \lambda = 0.8 \\ \eta = 1.0 \end{array}\right\} \text{ for strength classes} \leq \text{B50}$$

For a given concrete cross section and reinforcement amount A_s, the factor α needs to be decided such that the reinforcement strain ε_s corresponds to the equilibrium between T_c and S. When determining α, the strain condition in the cross section at bending moment failure must be known. Figure 3.6 shows three typical strain conditions.

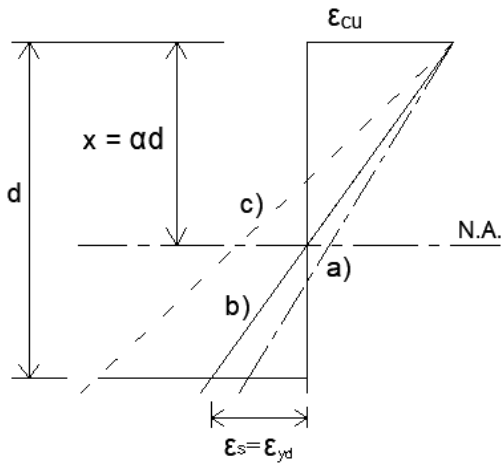

Figure 3.6: Typical strain conditions at bending moment failure

a) Over-reinforced cross section ($\varepsilon_s < \varepsilon_{yd}$) – the reinforcement doesn't yield before the concrete crushes

b) Balanced-reinforced cross section ($\varepsilon_s = \varepsilon_{yd}$) – the reinforcement starts to yield simultaneously as the concrete crushes

c) Under-reinforced cross section ($\varepsilon_s > \varepsilon_{yd}$) – the reinforcement starts to yield before the concrete crushes

By determining the balanced reinforcement amount, A_{sb}, and compare the relevant A_s with this one, it can be decided whether the cross section is over- or under-reinforced. The formula for A_{sb} is given by:

$$A_{sb} = \lambda \cdot \eta \cdot \frac{f_{cd}}{f_{yd}} \cdot b \cdot d \cdot \alpha_b \tag{3.2}$$

where

$$\alpha_b = \frac{\varepsilon_{cu}}{\varepsilon_{cu} + \varepsilon_{yd}}$$

When determining α, different equations should be used for over- and under-reinforced cross sections. In practice, it is desirable to dimension the cross section

as under-reinforced. The benefit of this is that the structure shows a certain ductility, which means that one can get a prewarning about the failure through relatively large deformations and visual cracks. Because of this, it was decided to make all of the beams under-reinforced. The following equation should then be used when determining α:

$$\lambda \cdot \eta \cdot f_{cd} \cdot b \cdot d \cdot \alpha - f_r \cdot A_s = 0 \tag{3.3}$$

The requirement for the minimum and maximum reinforcement amount given in NA.9.2.1.1(1) is also checked. The minimum reinforcement amount ensures that the reinforcement doesn't yield when the first crack occurs, as this would result in one large crack in the middle of the beam instead of several distributed cracks.

The moment capacity of each beam is used to find the failure loads by setting the occurring bending moment given for the 4-point bending test equal to the moment capacity. The equation can then be solved with respect to the failure load.

$$M_{Rd} = M_{Ed} = \frac{P_{cr}}{2} \cdot L_s \quad \Rightarrow \quad P_{cr} = \frac{2 \cdot M_{Ed}}{L_s} \tag{3.4}$$

This load will further be used to find the occurring shear force. In this way, the cross sections and reinforcement amounts for the beams can be chosen such that they would fail due to moment.

Table 3.3: Moment capacities

Identification	M_{Rd} [kNm]	M_{Ed} [kNm]	Utilization	P_{cr} [kN]
B2-2ø12-STEEL	13,8	12,1	81%	60,7
B2-3T-ALU1 B2-3T-ALU2	12,5	12,5	100%	62,7
B1-6ø10-ALU1 B1-6ø10-ALU2 B1-6ø10-ALU3	13,2	13,2	100%	66,1

Table 3.3 shows the calculated moment capacities for the beams, which is equal for the beams with the same reinforcement type. As the table shows, all of the aluminium reinforced beams are expected to obtain bending moment failure while

the steel reinforced beam is expected to fail due to shear. Equation (3.4), which gives the failure load can therefore only be used for the aluminium reinforced beams. The equation used to find the failure load for the steel reinforced beam is given in chapter 3.4.

3.4 Shear capacity

Rules for calculating the shear capacity are given in EC2, 6.2. The capacity should be controlled for both tensile failure and compressive failure. EC2 describes different methods for shear capacities, depending on whether there is a requirement for design shear reinforcement or not.

Shear tensile capacity

It was decided not to use shear reinforcement to get as few affecting factors as possible. EC2, 6.2.2(1) gives the following formula for the shear capacity without shear reinforcement:

$$V_{Rd,c} = C_{Rd,c} \cdot k \cdot (100 \cdot \rho_l \cdot f_{ck})^{1/3} \cdot b_w \cdot d \tag{3.5}$$

with a minimum of

$$V_{Rd,c} = v_{min} \cdot b_w \cdot d \tag{3.6}$$

where

$$k = 1 + \sqrt{\frac{200}{d}} \leq 2,0$$

$$\rho_l = \frac{A_{sl}}{b_w \cdot d}$$

$$C_{Rd,c} = k_2/\gamma_c$$

NA.6.2.2(1) gives k_2 and v_{min} as:

$k_2 =$ 0,18 for concrete with coarse aggregate, D $\geq$ 16 mm

$$v_{min} = 0,035 \cdot k^{3/2} \cdot f_{ck}^{1/2}$$

A formula developed for the new Eurocode, which is currently under editing, has also been viewed. This formula can be found in the *background documents to the interim draft* prEN 1992-1-1:2017-10, section 8.2.2(3). In difference to the current expression for the shear resistance, which is derived empirically on the basis of existing tests, the new formula is based on the Critical Shear Crack Theory for shear. (Muttoni et al., 2017) In this formula, the Young's Modulus of the reinforcement is included. This way the shear capacity differs for concrete reinforced with aluminium and concrete reinforced with steel.

$$V_{Rd,c} = 0.021^{2/3} \cdot \left(\rho_l \cdot E_r \cdot f_c \cdot \frac{d_{dg}}{a_{cs}} \cdot \frac{z}{d}\right)^{1/3} \cdot b_w \cdot d \tag{3.7}$$

where

E_r is Young's Modulus of the reinforcement, in Mpa

d_{dg} = 32 mm for normal weight concrete with $f_{ck} \leq 60$ MPa and $D_{lower} \geq 16$ mm, where D_{lower} is the coarsest aggregate size

a_{cs} = $\frac{M_{Ed}}{V_{Ed}} - \frac{d}{2}$ is the effective shear span, in mm

It is necessary to use shear reinforcement if $V_{Ed} > V_{Rd,c}$. Since shear reinforcement was undesirable, cross sections and reinforcement amounts were chosen such that the occurring shear force was smaller than the shear capacity, for the aluminium reinforced beams, resulting in bending moment failure.

Table 3.4: Shear tensile capacities - Current formula

Identification	$V_{Rd,current}$ [kN]	V_{Ed} [kN]	Utilization	P_{cr} [kN]
B2-2ø12-STEEL	30,4	30,4	100%	60,7
B2-3T-ALU1 B2-3T-ALU2	37,8	31,4	83%	62,7
B1-6ø10-ALU1 B1-6ø10-ALU2 B1-6ø10-ALU3	39,0	33,0	85%	66,1

Table 3.4 shows the calculated shear tensile capacities for the beams, given from equation (3.5) from the current Eurocode. As for the moment capacity, the shear tensile capacity is equal for the beams with the same reinforcement type. As the

table shows, the beam with steel reinforcement is expected to get shear tensile failure. For this beam, equation (3.8) is therefore used instead of equation (3.4) when calculating the failure load.

$$V_{Rd} = V_{Ed} = \frac{P_{cr}}{2} \quad \Rightarrow \quad P_{cr} = 2 \cdot V_{Ed} \tag{3.8}$$

The formula developed for the new Eurocode gives slightly different capacities than the current formula. A comparison between these formulas are given in Table 3.5, with comments on the failure type.

Table 3.5: Shear tensile capacities - Comparison of current and new formula

Identification	$V_{Rd,new}$ [kN]	$V_{Rd,current}$ [kN]	Comment
2ø12-STEEL	35,9	30,4	The new formula gives bending moment failure instead of shear failure.
B2-3T-ALU1 B2-3T-ALU2	29,9	37,8	The new formula gives shear failure instead of bending moment failure.
B1-6ø10-ALU1 B1-6ø10-ALU2 B1-6ø10-ALU3	32,6	39,0	The new formula gives shear failure instead of bending moment failure.

As the table shows, the current formula gives higher capacity for all of the aluminium reinforced beams. For the steel reinforced beam it is the opposite: the highest capacity is calculated from the formula developed for the new Eurocode.

Shear compressive capacity

The diagonal cracks that occur near the beam supports are caused by the shear force, and will form an angle of approximately 45° with the beam axis in the part of the beam that is below the neutral axis. This angle will decrease when the compression stress in the concrete σ_c increases, and the crack will then become more parallel with the beam axis upwards in the compression zone. Compression

stresses will occur parallel to the diagonal cracks as a so-called compression field as showed in Figure 3.7.

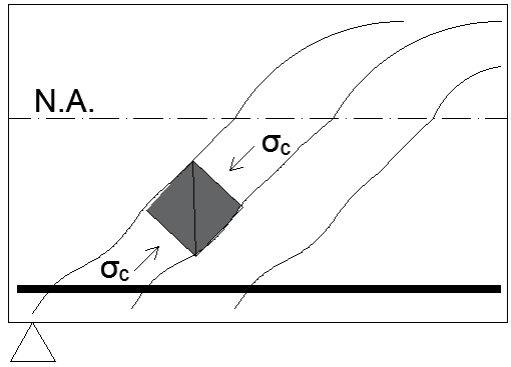

Figure 3.7: Compression field between diagonal cracks

The concrete needs to withstand these stresses to avoid compressive failure, and the shear compressive capacity can be used to control this. EC2 6.2.2(6) expresses this capacity as:

$$V_{Rd,max} = 0,5 \cdot b \cdot d \cdot \nu \cdot f_{cd} \tag{3.9}$$

where ν is a strength reduction factor for concrete cracked because of shear, given in NA.6.2.2(6) as:

$$\nu = 0,6 \cdot (1 - \frac{f_{ck}}{250})$$

The capacity requirement is that $V_{Ed} \leq V_{Rd,max}$. Table 3.6 shows the calculated shear compressive capacities for the beams, which for all beams is higher than the occurring shear force.

Table 3.6: Shear compressive capacity

Identification	$V_{Rd,max}$ [kN]	V_{Ed} [kN]
B2-2ø12-STEEL	235,6	30,4
B2-3T-ALU1 B2-3T-ALU2	227,8	31,4
B1-6ø10-ALU1 B1-6ø10-ALU2 B1-6ø10-ALU3	237,6	33,0

3.5 Anchorage

In this chapter, the necessary calculations of anchorage are performed according to EC2, 8.4 and the previous concrete standard NS-EN 3473, 12.8.5. The two standards are used based on different approaches of the ultimate bond stress, f_{bd}. Regulations according to the current Eurocode, 8.4. are only valid for reinforcement bars, which are either ribbed, mesh or prestressed tendons. The f_{bd} calculations of the beam with ordinary steel reinforcement were therefore performed based on regulations in the current Eurocode. On the other hand, the previous standard NS-EN 3473, takes into account the smooth surface of the reinforcement rods. Therefore the f_{bd} calculations of the beams with alloyed aluminium reinforcement were performed based on the previous standard.

Equation (3.10) below presents the formula of the required anchor length according to EC2. The final formula at the right hand side shows that this formula is only valid for reinforcement with circular cross section.

$$l_{b.rqd} \cdot \pi \cdot \phi \cdot f_{bd} = \frac{\pi \cdot \phi^2}{4} \cdot \sigma_{sd} \quad \Rightarrow \quad l_{b.rqd} = \frac{\phi \cdot \sigma_{sd}}{4 \cdot f_{bd}} \tag{3.10}$$

where

$l_{b.rqd}$	is the required anchoring length for each reinforcement rod, in mm
σ_{sd}	is the tensile strength of each reinforcement rod, in MPa
f_{bd}	is the ultimate bond stress, in MPa

However, the left hand side show how the formula includes the cross-sectional area and circumference of a circular reinforcement rod. By defining these with corresponding symbols A_r and O_r a universal formula develops, which means that reinforcement with different cross-sectional shapes can be used. Equation (3.11) below presents this universal formula.

$$l_{b.rqd} \cdot O_r \cdot f_{bd} = \frac{A_r}{n} \cdot \sigma_{sd} \quad \Rightarrow \quad l_{b.rqd} = \frac{A_r \cdot \sigma_{sd}}{n \cdot O_r \cdot f_{bd}} \tag{3.11}$$

where

A_r	is the total cross-sectional area of reinforcement, in mm^2
O_r	is the circumference of each reinforcement, in mm
n	is the number of reinforcement bars

According to calculations of required anchoring length and tensile stress, equation (3.11) was used for all reinforcement shapes. The maximal tensile stress were found by rearranging the equation on the right from equation (3.11) with respect to σ_{sd}. The required anchoring length is replaced by the anchoring length from the laboratory, $l_{bd,lab}$. Since the thesis presents reinforcement with circular and T-shaped cross sections, equation (3.11) were used for these calculations. Equation (3.10) could have been used for the reinforcement with circular cross section, but all of the calculations were done equally, using equation (3.11).

$$\sigma_{sd,max} = \frac{l_{bd,lab} \cdot O_r \cdot f_{bd} \cdot n}{A_r} \tag{3.12}$$

where

$l_{bd,lab}$ is the anchor length used in the laboratory studies, in mm

The tensile stress of each reinforcement bar is based on the failure load of each beam. Equation (3.13) shows how the tensile stress was calculated. P_{cr}, is the failure load calculated while V_{cr} is the total shear load in the reinforcement, which based on the 4-point bending test setup gives a load that is half of the failure load.

$$\sigma_{sd} = \frac{V_{cr}}{A_r \cdot n} \quad \Rightarrow \quad \sigma_{sd} = \frac{P_{cr}}{2 \cdot A_r \cdot n} \tag{3.13}$$

The formulas for the ultimate bond stress are different within the two standards. EC2, 8.4.2 presents the calculation of the ultimate bond stress, f_{bd}, and is given in equation (3.14).

$$f_{bd} = 2,25 \cdot \eta_1 \cdot \eta_2 \cdot f_{td} \tag{3.14}$$

where

η_1 = 1,0 based on that good conditions are contained

η_2 = 1,0 for $\phi \leq 32$ mm

f_{td} is the design value of the concrete tensile strength, in MPa

The previous standard NS-EN 3473, 12.8.5, presents the calculation of the ultimate bond stress, f_{bd}, and is given in equation (3.15). This equation contains the factor k_1, that considers the smooth surface of the reinforcement.

$$f_{bd} = k_1 \cdot f_{td} \tag{3.15}$$

where

k_1 = 0,9 for smooth surfaces, from Table 8 in NS-EN 3473

Equation (3.16) presents the formula for the final anchor length, l_{bd}, given in EC2, which is equal for all the reinforcement types. This formula contains different influencing factors that affect the design of a structure. In this laboratory experiment, these factors are not taken into account and the required anchor length is used instead.

$$l_{bd} = \alpha_1 \cdot \alpha_2 \cdot \alpha_3 \cdot \alpha_4 \cdot \alpha_5 \cdot l_{b,rqd} \tag{3.16}$$

where

α_{1-5} is influencing factors given in EC2, Table 8.2

In Table 3.7, the results from the anchorage calculations are shown, while the calculations are presented in Appendix C.

Table 3.7: Calculated anchorage

Identification	P_{cr} [kN]	f_{td} [MPa]	$l_{b,rqd}$ [mm]	$\sigma_{sd,max}$ [MPa]	$l_{bd,lab}$ [mm]	σ_{sd} [MPa]
B2-2ø12-STEEL	60,7	2,9	62	54,4	25	134,2
B2-3T-ALU1 B2-3T-ALU2	62,7	2,9	53	31,8	25	67,0
B1-6ø10-ALU1 B1-6ø10-ALU2 B1-6ø10-ALU3	66,1	2,9	67	26,1	25	70,1

Table 3.7 above shows poor anchoring where required anchor lengths are longer than what's actually used in the laboratory studies. Similarly, also the tensile stress that occurs from beam testing is larger than the maximal tensile stress requirement.

There were several possibilities of improving the anchoring e.g. transversal rods, adjustments of beam design, adjustments of distance between supports or bending of rods at the ends. However, based on restrictions of beam design discussed earlier in this chapter (chapter 3.1), it was decided to use transversal rods as anchoring.

3.6 Compression zone height

The size of the compression zone height affects the size of the failure load at bending moment failure. At an increasing load the compression zone height decreases. The relation between the loading and the compression zone height are presented here. The calculations are shown in Appendix D.

This relation can be found when the stress and strain distribution of the cross section is known. EC2, 3.1.7(1) gives the stress and strain relation in compression, which can be used for capacity calculations in the ultimate limit state, see Figure 3.8a. This relation can be simplified after EC2, 3.1.7(2) if it corresponds to or is more conservative than after EC2, 3.1.7(1), e.g. bi-linear relation as showed in Figure 3.8b.

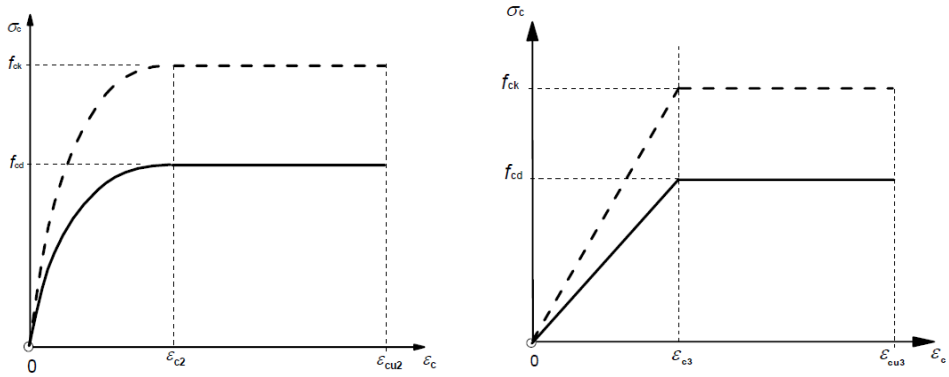

(a) Parabola-rectangle relation **(b)** Bi-linear relation

Figure 3.8: Stress and strain relations for the design of cross sections. (Standard, 1992)

For this task, it is assumed that the bi-linear relation is good enough to determine the relation between the loading and the compression zone height. This relation is based on a bi-linear stress block, simplified from the actual stress block which is parabolic.

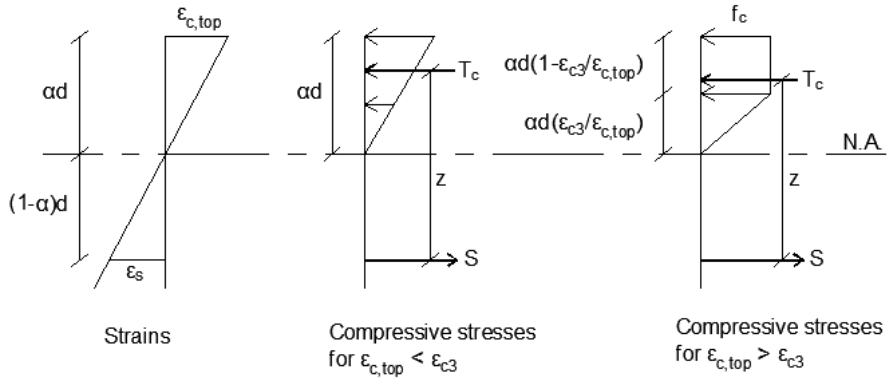

Figure 3.9: Calculation model for the relation between the loading and the compression zone height

Figure 3.9 shows the calculation model that is used to find the relation between the loading and the compression zone height. This relation is found by using the Solver Add-in in Excel. As the figure shows, the compressive stress distribution changes when the the top strain, $\varepsilon_{c,top}$, exceeds ε_{c3} (=1,75‰). The compressive resultant will therefore have two different equations, depending on the size of $\varepsilon_{c,top}$. For $\varepsilon_{c,top} < \varepsilon_{c3}$, the compressive stress distribution is linear, which gives the following equation for the compressive resultant:

$$T_c = b \cdot \frac{f_c}{\varepsilon_{c3}} \cdot \varepsilon_{c,top} \cdot \alpha d \cdot 0,5 \tag{3.17}$$

For $\varepsilon_{c,top} > \varepsilon_{c3}$, the compressive stress distribution is bi-linear, and equation (3.18) is used for the compressive resultant for these values.

$$T_c = b \cdot \frac{f_c}{\varepsilon_{c3}} \cdot \varepsilon_{c3} \cdot \alpha d \frac{\varepsilon_{c3}}{\varepsilon_{c,top}} \cdot 0,5 + f_c \cdot b \cdot \alpha d(1 - \frac{\varepsilon_{c3}}{\varepsilon_{c,top}}) \tag{3.18}$$

The tensile resultant is given from the following formula when the cross section is under-reinforced:

$$S = f_r \cdot A_r \tag{3.19}$$

The top strain $\varepsilon_{c,top}$ for a given compression zone height is solved with the Solver Add-in, by putting the compressive resultant and the tensile resultant equal to each other.

$$M_{Ed} = T_c \cdot z = S \cdot z \tag{3.20}$$

After the top strain is found, the internal lever arm, z, is found by geometry from Figure 3.9. Further, the loading can be solved from the occurring moment, and the relation between the loading and the compression zone height can then be found.

$$P = \frac{2 \cdot M_{Ed}}{L_s} = \frac{2 \cdot T_c \cdot z}{L_s} = \frac{2 \cdot S \cdot z}{L_s} \tag{3.21}$$

The relation between the loading and the compression zone height is shown in Figure 3.10 - Figure 3.12. The graphs show that the compression zone height is constant in stage I, until the crack load occurs. The crack load leads to a decrease in the compression zone height, from stage I to stage II. When the loading exceeds the crack load, the compression zone height is again constant, until either the reinforcement starts to yield or the concrete reaches its maximum stress. Next, the compression zone height decreases until the failure load (at moment failure).

The values for the different compression zone heights (αd, $(\alpha d)_I$ and (αd_{II})) and crack loads shown in Figure 3.10 - Figure 3.12 are taken from Appendix B. In the Solver Add-in in Excel, these values doesn't give quite correct strains. In addition, the Solver Add-in calculates the loading based on equation (3.21), while equation (3.4) is used in the calculations in Appendix B. The failure load is therefore slightly different. The difference is small, and will not affect the relation between the loading and the compression zone height significantly.

αd [mm]	Load [kN]
20,7	69,4
31,1	68,2
31,1	14,4
76,6	14,4
76,6	0

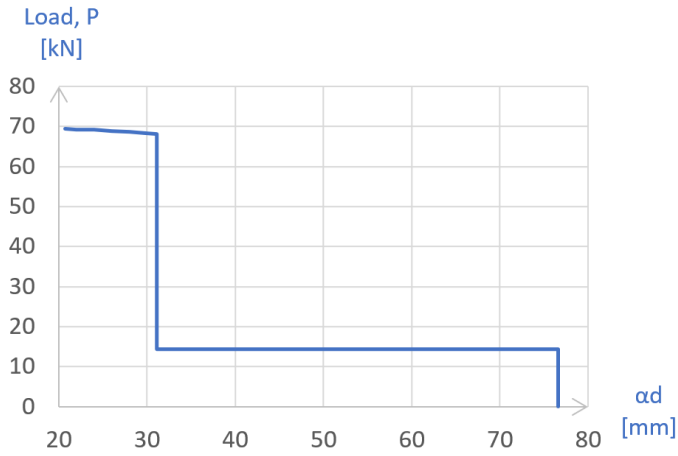

Figure 3.10: Load - compression zone height relation for beam B2-2ø12-STEEL

Figure 3.10 shows that the compression zone height decreases from 76,6 mm to 31,1 mm when the crack load of 14,4 kN occurs. From here, the compression zone height is constant until the reinforcement starts to yield at 68,2 kN. Next, the compression zone height decreases until the failure at 69,4 kN.

αd [mm]	Load [kN]
19,5	65,5
26,5	64,9
26,5	14,1
76,0	14,1
76,0	0

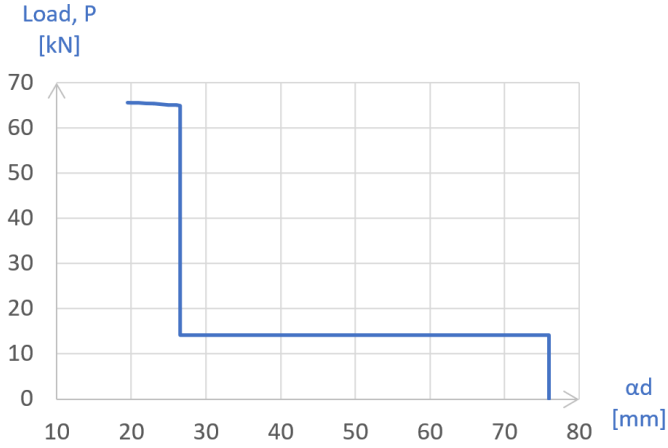

Figure 3.11: Load - compression zone height relation for beams B2-3T-ALU1 and B2-3T-ALU2

Figure 3.11 shows that the compression zone height decreases from 76,0 mm to 26,5 mm when the crack load of 14,1 kN occurs. From here, the compression

zone height is constant until the reinforcement starts to yield at 64,9 kN. Next, the compression zone height decreases until the failure at 65,5 kN.

αd [mm]	Load [kN]
19,6	66,0
27,2	65,2
27,2	14,2
76,2	14,2
76,2	0

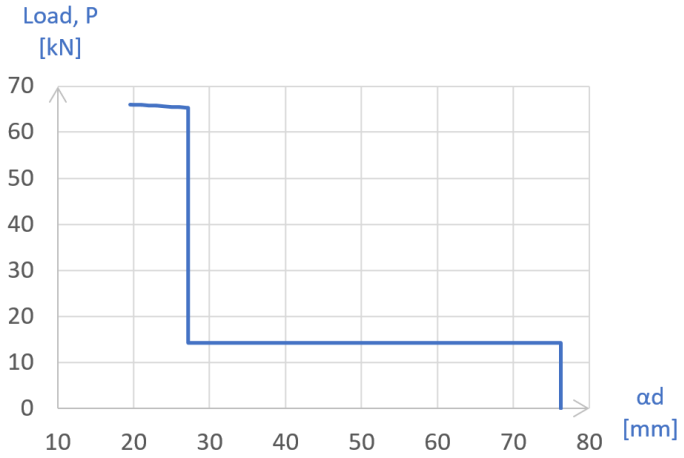

Figure 3.12: Load - compression zone height relation for beams B1-6ø10-ALU1, B1-6ø10-ALU2 and B1-6ø10-ALU3

Figure 3.12 shows that the compression zone height decreases from 76,2 mm to 27,2 mm when the crack load of 14,2 kN occurs. From here, the compression zone height is constant until the reinforcement starts to yield at 65,2 kN. Next, the compression zone height decreases until the failure at 66,0 kN.

3.7 Deflection

Control calculations of a construction's displacement is usual, and necessary. The computational deflection of the beams are studied. According to EC2, the deformation of a structure or a structural element shall not affect the intended usage or appearance.

This chapter covers the deflection calculations caused by the bending deformation. The calculation of the bending stiffness, EI, is divided into two stages;

- Stage I: Uncracked concrete cross section, linear properties
- Stage II: Cracked concrete cross section, linear properties

Stage I: Uncracked

When the loads are kept relatively small the temporary tension stresses that occur in the concrete will be less than the tensile strength, and the cross section will be described as uncracked. For the uncracked cross section, the neutral axis (N.A.) would be equal to the centre of gravity (C.G.). (Sørensen, 2013)

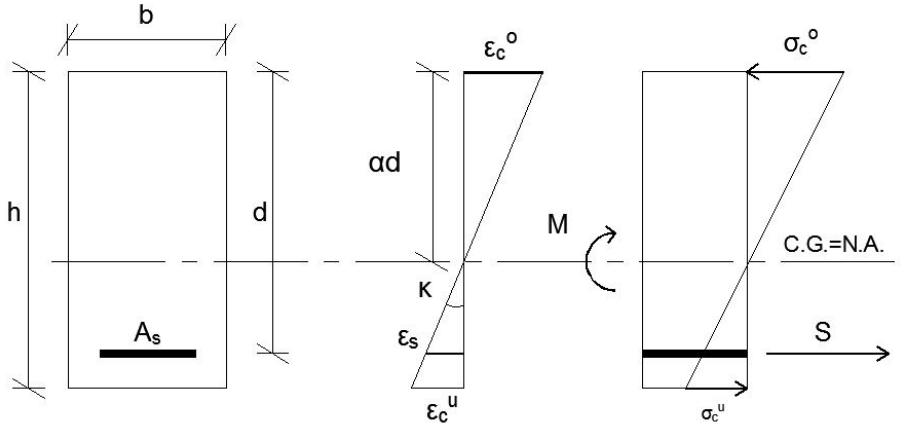

Figure 3.13: Unracked cross section

The calculations of the bending stiffness and the placement of the axis are presented in the formulas below:

$$\alpha d = \frac{A_c \cdot 0,5h + \eta A_r d}{A_c + \eta A_r} \tag{3.22}$$

where

$\eta = \dfrac{E_r}{E_c}$ is the material stiffness relation

$$(EI)_I = E_c I_{c1} + E_r I_{r1} \tag{3.23}$$

where

$I_{r1} = A_r(d - \alpha d)^2$ is the contribution from the reinforcement to the moment of inertia for the uncracked cross section, in mm^4

$I_{c1} = \dfrac{bh^3}{12} + bh \cdot \left(\alpha d - \dfrac{h}{2}\right)^2$ is the contribution from the concrete to the moment of inertia for the uncracked cross section, in mm^4

Stage II: Cracked

The cross section cracks in the tension zone when the crack load is exceeded. When the crack load increases, the deflection instantaneous moves from Stage I to Stage II, but in reality this happens more gradually. This may be taken into account for structural elements that are mainly exposed to bending, and is given in EC2, 7.4.3(3). However, this is not accounted for in this study.

In stage I, the compression zone height doesn't depend on the size of the bending moment, which means that the position of the neutral axis remains constant.

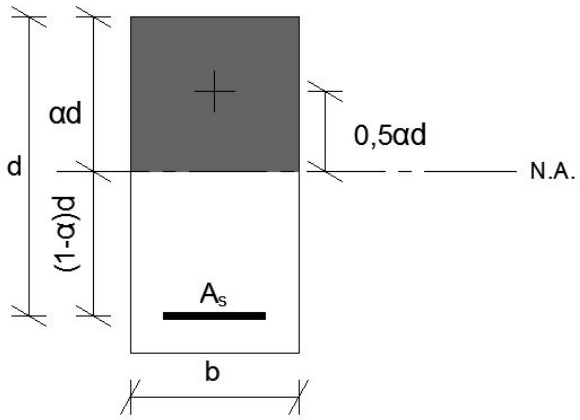

Figure 3.14: Cracked cross section

The compression zone height and bending stiffness is calculated as follows:

$$\alpha = \sqrt{(\eta\rho_l)^2 + 2\eta\rho_l} - \eta\rho_l \tag{3.24}$$

$$(EI)_{II} = E_c Ic \tag{3.25}$$

where

$I_c = \frac{1}{2} \cdot \alpha^2 \left(1 - \frac{\alpha}{3}\right) bd^3$ is the contribution form the concrete to the moment of inertia for the cracked cross section, in mm^4

Crack load

The cross section from Figure 3.13 is assumed to crack when the tensile stress in the lower edge exceeds the concrete's tensile strength. The crack moment and crack load which indicates the change from uncracked to cracked cross section, can then be found.

The same figure gives the following formula for the curvature:

$$\kappa = \frac{1}{r} = \frac{M}{(EI)_I} = \frac{\varepsilon_c^u}{h - \alpha d} \tag{3.26}$$

where

ε_c^u is the concrete strain at the bottom of the cross section

The bending stiffness from equation (3.23) can be rewritten using the material stiffness relation:

$$(EI)_I = E_c \cdot \left(I_{c1} + \frac{E_r}{E_c} \cdot I_{r1} \right) = E_c \cdot (I_{c1} + \eta I_{r1}) \tag{3.27}$$

Equation (3.27) inserted in equation (3.26) gives:

$$M = \frac{\varepsilon_c^u \cdot E_c \cdot (I_{c1} + \eta I_{r1})}{h - \alpha d} = \frac{\sigma_c^u (I_{c1} + \eta I_{r1})}{h - \alpha d}$$

where

σ_c^u is the concrete stress at the bottom of the cross section, in MPa

Inserting of the crack criterion $\sigma_c^u = f_{ctm}$ gives the crack-moment M_{crack}:

$$M_{crack} = \frac{I_{c1} + \eta I_{r1}}{h - \alpha d} \cdot f_{ctm} \tag{3.28}$$

Finally, the crack load P_{crack} can be found from the following formula, given for the statically system with two point loads:

$$P_{crack} = \frac{2 \cdot M_{crack}}{L_s} \tag{3.29}$$

Table 3.8 shows the calculated crack loads for the beams.

Table 3.8: Crack-loads

Identification	P_{crack} [kN]
2ø12-STEEL	14,4
B2-3T-ALU1 B2-3T-ALU2	14,1
B1-6ø10-ALU1 B1-6ø10-ALU2 B1-6ø10-ALU3	14,2

Calculated deflections

The deflection of the beams are calculated by the following formula, given for the 4-point bending test:

$$\delta = \frac{\frac{P}{2}L_s}{24EI}(3L^2 - 4L_s^2) \tag{3.30}$$

As mentioned, the bending stiffness varies for uncracked and cracked cross sections. The deflections that are calculated for loads smaller than the crack load will therefore use the bending stiffness from equation (3.23), while the deflections for loads greater than the crack load will use the bending stiffness from equation (3.25).

The loads and deflections for all beams are plotted in Figure 3.15. The curves start off pretty steep in stage I, i.e. less deflection per load unit, before they get a break in the curve. This is when the first crack appears and the beams go from stage I to stage II. In stage II, the deflections are linear and a little less steep than in stage I.

Stage II continues until the failure load. The deflection calculations are only valid in the serviceability limit state (SLS), and not in the ultimate limit state (ULS). The deflection at failure is therefore not correctly calculated. However, the distinction between the SLS and ULS is unknown, so the graphs show the deflection from zero loading and up to the failure load.

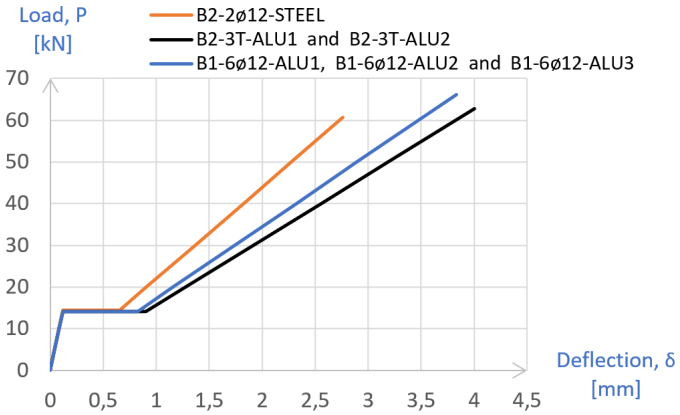

Figure 3.15: Load - deflection curves

Table 3.9 shows the values of both loading and deflection for the different stages for each beam.

Table 3.9: Calculated load-deflection values

Identification	P_{crack} [kN]	$\delta_{crack,I}$ [mm]	$\delta_{crack,II}$ [mm]	P_{cr} [kN]	δ_{cr} [mm]
B2-2ø12-STEEL	14,4	0,12	0,65	60,7	2,76
B2-3T-ALU1 B2-3T-ALU2	14,1	0,12	0,90	62,7	4,01
B1-6ø10-ALU1 B1-6ø10-ALU2 B1-6ø10-ALU3	14,2	0,12	0,82	66,1	3,83

Figure 3.15 and Table 3.9 shows that all of the beams have a deflection of 0,12 mm in the end of stage I. From here, the loading and deflection varies for all of the beams.

The steel beam (B2-2ø12-STEEL) cracks at a loading of 14,4 kN, which leads to an increase of the deflection from 0,12 mm to 0,65 mm. When the beam reaches

stage II, the deflection varies linearly until the failure load of 60,7 kN occurs, giving a final deflection of 2,76 mm.

The aluminium beams with T-shaped reinforcement (B2-3T-ALU1 and B2-3T-ALU2) crack at a loading of 14,1 kN, which leads to an increase of the deflection from 0,12 mm to 0,90 mm. When the beam reaches stage II, the deflection varies linearly until the failure load of 62,7 kN occurs, giving a final deflection of 4,01 mm.

The aluminium beams with circular reinforcement (B1-6ø10-ALU1, B1-6ø10-ALU2, B1-6ø10-ALU3) crack at a loading of 14,2 kN, which leads to an increase of the deflection from 0,12 mm to 0,82 mm. When the beam reaches stage II, the deflection varies linearly until the failure load of 66,1 kN occurs, giving a final deflection of 3,83 mm.

3.8 Crack spacing

Cracks usually appear in reinforced concrete structures affected by bending, shear, torsion or tension as a result from either restrained or directly loaded structures or imposed deformations (external factors). Development of cracks also arise from internal factors e.g. due to volume instability like plastic shrinkage or expansion from chemical reactions within the hardening concrete.

Concrete cracks are limited such that the proposed function or durability of the structure is unaltered or it gives an unacceptable appearance.

EC2, 7.3.4(3) gives the maximum final crack spacing $S_{r,max}$, depending on the spacing of the reinforcement within the tension zone. In situations where the spacing $\leq 5(c + \frac{\phi}{2})$, the maximum final crack spacing can be calculated from equation (3.31).

$$S_{r,max} = k_3 c + k_1 k_2 k_4 \frac{\phi}{\rho_{p,eff}} \tag{3.31}$$

where

ϕ is the bar diameter, in mm
c is the cover to the longitudinal reinforcement, in mm
k_1 is a coefficient which takes account of the bond properties of the bonded reinforcement:
= 0,8 for high bond bars
= 1,6 for bars with an effectively surface
k_2 is a coefficient which takes account of the distribution strain:
= 0,5 for bending

$$\rho_{p,eff} = \frac{A_r}{A_{c,eff}} = \frac{A_r}{b \cdot h_{c,eff}} = \frac{A_r}{b \cdot min\{2, 5(h - \alpha d), \frac{h-\alpha d}{3}, \frac{h}{2}\}}$$

NA.7.3.4(3) gives k_3 and k_4 as:

k_3 = 3,4

k_4 = 0,425

If the spacing of the reinforcement within the tension zone $> 5(c + \frac{\phi}{2})$, the maximum final crack can be calculated from equation (3.32).

$$S_{r,max} = 1,3(h - \alpha d) \tag{3.32}$$

The maximum final crack spacing is only calculated for the beams with circular reinforcement shapes because the factor ϕ is included in the calculations, and is unknown for the T-profiles. The results from the calculations are shown in Table 3.10.

Table 3.10: Maximum final crack spacing

Identification	Reinforcement spacing [mm]	$5(c + \frac{\phi}{2})$ [mm]	Equation number	$S_{r,max}$ [mm]
B2-2ø12-STEEL	176	155	(3.32)	168
B1-6ø10-ALU1 B1-6ø10-ALU2 B1-6ø10-ALU3	28	150	(3.31)	124

The full calculation can be found in Appendix E.

Chapter 4

Experimental program

The experimental program is presented in this chapter and includes the practical information about how the task has been solved. The chapter is divided into three parts. In the first section, the beam production is described. The next section presents the description of the executed tests for the material properties, while the beam testing is presented in the last section.

4.1 Production

This chapter contains the production of all the small specimens and beams, from raw material, until the products are wrapped and stored away for hardening.

4.1.1 Proportioning

Proportioning of concrete means selecting materials and putting them together to obtain desirable properties for the fresh and hardened concrete. In our project, SINTEF calculated the necessary quantity of each material and put together a prescription. It is necessary to perform a test compound of the prescription to ensure reliable results. SINTEF performed this test compound where several procedure tests of fresh and hardened concrete were executed, to evaluate the given prescription.

Prescription

The materials used in the concrete mix, provided by NTNU and SINTEF, are presented as a prescription in Table 4.1. The total mixing form and the grading curves can be found in Appendix A.

Table 4.1: Concrete prescription

Materials	**Quantity** [kg/m^3]
Norcem Anlegg	143,9
Calcined clay, A-5011	175,9
Free water	223,9
Absorbed water	5,7
0-8mm Årdal 08-16	970,9
8-16mm Årdal 02-18	702,4
Sika-Viscocrete RMC-315 A-4871	1,9
Soluble magnesium salt	19,2

The cement is the adhesive part of the concrete. The choice of cement depend on several factors; the end-use of the concrete, hardening conditions and the environmental affect. Norcem Anlegg cement was used, which had good casting and durability properties. This cement is known to give low strength at an early stage, and high strength for the final condition. As mentioned earlier, calcined clay replaces parts of the cement to reduce the pH value in the concrete. The aggregate was a composition of different grain sizes, from 0-8mm and 8-16mm. To obtain the right w/c-ratio, the moisture of the aggregate was measured for both batched. The moisture was found by measuring the moisture content of a sample before and after drying it. Admixture liquids can be added to the concrete to change its properties for both fresh and hardened condition. In our case it was the superplasticizer Sika-Viscocrete, which is used to make the concrete more workable without affecting the w/c-ratio. The purpose of adding the soluble magnesium salt in the water was to lower the initial pH-value of the fresh mix by precipitating hydroxide ions as brucite. Then, the remaining alkalies in the pore water was neutral alkali salt instead of alkali hydroxide, which gave the high pH-value.

Working procedure

The mix of the concrete was done in a specific order and was mixed in a specific amount of time. First, the aggregate was added to the machine, then the cement and the calcined clay. This was mixed for one minute. The soluble magnesium

salt was added to the water before the water was added to the mix, and mixed for two minutes. Next, the machine was stopped for two minutes for the mix to rest. Then the machine was started again, and the superplasticizer was added to the mix and mixed until the consistency was as desired. For this purpose, this is when the concrete has a slump of around 15 cm, verified by performing a slump test. The amount of Sika-Viscocrete added to the concrete to obtain the desired consistency was less than the amount given in the mixing form. Respictively, 0,205 kg for batch 1 and 0,171 kg for batch 2. After the desired consistency was obtained, the concrete was distributed into the beam and cylinder formwork. One mix was enough for 3 beams and 12 cylinders.

4.1.2 Small specimen

Cylinders with dimensions ø100x200 mm were produced for testing of the hardened concrete properties. 12 cylinders for each concrete mix, in total 24 cylinders were produced. The dimension of the cylinders is a standard dimension, and the formworks were therefore already produced. The formwork only had to be oiled before pouring the concrete into them.

The cylinders were first filled halfway with the concrete mix, before it was compressed by stamping a steel rod and vibrated gently by hammering with a hammer. After the next layer was poured into the cylinders, the compression process was repeated. At the end, the top was smoothed with a metal ruler to make even top surfaces. At last, the cylinders were covered with plastic to prevent evaporation.

Figure 4.1: Cylinders from one of the concrete mixes

4.1.3 Beams

The execution of the progression, from empty formworks to storage of reinforced beams, are explained below.

Formwork

The formworks were made out of smooth laminated timber. There were a total of three forms, where each form was divided into two parts with inner dimensions equal to the beam dimensions, resulting in two beams per form.

Figure 4.2: Beam formwork

The beam formwork was also oiled before casting, to make it easier to demould the timber from the concrete.

Reinforcement bars

The aluminium rebars were produced through an extrusion process. This is a process used to create different objects like pipes and profiles. The idea was that the rebars were going to be manufactured by use of a screw extrusion process, patented by Hydro, with usage of scrap materials of the aluminium production. The screw extruder tool wasn't ready for use in time, and bolt extrusion was used instead.

The extrusion process was carried out under the management of Hydro with help from SINTEF and NTNU, at SINTEF's laboratory at "Verkstedteknisk". The Al-5Mg bolts were heated to 430 °C and pushed through a die of the desired cross sections. After the extrusion process, the rods were cooled and cured before they were cut into desired lengths.

To make sure that no hydrogen gas would be formed in contact between the aluminium rods and the concrete, the rods were dipped in an inhibitor solution prior to use for around 16 hours to form an oxide layer on the surface. This oxide layer lead to binding the transversal rods for anchoring instead of welding, as welding could cause development of toxic gases. In Figure 4.3, the manual binding of the rebars are shown.

Figure 4.3: Binding of the aluminium reinforcement

The rebars should have been welded before they were placed in the inhibitor solution for welding to be carried out. The steel reinforcement on the other hand was still welded as planned, where four transversal steel rods were welded onto the reinforcement in each end. The available amount of aluminium alloy gave a total of 38 transversal rods, which resulted in four transversal rods in each end for four of the beams, and three transversal rods in each end for one of the beams (beam B1-6ø10-ALU3).

Beam casting

The reinforcement was held in place before the concrete was poured into the formwork, enough to fill it halfway up. Square trowels were used to distribute the concrete in the formwork and stamp around the reinforcement and along the formwork walls. A hammer was used to hit the formwork on the outside to vibrate the concrete. All to ensure contact between the concrete and the reinforcement, and that the concrete was well distributed. Next, concrete was filled all the way up in the formwork, and further stamping was carried out. The concrete at the top of the beams were then leveled out, and two lifting points were placed at 30 cm from each edge. The beams were then covered with plastic to harden without evaporation for

two days, before taking them out of the formwork and storing them to harden until testing.

4.1.4 Storage and concrete hardening process

The beams and cylinders were demoulded and placed in humid areas for storage, two days after the casting day. This was because the concrete mix including calcined clay had a lower strength development at the early stage of the hardening process, compared to ordinary concrete. Therefore, it was decided to add an extra day of hardening before demoulding them. After demoulding, the beams were marked with correct names as given in Table 3.2, and the cylinders were marked from 1 to 12 with the batch number in front (e.g 1-1 to 1-12 for batch 1). The specimens were also marked with the production date.

Each beam had a total mass of approximately 100 kg, and a crane was therefore used to move them. The beams were stored together on a pallet, covered in moisture burlap sacks and wrapped up in plastic to avoid fluid loss. The same procedure was carried out for the cylinders. Before wrapping up the cylinders, they were all weighted both in dry and wet climate.

Fluid loss appears when the concrete's w/c-ratio is less than 0,4. The prescription used in this project had a w/c-ratio of 0,7 and it was therefore unlikely to dry out. (SNL, 2018)

4.2 Material property testing

Different tests are performed to verify the quality and strength of the concrete. In this chapter, the executed tests for the material properties are presented. In order to separate the tests they are divided into two main groups, fresh and hardened concrete properties.

Standards that concern testing of concrete were used, hence NS-EN 12350 *testing of fresh concrete* and NS-EN 12390 *testing of hardened concrete*.

Testing of fresh concrete, NS-EN 12350:

Part 2: Slump test
Part 6: Density
Part 7: Air content

Testing of hardened concrete, NS-EN 12390:

Part 3: Compressive strength of test of specimens
Part 6: Tensile splitting strength of test specimens
Part 7: Density of hardened concrete
Part 13: Determination of secant modulus of elasticity in compression

4.2.1 Fresh concrete properties

The fresh concrete tests give an indicator of the workability of the concrete, which affects its strength and durability. The aim is to obtain the concrete as compact and homogeneous as possible, and provide dense surfaces to avoid unnecessary treatment later on.

Workability is a word of wide range in conjunction with fresh concrete. In this case, the word describes the mobility of the concrete to spread itself, ability to be compressed and stability of composition, e.g. when it is exposed to falls or other processing phases. The fresh concrete tests are therefore also verifying the quality of the concrete. (Gjerp et al., 2014)

(a) Slump test

(b) Air content test

Figure 4.4: Fresh concrete testing

Slump test

The slump test is a method which is used to determine the consistence of the fresh concrete. Equipment used was a steel cone, steel stamp and plane base surface. The cone had a minimum and maximum diameter of respectively 100 and 200 mm, and a height of 300 mm. The steel rod had a circular cross section with rounded ends, a diameter of 16 mm and a length of about 600 mm.

The procedure executed was performed in accordance to NS-EN 12350-2. The test procedure started by placing the steel cone on the plane base surface, then it was filled with concrete divided into three layers. In between each layer, the rod was stamped 25 times to make the layers equally compact. After the cone was filled and stamped, the surface was straightened before the container was lifted slowly upwards. The concrete flowed out on the base, and when the concrete flow was stabilized, the measured distance between the initial height and the remaining height of the concrete cone gave the slump value.

Density test

The density test tells how compact the fresh concrete is, and the procedure used for this test is described in NS-EN 12350-6. Equipment used for this test was a metal container, a plate in glass, a scale with accuracy of 0,01 kg and other smaller equipment for preparing and moving of the concrete mass. The concrete was compressed into a rigid and watertight container with known volume and weight. Then, the container was weighted. The density of the fresh concrete was found by equation (4.1), where the mass of the container was subtracted from the total mass of the concrete filled container, and then the mass was divided by the containers volume.

$$\rho_c = \frac{m_2 - m_1}{V_{ol}} \tag{4.1}$$

where

ρ_c concrete density, in kg/m^3

m_1 mass of container, in kg

m_2 mass of container filled with compacted concrete, in kg

V_{ol} volume of the container, in m^3

Air Content

Measurement of the air content of compacted fresh concrete was executed by using the water column method, described in NS-EN 12350-7. The procedure started with injecting water into a sealed container at a predetermined height above a sample of compacted concrete, with known volume. Next, a predetermined air pressure was applied above the water. By observing the lowered value of the water column, the air content of the concrete was measured.

The concrete on top of the container in this test couldn't be used further, due to the injected water which damages the prescription, so the top layer had to be removed.

4.2.2 Hardened concrete properties

In the design of concrete structures, it is the mechanical properties of the hardened concrete that are of greatest interest. The most important property in the hardened condition is the strength, especially the compressive strength. The hardened concrete density is also of great interest as this is the most important factor for the concrete durability. The properties of the hardened concrete are found by testing the smaller specimens.

The compressive strength, tensile splitting strength, density of hardened concrete and Young's Modulus where the different tests that were executed for the small specimens. In total 16 cylinders were tested, where the remaining eight cylinders were kept as a backup. The density of hardened concrete was measured for all 16 cylinders. For the remaining tests, the cylinders were distributed on different tests. After 28 days of hardening, 12 cylinders were tested, six from each batch. In order to obtain the most accurate results, the strength should be based on the average of at least two test specimens. Two cylinders were therefore used for each test. It was necessary to test the compressive strength at the beam testing day as well. Therefore, two cylinders from each concrete mix were tested at this point.

Compressive strength

The compressive strength test is a measure of how much load the hardened concrete can withstand per unit area before it fails. For this test, the procedure in NS-EN 12390-3 was followed. The specimens used in this test were cylinders with a diameter of 100 mm and a height of 200 mm. Cubes could also have been used to find the compressive strength, but testing of cylinders were beneficial in this case as the result could be used directly as an input for the Young's Modulus

test, described later in this chapter. The cylinders were grounded on the top and the bottom to ensure parallel surfaces.

Once the specimens were prepared and ready for testing, they were centered with respect to the lower plate. The load was applied at a constant rate within the range 0,6 $\pm$ 0,2 MPa/s. This initial load did not exceed approximately 30 % of the failure load. Next, load was applied to the specimen without shock and increased continuously at the rate $\pm$ 10 % until failure.

There are certain types of failure for the specimens that are satisfactory and certain types that are unsatisfactory. The satisfactory failure types for cylinders are shown in Figure 4.5.

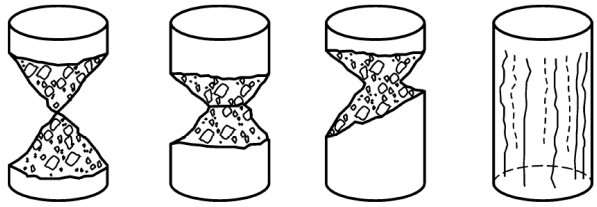

Figure 4.5: Satisfactory failure of cylinder specimens. (Standard, 2009)

The compressive strength is given by the following equation:

$$f_c = \frac{F}{A_c} \tag{4.2}$$

where

f_c is the compressive strength, in MPa

F is the maximum load at failure, in N

A_c is the cross-sectional area of the specimen on which the compressive force acts, in mm^2

Tensile splitting strength

The test for the tensile splitting strength was performed after NS EN-12930-6. In the tensile splitting strength test, the cylindrical specimen was tilted as shown in Figure 4.6a, and a compressive force was applied to a narrow region along its

length. The loading results in a tensile force orthogonal to the loading direction, which causes the specimen to split and fail in tension.

The specimen was placed in the loading machine between two parallel plates, and wooden pieces were placed between the plates and the specimen to ensure an even load distribution. The specimen was then loaded at a constant rate of stress at 0,05 MPa/s. The initial load did not exceed approximately 20 % of the failure load. Next, load was applied to the specimen without shock and increased continuously at the same rate until failure.

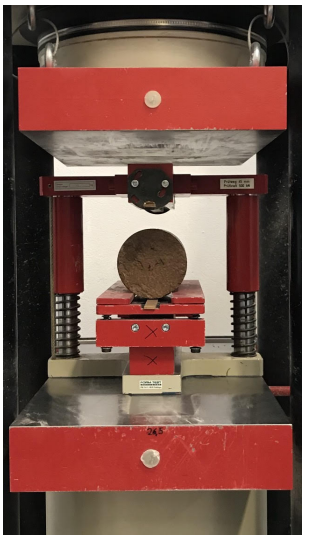

(a) Test setup

(b) Result of one specimen

Figure 4.6: Testing of the tensile splitting strength

The tensile splitting strength is determined by the equation:

$$f_{ct} = \frac{2 \cdot F}{\pi \cdot L \cdot d} \tag{4.3}$$

where

f_{ct} is the tensile splitting strength, in MPa

F is the maximum load, in N

L is the length of the line of contact of the specimen, in mm

d is the diameter of the specimen, in mm

Density of hardened concrete

The density of hardened concrete was determined based on the procedure in NS-EN 12390-7. For this test, the mass and volume had to be determined first. The specimen's mass in air m_a, was found by placing the specimen on a scale and recording the mass. The specimen's volume was determined by water displacement. The mass of the specimen in water m_w, was found by hanging a stirrup from a scale such that it was immersed in a water tank without touching the bottom. The scale was reset to zero and the specimen was placed in the stirrup. The mass m_w, of the immersed specimen was then recorded. The volume of the specimen was calculated using the following equation:

$$V_{ol} = \frac{m_a - m_w}{\rho_w} \tag{4.4}$$

where

V_{ol} is the volume of the specimen, in m^3

m_a is the mass of the specimen in air, in kg

m_w is the mass of the immersed specimen, in kg

ρ_w is the density of the water at 20 °C, taken as 998 kg/m^3

The density of the specimen was calculated by using the determined values for mass and volume, inserted into the equation:

$$\rho_c = \frac{m_a}{V_{ol}} \tag{4.5}$$

where

ρ_c is the density, in kg/m^3

Young's Modulus test

This test determines the secant modulus of elasticity in compression of hardened cylindrical test specimens, $E_{c,s}$, and was performed in conjunction with NS-EN 12390-13. Four cylindrical specimens, two from each batch, were exposed to axial pressure in three loading cycles with instruments measuring and recording the strain. The test specimen was placed centrically into a compression machine, with measuring instruments attached axially to it. A preload stress σ_p of 0,5 MPa was applied. After the preload stress stabilized, the strain measure instruments were set to zero.

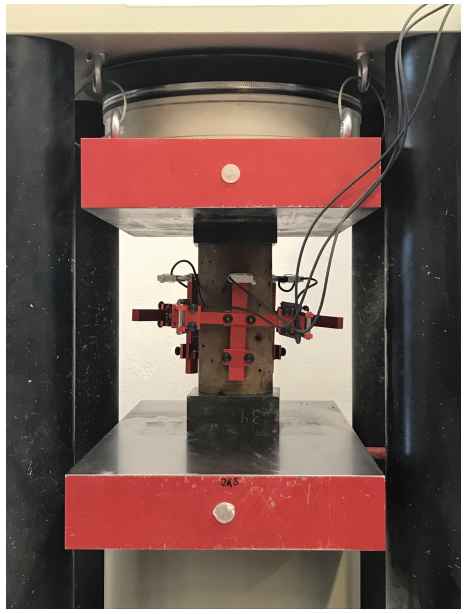

Figure 4.7: Testing of Young's Modulus

In the first cycle, the specimen was exposed to an increasing stress from the preload stress until the upper stress σ_a, with a rate of 0,6 MPa/s. For this first cycle, the upper stress level was 45 % of the expected fracture stress measured in the compression test. The corresponding stress values, 24 MPa from the first batch and 23 MPa for the second batch, are both input values for the test machine. These values are not based on the failure load and the specimen's surface area, but were given from the testing machine. Hence, they don't correspond to the values in

Table 6.3. When the increasing stress reached the upper stress, it was held for 60 seconds before it was reduced with the same rate down to the preload stress and held for another new 60 seconds.

The same procedure was carried out for the second and third cycle, where the upper stress value was reduced to 33,3 % of the expected fracture stress for both cycles. After the third cycle was completed, the stress was held for 60 seconds at the preload stress before the specimen was compressed until failure. The measuring instruments were removed after the last hold in order to prevent them from permanent damage.

The test routine executed was not done exactly as described in the Eurocode, because some modifications were done based on SINTEF Byggforsk's own specifications.

4.3 Beam testing

The beam testing was executed at NTNU's large test hall. In total 6 beams were tested, and the testing for each batch took place over two days. The beam testing was originally planned to start the 17.04.18 (week 16) and proceed for three days, but the date was postponed until 08.05.18 (week 19) based on absent personnel at the laboratory. At the first test date, 08.05.18, two beams from batch 2, one with steel reinforcement and one with T-shaped aluminium reinforcement were tested. The following day, 09.05.18, the last beam from batch 2 was tested, also with T-shaped aluminium reinforcement. Beams from batch 1 with circular aluminium reinforcement were tested the upcoming week, two beams at the 14.05.18 and the final beam on the 15.05.18.

The beams were exposed to a 4-point bending test, and were loaded in several load steps until failure. Deflection, strain, crack development, failure load and failure type were the analyzed subjects for each beam.

Test setup

The test rig used for the beam testing was assembled by several different components. The loading cylinder was called Instron 8800, and had a maximum capacity

of 312 kN. The test setup was supposed to be a 4-point bending test as shown in Figure 4.8.

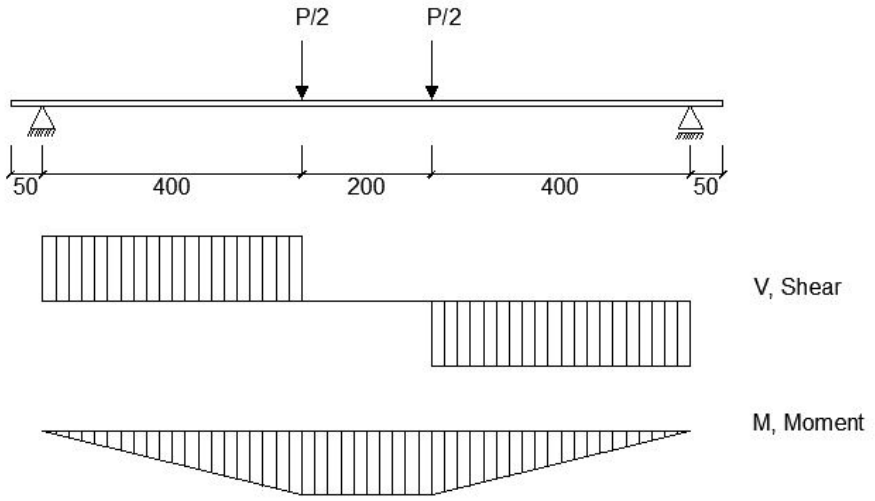

Figure 4.8: 4-point bending test

To obtain a 4-point bending test, the test rig was set up as in Figure 4.9. The load distribution beam divides the load from the loading cylinder into two separate point loads on the top of the beam. The remaining point loads are applied through the supports at the bottom of the beam. Both the beam and the load distribution beam had roller and pinned bearings, giving a simply supported system.

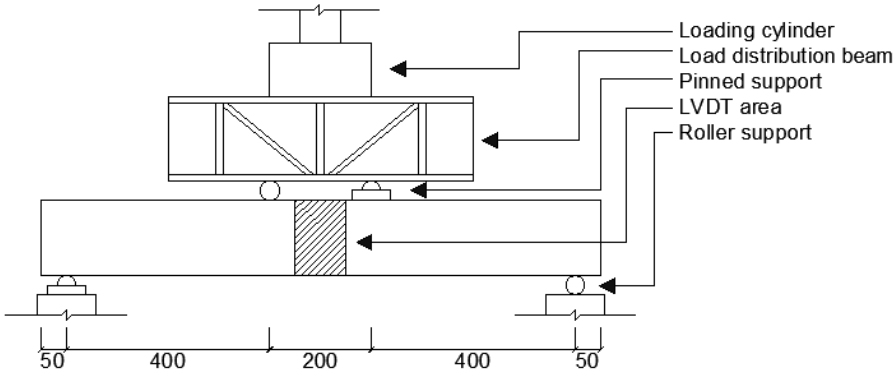

Figure 4.9: Beam test setup

For this setup, the load was calculated to be applied by a constant deflection of 0,3

mm/min in several load steps of 10 kN. This feeding rate was determined based on calculated deflections and desired loading time for each step (1-2 min). The load was applied until failure, defined as the time when the loading cylinder started to unload.

LVDT

LVDTs (Linear Variable Differential Transformer) are inductive transducers, which are coupled to the beams to measure the deformation and strain of the beams during testing. These electromechanical transducers determine the deformation by measuring the rectilinear motion of an object that is coupled mechanically into an electrical signal. (Connectivity, 2017) A total number of four LVDTs are glued to each beam. A HBM QuantumX XM840B connected to an external computer registers the output records and stores them using the software program CatmanAP V5.1.1.13.

(a) LVDTs in the front of the beam

(b) LVDTs in the back of the beam

Figure 4.10: Placing of the LVDTs

To measure the deflections, two LVDTs were placed in the middle of the LVDT area, as shown in 4.9. One LVDT was placed at each side of the beam, in case the beam deflected more on one side than the other. The one facing the camera was marked as North-East (NE), while the one on the opposite side was marked as South-West (SW). These LVDTs had a maximum contraction length of 15 mm.

Additionally, two LVDTs were used to measure the strains over a distance of 10 cm. They were placed horizontally in the middle of the LVDT area, one at each

side of the beam, but at different heights. The first one was located on the top of the front side of the beam (facing the camera), while the other one was placed at the bottom of the opposite side.

Crack development

The beams were, previous to the testing days, unwrapped from plastic and damp burlap sacks, lifted and placed onto steel trestles. Next, they were inspected for any crack development from the hardening period which was none or negligible. To improve the concrete crack development investigation, all of the beams were partly painted in white. The paint made it easier to discover the crack development during the 4-point bending test. The test was, as mentioned, divided into several loading steps, where each step was increased by 10 kN. Between each interval, the machine was paused to make sure it was enough time to draw the crack development onto the beams.

Chapter 5

Modifications

Chapter 6.2 presented later in this study, explains that the testing of the aluminium reinforced beams didn't go as planned. It was therefore decided to change the setup for the remaining beams. This, together with different material properties than expected, mainly lower concrete strength, made it necessary to perform new calculations for comparison with the beam testing results.

All modifications that is done as a result of the laboratory outcomes is presented in this chapter.

5.1 Modified beam setup

It was supposed that all of the beams should have the same statical system as shown in Figure 3.1. As mentioned above, modifications of the beam setup were done for several beams. The setups that were used during testing for each beam are presented in Figure 5.1. An explanation for each of the changes are presented later, in chapter 6.2.

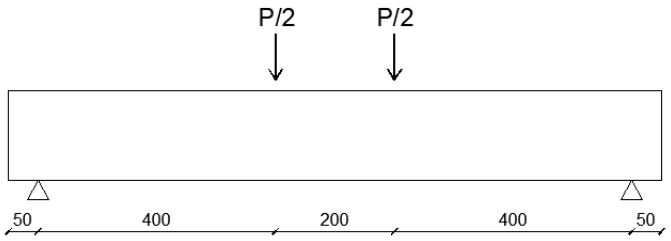

(a) B2-2ø12-STEEL and B2-3T-ALU1

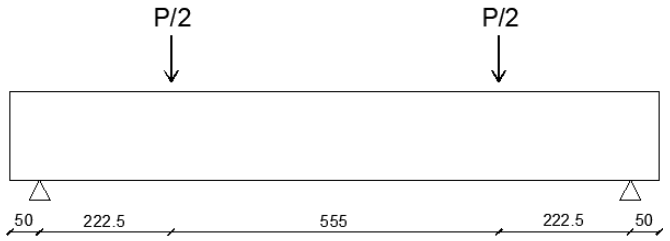

(b) B2-3T-ALU2 and B1-6ø10-ALU1

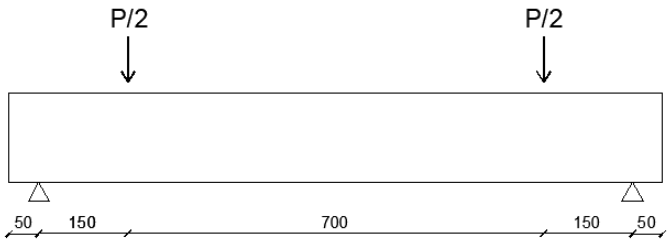

(c) B1-6ø10-ALU2

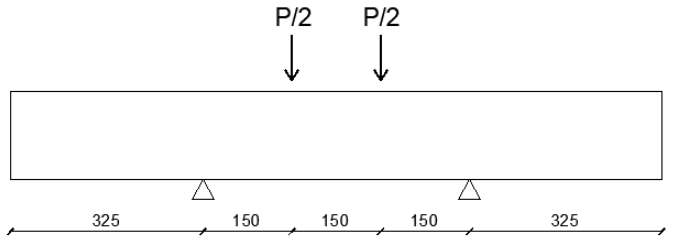

(d) B1-6ø10-ALU3

Figure 5.1: Statical systems of the beams

5.2 Modified calculations

The beam design calculations done in Chapter 3 are based on the statical system from Figure 3.1, which is the same as in Figure 5.1a, together with expected values for the material properties. Because of the modified beam setups and results from the material property testing, given in chapter 6.1, new calculations have been carried out to ensure as accurate results as possible for comparison with the beam testing results.

Material properties used for the calculations in this chapter are therefore based on results from laboratory testing. The Young's Modulus and tensile splitting strength are values from the testing at 28 days, while the compressive strength values are from the test days. As for chapter 3, mean values for the steel reinforcement is used. For the aluminium reinforcement, the yield strength is set to 274 MPa which is the mean value from tensile testing of three aluminium alloyed test specimens, see Appendix J.

5.2.1 Moment capacity

The modified moment capacities are given in Table 5.1.

Table 5.1: Modified moment capacities

Identification	M_{Rd} [kNm]	M_{Ed} [kNm]	Utilization	P_{cr} [kN]
B2-2ø12-STEEL	13,5	11,2	83%	56,1
B2-3T-ALU1	13,4	13,4	100%	66,8
B2-3T-ALU2	13,4	8,1	60%	72,2
B1-6ø10-ALU1	14,2	8,8	62%	79,3
B1-6ø10-ALU2	14,2	8,8	62%	117,6
B1-6ø10-ALU3	14,2	8,8	62%	117,6

As the table shows, only beam B2-3T-ALU1 is expected to obtain bending moment failure in difference to the first calculations where all of the aluminium reinforced beams were expected to obtain bending moment failure.

5.2.2 Shear capacity

Shear tensile capacity

Because of the modified beam setup, EC2, 6.2.2(6) needs to be taken into account when calculating the shear tensile capacity.

This section allows a reduction of loads applied on the upper side of beams/plates within a distance of 0,5d $\leq$ a_v $\leq$ 2d from the edge of a support, when calculating the shear tensile capacity. The contribution from the loading to the shear force, within this area, may be multiplied by β = a_v / 2d. One can also divide the shear tensile capacity with the same factor so that the capacity increases, instead of reducing the applied load. This can be done because a significant portion of the shear force may be transferred directly to the support, leading to an increased capacity. For this to be valid, the longitudinal reinforcement needs to be fully anchored at the supports. It is assumed that this requirement is satisfied because of the transversal rods that are fastened at each end of the longitudinal reinforcement.

An increase of the shear tensile capacity is done for beam B2-3T-ALU2, B1-6ø10-ALU1, B1-6ø10-ALU2 and B1-6ø10-ALU3. Table 5.2 shows the modified shear tensile capacities, calculated from the current formula of the shear tensile capacity.

Table 5.2: Modified shear tensile capacities - Current formula

Identification	$V_{Rd,current}$ [kN]	V_{Ed} [kN]	Utilization	P_{cr} [kN]
B2-2ø12-STEEL	28,0	28,0	100%	56,1
B2-3T-ALU1	34,9	33,4	96%	66,8
B2-3T-ALU2	36,1	36,1	100%	72,2
B1-6ø10-ALU1	39,6	39,6	100%	79,3
B1-6ø10-ALU2	58,8	58,8	100%	117,6
B1-6ø10-ALU3	58,8	58,8	100%	117,6

As the table shows, all of the beams except for beam B2-3T-ALU1 is expected to obtain shear failure, even with the increased shear tensile capacity, after EC2, 6.2.2(6), for some of the beams.

A comparison of the shear tensile capacities given from the current formula and the formula developed for the new Eurocode is also done here, and is shown in Table 5.3.

Table 5.3: Modified shear tensile capacities - Comparison of current and new formula

Identification	$V_{Rd,new}$ [kN]	$V_{Rd,current}$ [kN]	Comment
B2-2ø12-STEEL	32,9	28,0	The new formula gives bending moment failure instead of shear failure.
B2-3T-ALU1	27,3	34,9	The new formula gives shear failure instead of bending moment failure.
B2-3T-ALU2	34,4	36,1	The new formula still gives shear failure.
B1-6ø10-ALU1	37,9	39,6	The new formula still gives shear failure.
B1-6ø10-ALU2	64,0	58,8	The new formula still gives shear failure.
B1-6ø10-ALU3	64,0	58,8	The new formula still gives shear failure.

As for the first calculations, the formula developed for the new Eurocode gives slightly different capacities than the current formula. It can be interesting to see which calculations the laboratory results will be closest to, if some of the beams fail due to shear.

Shear compressive capacity

The modified shear compressive capacities are given in Table 5.4. The compressive strength used in the formula is the average value from the two cylinders from each batch, tested at the beam testing days.

Table 5.4: Modified shear compressive capacity

Identification	$V_{Rd,max}$ [kN]	V_{Ed} [kN]
B2-2ø12-STEEL	190,7	28,0
B2-3T-ALU1	184,4	33,4
B2-3T-ALU2	184,4	36,1
B1-6ø10-ALU1	203,2	39,6
B1-6ø10-ALU2	203,2	58,8
B1-6ø10-ALU3	203,2	58,8

As seen from the table, the requirement is still satisfied with a good margin for all beams.

5.2.3 Anchorage

Adjusted results of anchoring lengths, tensile strengths and stresses are shown in Table 5.5. Anchorage modification calculations are presented in Appendix G.

Table 5.5: Modification anchorage calculation

Identification	P_{cr} [kN]	f_{td} [MPa]	$l_{b,rqd}$ [mm]	$\sigma_{sd,max}$ [MPa]	$l_{bd,lab}$ [mm]	σ_{sd} [MPa]
B2-2ø12-STEEL	56,1	2,16	77	40,5	25	124,0
B2-3T-ALU1	66,8	2,16	75	23,7	25	71,4
B2-3T-ALU2	72,2	2,16	81	23,7	25	77,1
B1-6ø10-ALU1	79,3	2,38	98	21,4	25	84,1
B1-6ø10-ALU2	117,6	2,38	146	21,4	25	124,8
B1-6ø10-ALU3	117,6	2,38	146	257,0	300	124,8

Table 5.5 shows that the results from Table 3.7 have changed in correspondence to the modifications. Further, the modified calculations show that all the beams can obtain higher failure loads. Increasing loads will affect the tensile stresses and required anchor lengths.

In the previous calculations none of the anchoring lengths compared with required anchoring lengths, were long enough for the beam to obtain the calculated failure loads. After the modifications were executed, only the beam with 300 mm anchoring length fulfilled the anchoring length requirement. However, as mentioned earlier, transversal rods were fastened at the ends to obtain sufficient anchorage.

5.2.4 Compression zone height

The modified relation between the loading and the compression zone height is shown in Figure 5.2 - Figure 5.6. The values for the different compression zone heights (αd, $(\alpha d)_I$ and (αd_{II})) and crack loads shown in the figures, are taken from Appendix F.

αd [mm]	Load [kN]
26,4	67,9
38,5	66,6
38,5	11,1
77,5	11,1
77,5	0

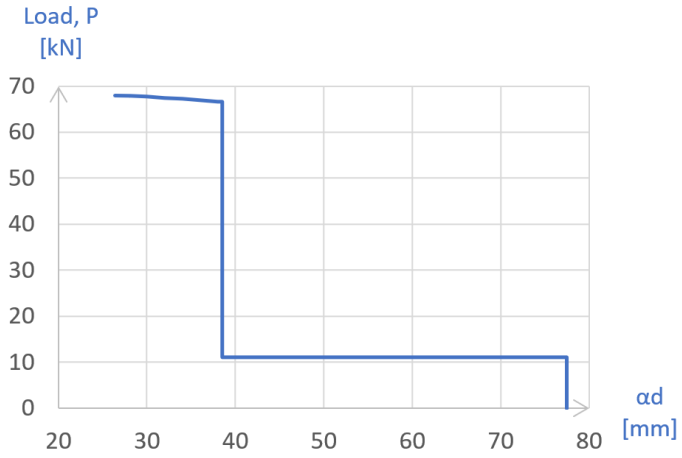

Figure 5.2: Load - compression zone height relation for beam B2-2ø12-STEEL

Figure 5.2 shows that the compression zone height decreases from 77,5 mm to 38,5 mm when the crack load of 11,1 kN occurs. From here, the compression zone height is constant until the reinforcement starts to yield at 66,6 kN. Next, the compression zone height decreases until the failure at 67,9 kN.

αd [mm]	Load [kN]
27,2	69,8
33,0	69,3
33,0	10,7
76,7	10,7
76,7	0

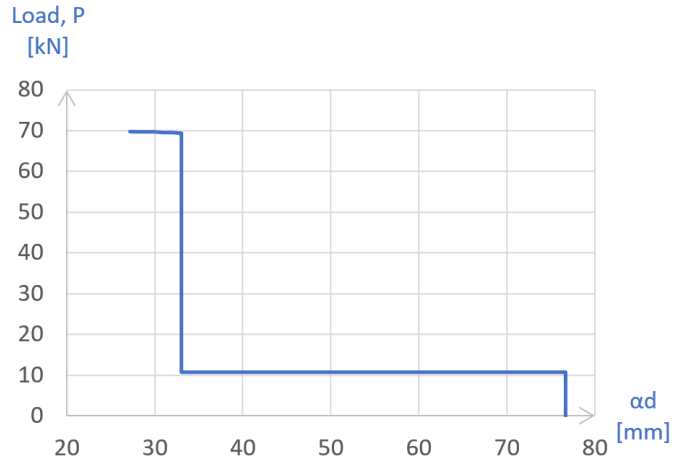

Figure 5.3: Load - compression zone height relation for beam B2-3T-ALU1

Figure 5.3 shows that the compression zone height decreases from 76,7 mm to 33,0 mm when the crack load of 10,7 kN occurs. From here, the compression zone

height is constant until the concrete reaches its maximal stress at 69,3 kN. Next, the compression zone height decreases until the failure at 69,8 kN.

αd [mm]	Load [kN]
27,2	125,5
33,0	124,7
33,0	19,3
76,7	19,3
76,7	0

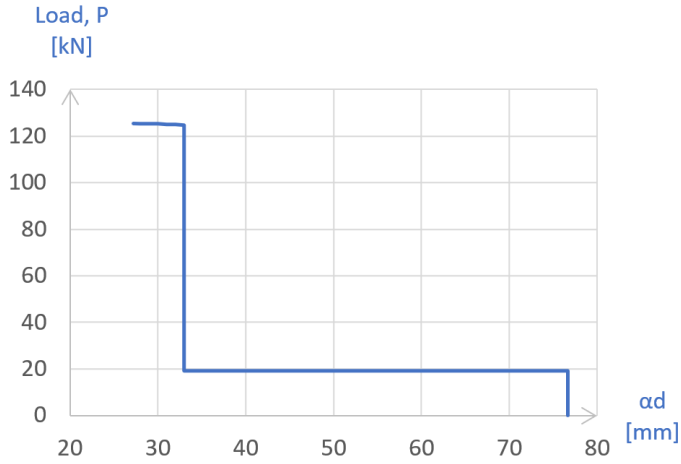

Figure 5.4: Load - compression zone height relation for beam B2-3T-ALU2

Figure 5.4 shows that the compression zone height decreases from 76,7 mm to 33,0 mm when the crack load of 19,3 kN occurs. From here, the compression zone height is constant until the concrete reaches its maximal stress at 124,7 kN. Next, the compression zone height decreases until the failure at 125,5 kN.

αd [mm]	Load [kN]
25,7	127,1
33,1	125,9
33,1	21,4
76,8	21,4
76,8	0

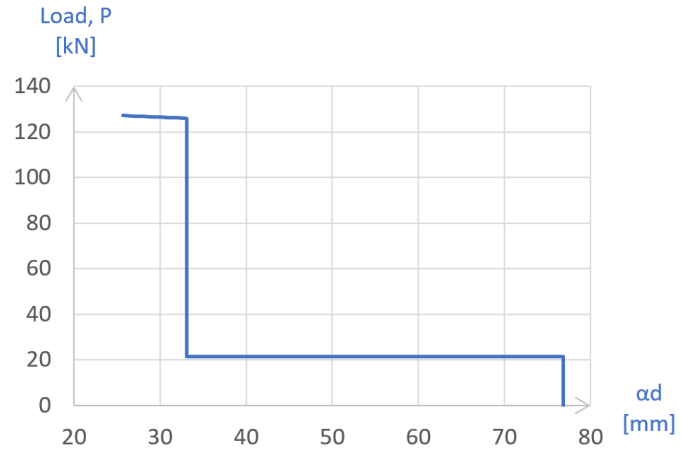

Figure 5.5: Load - compression zone height relation for beam B1-6ø10-ALU1

Figure 5.5 shows that the compression zone height decreases from 76,8 mm to 33,1 mm when the crack load of 21,4 kN occurs. From here, the compression zone

height is constant until the concrete reaches its maximal stress at 125,9 kN. Next, the compression zone height decreases until the failure at 127,1 kN.

αd [mm]	Load [kN]
25,7	188,5
33,1	186,7
33,1	31,8
76,8	31,8
76,8	0

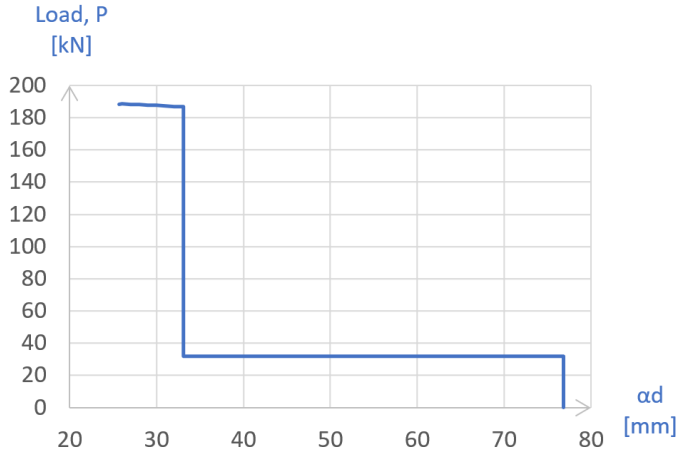

Figure 5.6: Load - compression zone height relation for beams B1-6ø10-ALU2 and B1-6ø10-ALU3

Figure 5.6 shows that the compression zone height decreases from 76,8 mm to 33,1 mm when the crack load of 31,8 kN occurs. From here, the compression zone height is constant until the concrete reaches its maximal stress at 186,7 kN. Next, the compression zone height decreases until the failure at 188,5 kN. Full calculations of the compression zone height are shown in Appendix H.

5.2.5 Deflection

The modified loads and deflections for all beams are plotted in Figure 5.7.

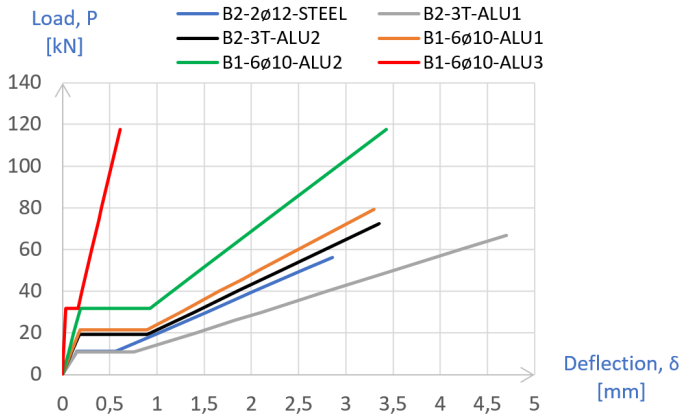

Figure 5.7: Load - deflection curves

Table 5.6 shows the modified values of both loading and deflection for the different stages for each beam.

Table 5.6: Calculated load-deflection values, modified

Identification	P_{crack} [kN]	$\delta_{crack,I}$ [mm]	$\delta_{crack,II}$ [mm]	P_{cr} [kN]	δ_{cr} [mm]
B2-2ø12-STEEL	11,1	0,15	0,56	56,1	2,85
B2-3T-ALU1	10,7	0,15	0,75	66,8	4,70
B2-3T-ALU2	19,3	0,17	0,90	72,7	3,36
B1-6ø10-ALU1	21,4	0,18	0,89	79,3	3,30
B1-6ø10-ALU2	31,8	0,19	0,93	117,6	3,43
B1-6ø10-ALU3	31,8	0,03	0,16	117,6	0,61

As seen from Figure 5.7 and Table 5.6, the loading and deflection varies more here than before the modifications.

5.2.6 Crack spacing

The modified maximum final crack spacing is shown in Table 5.7.

Table 5.7: Maximum final crack spacing - modified

Identification	Reinforcement spacing [mm]	$5 \cdot (c + \frac{\phi}{2})$ [mm]	Equation number	$S_{r,max}$ [mm]
B2-2ø12-STEEL	176	155	(3.31)	161
B1-6ø10-ALU1 B1-6ø10-ALU2 B1-6ø10-ALU3	28	150	(3.32)	122

As the table shows, the spacing is changed by a few millimeters for the beams. This change is caused by the increased compression zone height, as the compressive strength is lower than in the first calculations. The modified setups do not affect these calculations. Modified calculations are shown in Appendix I.

Chapter 6

Results

This chapter presents the results from the laboratory testing of beams and cylinders.

The test setup was not executed equally for all beams. After testing the second beam, it was decided to do some setup changes, to try to obtain desirable results. The feeding rate was set to be 0,3 mm/min for all beams, but was modified for some of the beams during testing according to slow progress in the testing. Adjustments for each beam are commented below, and are further discussed in Chapter 7. Except for replacing the load distribution beam with a larger one for the last two beam tests, the same equipment was used during testing.

6.1 Material properties

The material properties are divided into fresh and hardened concrete as mentioned earlier, and the results from the tests are presented in this chapter.

6.1.1 Fresh concrete properties

The properties of the fresh concrete were determined as described in chapter 4.2.1. The fresh concrete test results are presented in Table 6.1 below. Almost equal values were measured for both batches.

Table 6.1: Fresh concrete testing results

Fresh concrete tests	Batch 1	Batch 2
Slump test	19 cm	19 cm
Density test	2299 kg/m^3	2297 kg/m^3
Air Content	1,3 %	1,3 %

The slump test results classified as flowing with a value between 15-20 cm which means that the casting property is good (Gjerp et al., 2014). The density tests of fresh concrete show a density of approximately 2300 kg/m^3 and the air content values lie in the gap between 1-2 % which is also good.

The fresh concrete tests are a quality assurance of the concrete properties, and the results are not used further in the thesis.

6.1.2 Density of hardened concrete

The density of all 16 relevant cylinders were determined as described in chapter 4.2.2. The average densities of the cylinders are presented in Table 6.2.

Table 6.2: Density of hardened concrete

	Batch 1	Batch 2
Density, ρ [kg/m^3]	2324	2317

The densities for the hardened concrete have normal values which are between the range of 2200-2500 kg/m^3 (SNL, 2018). The fresh concrete densities, where batch 1 and 2 had a density of respectively 2299 kg/m^3 and 2297 kg/m^3, show that the density of the concrete changes according to the hydration and hardening phase, and becomes somewhat more dense after hardening.

6.1.3 Compressive strength

In total, eight cylinders were tested for the compressive strength. After 28 days of hardening four cylinders were tested, two from each batch. The remaining four cylinders, also two from each batch, were tested the same day as the corresponding beams. Each test was executed in accordance to the description in chapter 4.2.2. The fracture was ductile, which resulted in some small visible cracks on the

cylinder surfaces. Compared to the fracture types given in Figure 4.5, all of the cylinders had a satisfied fracture type, similar to the cylinder on the far right in the figure.

Table 6.3: Compressive strength test results

Cylinder	Days of hardening	Fracture load [kN]	Compressive strength, f_c [MPa]	$f_{c,avg}$ [MPa]
1-1	28	175,8	22,3	23,0
1-2	28	186,1	23,7	
1-5	55	194,8	24,8	25,1
1-6	55	200,0	25,4	
2-1	28	170,9	21,6	21,4
2-2	28	170,4	21,2	
2-5	50	191,2	24,3	23,6
2-6	50	179,5	22,9	

According to the concrete prescription, a compressive strength of 30 MPa was desired. The desired compressive strength of 30 MPa was a qualified guess based on previous research, as presented in chapter 2.2. As seen in Table 6.3, the compressive strength of 30 MPa wasn't attained, which impacted the laboratory beam testing results.

6.1.4 Tensile splitting strength

After the concrete had hardened for 28 days, the tensile splitting strength was tested according to the method described in chapter 4.2.2. In total four cylinders were tested, two from each batch. All the cylinders were split in half during testing, which is shown in Figure 4.6b. An overview of the testing results are given in Table 6.4.

Table 6.4: Tensile splitting strength values, f_{ct}

Cylinder	Calculated f_{ct} from eq (4.4) [MPa]	$f_{ct,avg}$ [MPa]
1-7	2,26	2,38
1-8	2,49	
2-7	1,95	2,16
2-8	2,36	

6.1.5 Young's Modulus

In order to obtain the Young's Modulus values, two cylinders from each batch were tested, after 28 days of hardening. As mentioned, in the end of chapter 4.2.2, this test was executed after NS-EN 12390-13 with modifications from SINTEF Byggforsk's own specifications. The Young's Modulus results are presented in table 6.5.

Table 6.5: Young's Modulus testing results

Cylinder	E_c [MPa]	$E_{c,avg}$ [MPa]
1-3	21337	20868
1-4	20399	
2-3	20206	19676
2-4	19145	

These test values are collected from a report given by the testing machine. This report can be found in Appendix J.

6.2 Beams

The beams are presented in the same order as they were tested. As mentioned earlier, the test was divided into several load steps of 10 kN. These load steps were marked with a number beside the drawn cracks for each step, to easier recognize when they occurred. Series of images of crack development for each beam at each load step are presented in Appendix K.

The compression zone heights in this chapter are calculated from the strains measured from the LVDTs, and are not a direct output from the laboratory results.

6.2.1 Beam B2-2ø12-STEEL

The beam with steel reinforcement was tested at 08.05.18, and was the first beam to be tested. After 50 days of hardening, the concrete had a compressive strength of 23,6 MPa. The beam setup for this beam was performed as planned with a distance

of 200 mm between the point loads, as shown in Figure 6.1, and the calculated feeding rate of 0,3 mm/min. This feeding rate stayed the same throughout the whole test.

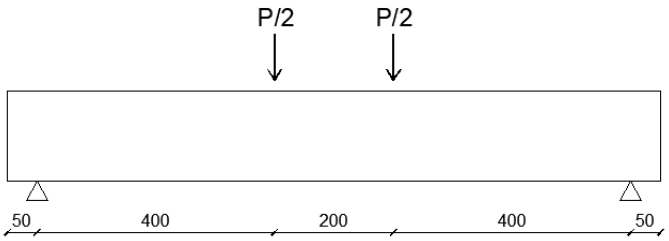

Figure 6.1: Setup for beam B2-2ø12-STEEL

The first observed crack was a bending crack and occurred in the lower part of the beam at the middle section, within the moment zone, at a point load of 16,4 kN. Further on, several bending cracks arose along the beam as the test ran. In the load-gap between 30-40 kN, the first shear crack was observed by the pinned support. At the load of 56,2 kN, the shear crack lead to shear failure, which was expected. A picture of the shear failure is shown in Figure 6.2.

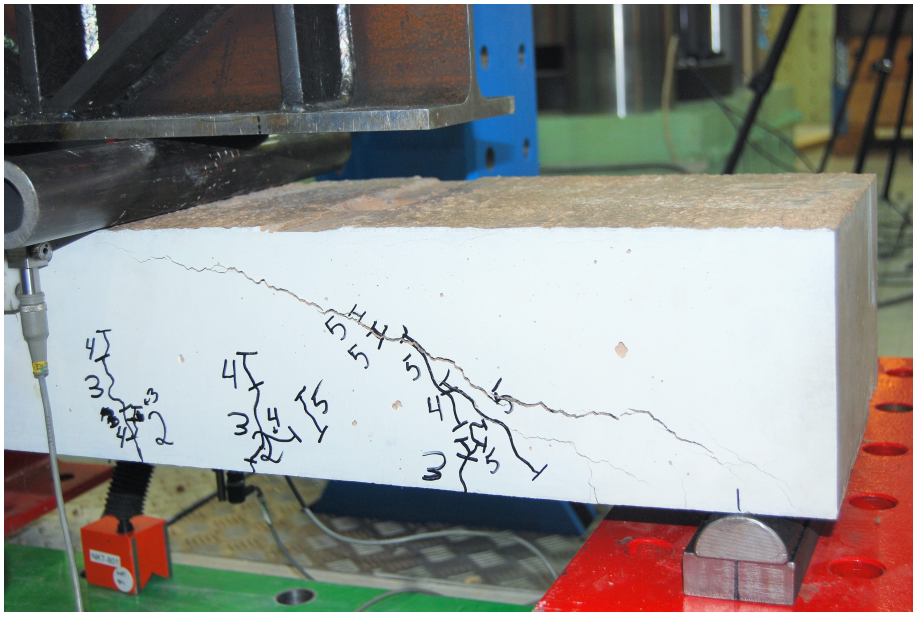

Figure 6.2: Shear failure of beam B2-2ø12-STEEL

Figure 6.3 shows the total crack development, with numbers corresponding to the load steps from Table 6.6. The maximum final crack spacing was measured in the middle of the beam, and was 161 mm.

Table 6.6: Load steps for beam B2-2ø12-STEEL

Step	1	2	3	4	5
Load [kN]	10	20	30	40	50

Figure 6.3: Crack development of beam B2-2ø12-STEEL

The compression zone height from the testing is shown in Figure 6.4. The first crack was observed at 16,4 kN, and the graph shows that the the compression zone height was approximately 39 mm at this load. The graph also shows how the compression zone height is close to constant after the crack load appears, and only

changes from 39 mm at 16,4 kN to 32,7 mm at the failure load of 56,2 kN.

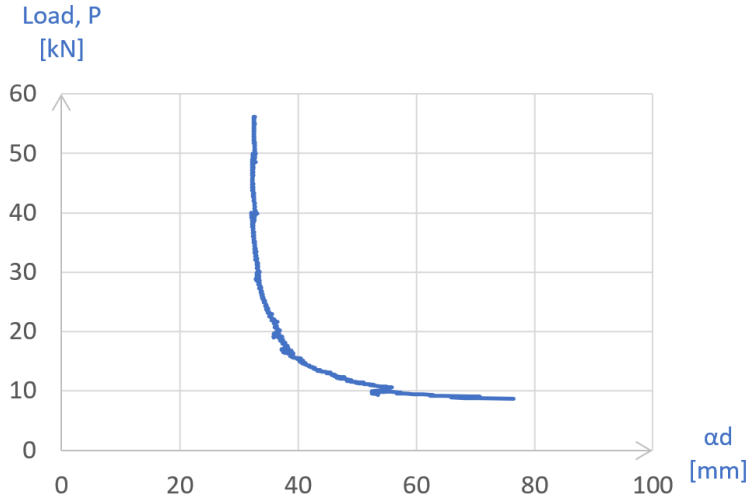

Figure 6.4: Load-deflection of beam B2-2ø12-STEEL

The graph in Figure 6.5 illustrates the relation between load and deflection. The graph shows that the beam failed at 56,2 kN, which, as mentioned, was shear failure. The deflection at this point was 6,08 mm. The first crack was observed at 16,4 kN when the deflection was 1,39 mm.

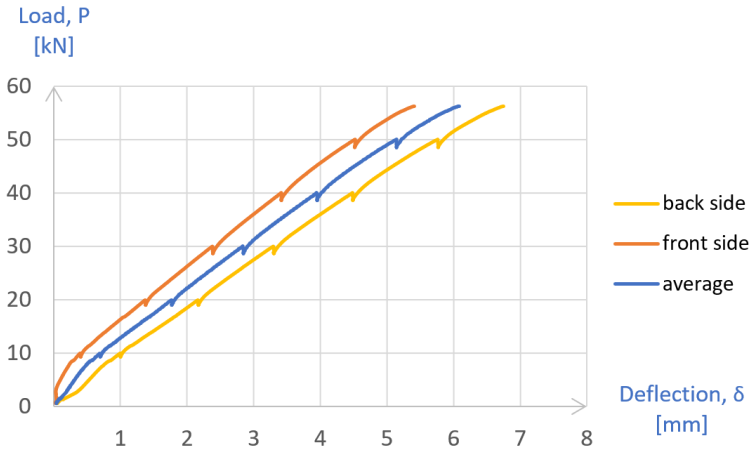

Figure 6.5: Load-deflection of beam B2-2ø12-STEEL

6.2.2 Beam B2-3T-ALU1

The second beam to be tested was beam B2-3T-ALU1 with T-shaped reinforcement bars. The testing day was the same as for beam B2-2ø12-STEEL (08.05.18),

and therefore the compressive strength was the same as for the steel reinforced beam (23,6 MPa). The beam was also equally set up as the previous beam test, with a distance of 200 mm between the point loads.

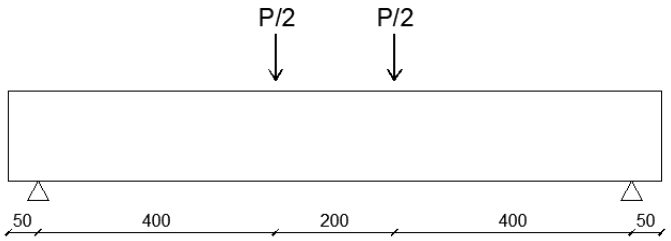

Figure 6.6: Setup for beam B2-3T-ALU1

The feeding rate started at the same rate as for the steel reinforced beam. During the test, the progress was so slow that it was decided to increase the feeding rate, which had the start value of 0,3 mm/min, before it was increased to 0,7 mm/min at a point load of 31,5 kN. Further on, the feeding rate was doubled to 1,4 mm/min at the point load of 34 kN. The last change of the feeding rate was to a value of 3,0 mm/min at 37 kN.

The first crack observed was a bending crack in the lower middle region, at a point load of 11,7 kN. During further load application, new cracks developed. After a while, the bending cracks at the centre started to expand until they went beyond all requirements, as shown in Figure 6.7a. The reinforcement had slipped due to poor bond, leading to large and wide cracks at the lower edge of the beam. These cracks were so large, it was even possible to directly view the T-shaped aluminium reinforcement bars through the cracks, as shown in Figure 6.7b.

(a) Closer look on the large bending cracks

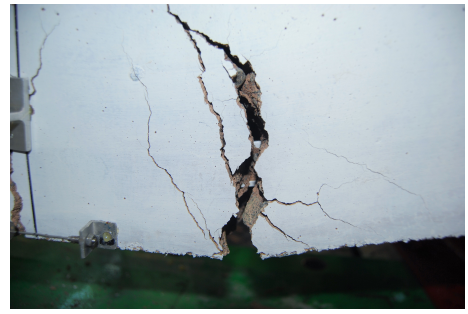

(b) Direct view of the T-shaped aluminium reinforcement.

Figure 6.7: Anchoring failure of beam B2-3T-ALU1

The beam reached a load of 39,5 kN before the machine was manually stopped. This was beyond failure, and there was no purpose in further loading. It can be seen in Figure 6.10 that the actual failure load was 26 kN. Figure 6.8 shows the total crack development with numbers corresponding to the load steps shown in Table 6.7. After load step 5 the loading continued without any stops (except for brief stops when the loading rate was changed), and the test ran until the final load of 39,5 kN. The maximum final crack spacing was measured to 126 mm, in the left part of the beam.

Figure 6.8: Crack development of beam B2-3T-ALU1

Table 6.7: Load steps for beam B2-3T-ALU1

Step	1	2	3	4	5
Load [kN]	10	20	30	40	50

When the reinforcement couldn't help the concrete withstand the load anymore, large deformations occurred. These deformations surpassed the expectations of maximum 15 mm deflection, so the LVDTs measuring the midspan deflections had to be removed during testing due to limited contraction ability.

The compression zone height from the testing is shown in Figure 6.9. The first

crack was observed at 11,7 kN. The first value of the compression zone height can be found when the strain in the reinforcement starts developing which was at 13,6 kN, i.e. in stage II where cracks had started to develop. Between this load and the failure load at 26 kN, the compression zone height varied from 76,5 mm at 13,6 kN to 35,5 mm at 26 kN.

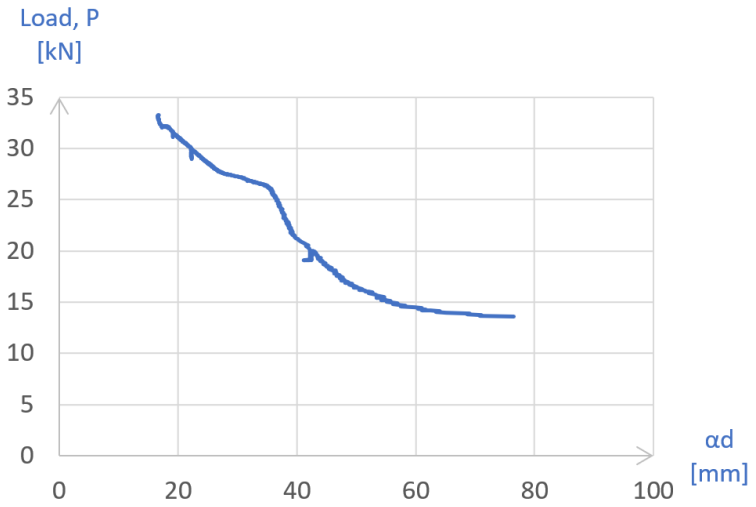

Figure 6.9: Load - compression zone height of beam B2-3T-ALU1

The graph in Figure 6.10 illustrates the relation between load and deflection. The beam was loaded until the machine reached 39,5 kN, but the graph only shows until 33,3 kN because the deflection could not be recorded further than 15 mm. The graph also shows that failure occurred at 26 kN, which is where the reinforcement

started to slip. The deflection at this point was 2,69 mm. The first crack was observed at 11,7 kN when the deflection was 0,74 mm.

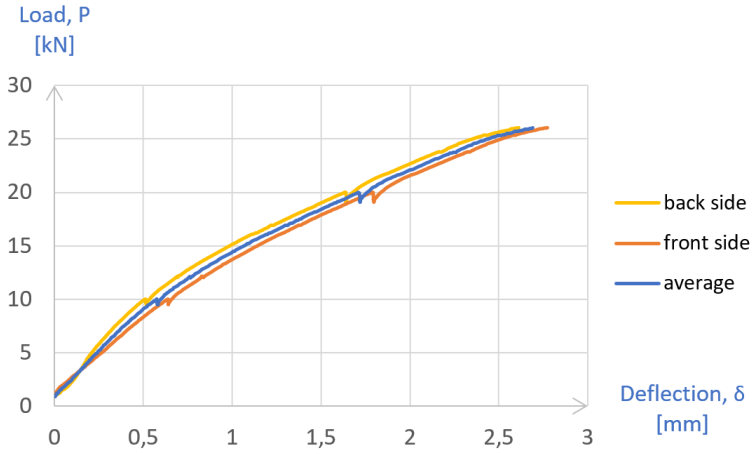

Figure 6.10: Load-deflection of beam B2-3T-ALU1

After this beam was tested, one of the beam ends was cut off to investigate the corrosion status. The aluminium reinforcement showed no sign of corrosion products, which indicates that this concrete chemically functions with the alloyed aluminium reinforcement.

6.2.3 Beam B2-3T-ALU2

Beam B2-3T-ALU2 with equal reinforcement as the previous tested beam, was the final beam from batch 2 to be tested. This beam was tested the 09.05.18, and had approximately the same compressive strength as the previous beams (23,6 MPa). This can be assumed since 95 % of the strength is reached after 28 days of hardening, and the strength development after this is slow. The setup for this beam was the first to be modified. Originally, bending moment failure was desired, but since the test for the previous beam resulted in bond failure instead of the desired bending moment failure, shear failure was now desired. The distance between the point loads were therefore increased from 200 mm to 555 mm, as seen in Figure 6.11. This length was chosen to be as long as possible, but was limited by the load distribution beam length and the desire to avoid point loads at the lifting points.

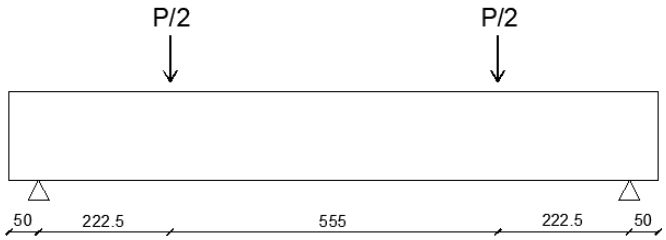

Figure 6.11: Setup for beam B2-3T-ALU2

The feeding rate was set to 0,3 mm/min, and was kept constant during the whole test. The first sight of cracks appeared in the middle section at a load of 13,9 kN.

Figure 6.12: Crack development of beam B2-3T-ALU2

Unfortunately, also this beam failed due to anchorage, this time at a point load of 55,5 kN. It can be seen in Figure 6.14 that the actual failure load was 45 kN. The beam could withstand more than the previous beam with the same reinforcement, but also here large deflections occurred. Figure 6.12 shows the crack development of this beam, with numbers corresponding to the load steps in Table 6.8. After the final load step, the test ran continuously until the load reached 55,5 kN. The maximal final crack spacing was measured to be 125 mm, at two places, both

within the moment zone.

Table 6.8: Load steps for beam B2-3T-ALU2

Step	1	2	3	4	5
Load [kN]	10	20	30	40	50

The compression zone height from the testing is shown in Figure 6.13. The first crack was observed at 13,9 kN, and the graph shows that the the compression zone height was approximately 115,7 mm at this load. Between this load and the failure load at 45 kN, the compression zone height varied from 115,7 mm at 13,9 kN to 61,3 mm at 45 kN. However, this indicates that the compression zone height from the laboratory at the crack load can't be calculated, because the compression zone height is never much larger than approximately $\frac{h}{2}$.

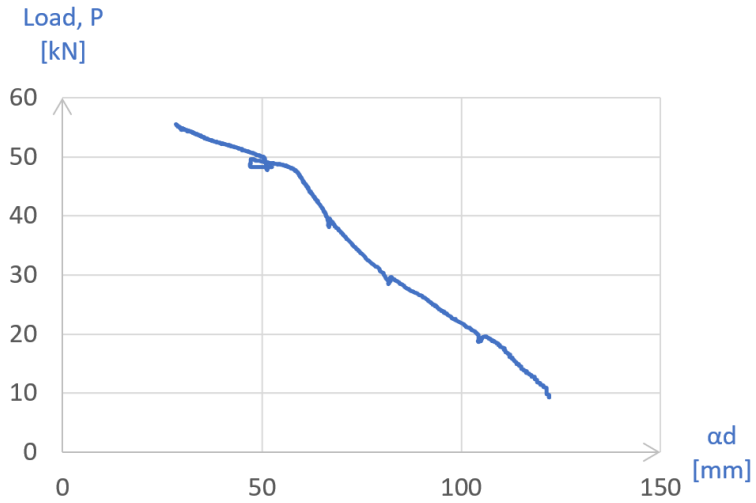

Figure 6.13: Load - compression zone height of beam B2-3T-ALU2

The graph in Figure 6.14 illustrates the relation between load and deflection. The graph shows that failure occurred at 45 kN, which is where the reinforcement

started to slip. The deflection at this point was 4,43 mm. The first crack was observed at 13,9 kN when the deflection was 0,77 mm.

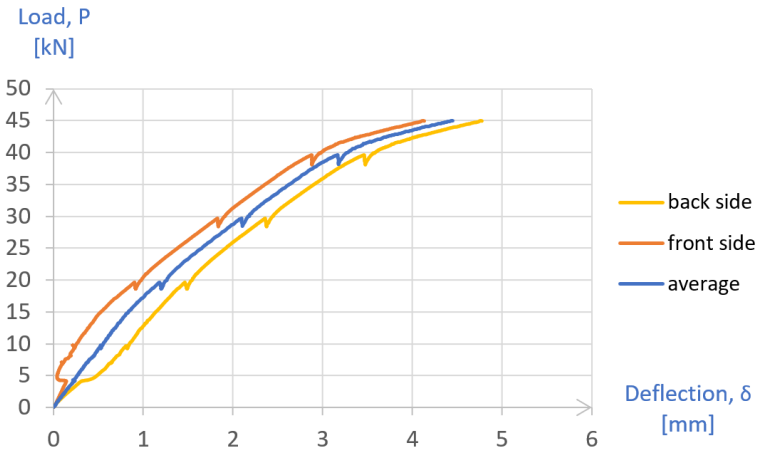

Figure 6.14: Load-deflection of beam B2-3T-ALU2

6.2.4 Beam B1-6ø10-ALU1

The first beam from batch 1, beam B1-6ø10-ALU1, was tested the 14.05.18. After 55 days of hardening, the concrete had a compressive strength of 25,1 MPa. It was decided to use the same setup as for the previous beam, with a distance of 555 mm between the point loads, to easier compare the results from different shapes of the aluminium reinforcement. The feeding rate of 0,3 mm/min was the same throughout the test.

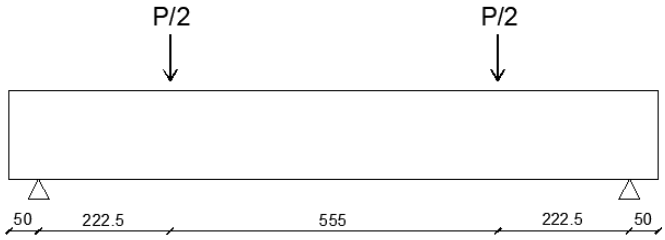

Figure 6.15: Setup for beam B1-6ø10-ALU1

The first observed crack was a bending crack, occured at a point load of 12 kN, which was a bit lower than for the T-shaped rods. Further on, a shear crack devel-

oped at the point load of approximately 50 kN, just before the beam failed at the load of 53,13 kN. Once again, the beam failed due to anchorage. It can be seen in Figure 6.17 that the actual failure load was 45,6 kN. The crack development with numbers corresponding to the load steps, presented in Table 6.9, is shown in Figure 6.16. After load step 5 the loading continued without any stops, and the test ran until the final load of 53,13 kN. The maximal final crack spacing was measured to 199 mm, just to the left of the beam center.

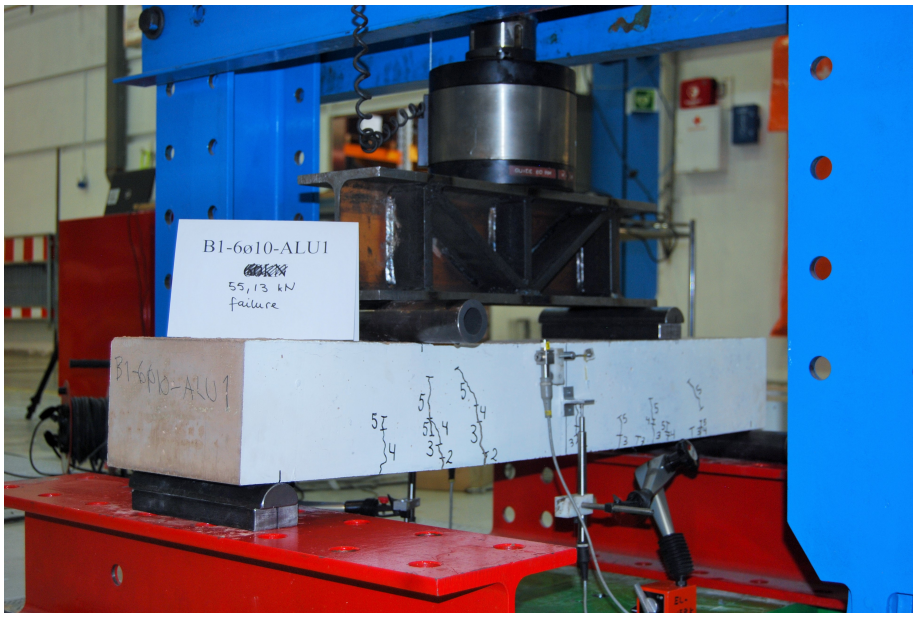

Figure 6.16: Crack development of beam B1-6ø10-ALU1

Table 6.9: Load steps for beam B1-6ø10-ALU1

Step	1	2	3	4	5
Load [kN]	10	20	30	40	50

In the laboratory, the LVDTs for the strains did not work for this beam. Since the relation between the loading and the compression zone height is calculated based on the strain values, it couldn't be found for this beam.

The graph in Figure 6.17 illustrates the relation between load and deflection. The graph shows that failure occurred at 45,6 kN, which is where the reinforcement

started to slip. The deflection at this point was 3,50 mm. The first crack was observed at 12 kN when the deflection was 0,58 mm.

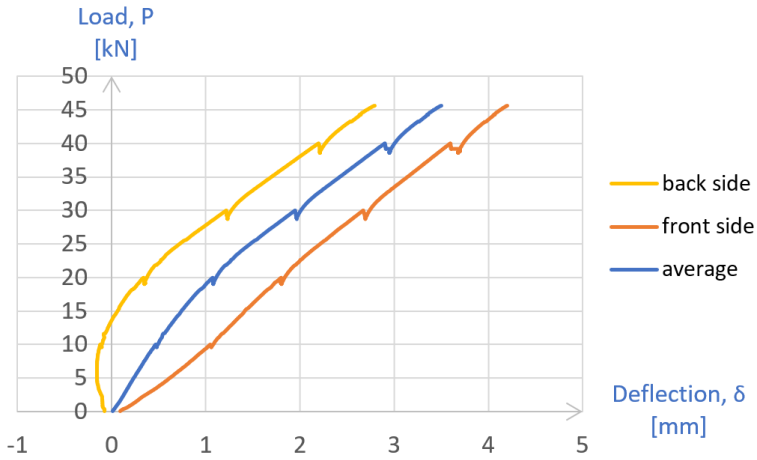

Figure 6.17: Load-deflection of beam B1-6ø10-ALU1

6.2.5 Beam B1-6ø10-ALU2

Beam B1-6ø10-ALU2 was the next beam to be tested. This beam was also tested the 14.05.18 as the previous beam, and had the same compressive strength of 25,1 MPa. After developing anchoring failure for another beam, it was decided to change the test setup once more. The distance between the point loads was increased even further, from 555 mm to 700 mm, still in the hope of shear failure. In conjunction with the modified spacing, a new and longer load distribution beam had to be used. As for several of the previous beams, the feeding rate stayed at the calculated value of 0,3 mm/min through the entire test.

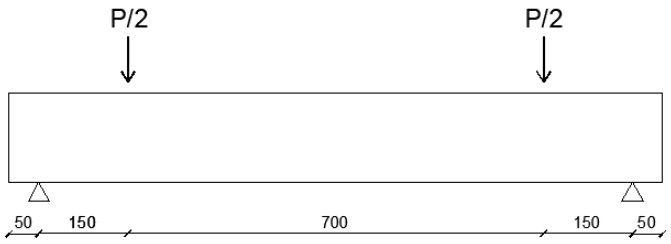

Figure 6.18: Setup for beam B1-6ø10-ALU2

The first bending crack was observed at 25 kN. At the load of 78,2 kN, the beam failed due to anchorage. Figure 6.19 shows the crack development with numbers corresponding to the load steps in Table 6.10. After the final load step, the test ran continuously until the load reached 80 kN. The maximum crack spacing was measured to 148 mm, in the middle of the beam.

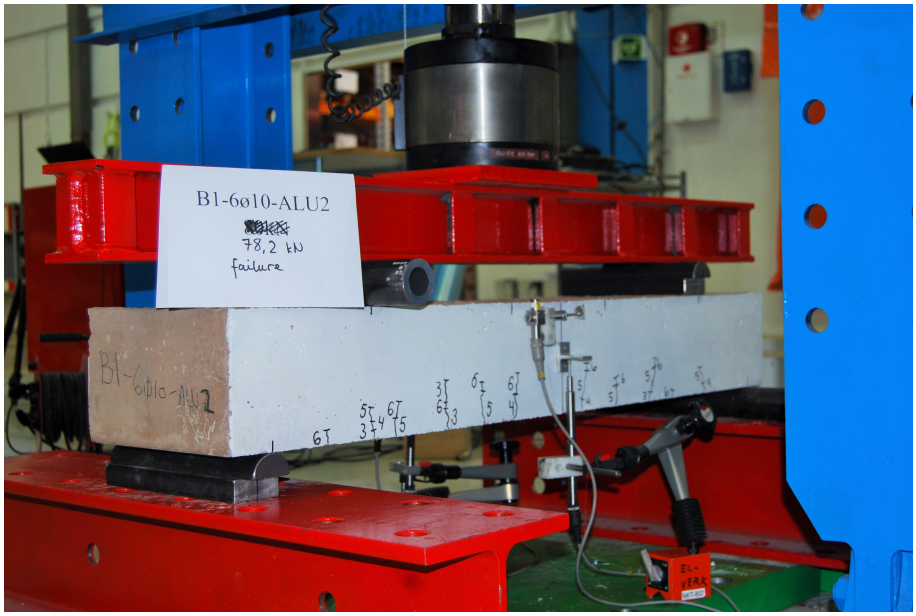

Figure 6.19: Crack development of beam B1-6ø10-ALU2

Table 6.10: Load steps for beam B1-6ø10-ALU2

Step	1	2	3	4	5	6
Load [kN]	10	20	30	40	50	60

Since the changes of the beam setup was done just before the testing of the beam, the correct calculations were not done prior to the testing. From the calculations done after the test, the beam was calculated to have a capacity of 117,6 kN. Since the calculated failure load increased from 66,1 kN to 117,6 kN, load steps of 20 kN would be more suitable than the load steps of 10 kN that was used for this beam. The graph in Figure 6.20 illustrates the relation between load and deflection.

In the laboratory, the LVDTs for the strains did not work for this beam. Since the relation between the loading and the compression zone height is calculated based

on the strain values, it couldn't be found for this beam.

The graph shows that the failure occurred at 78,2 kN, which is where the reinforcement started to slip. The deflection at this point was 3,75 mm. The first crack was observed at 25 kN when the deflection was 1,00 mm.

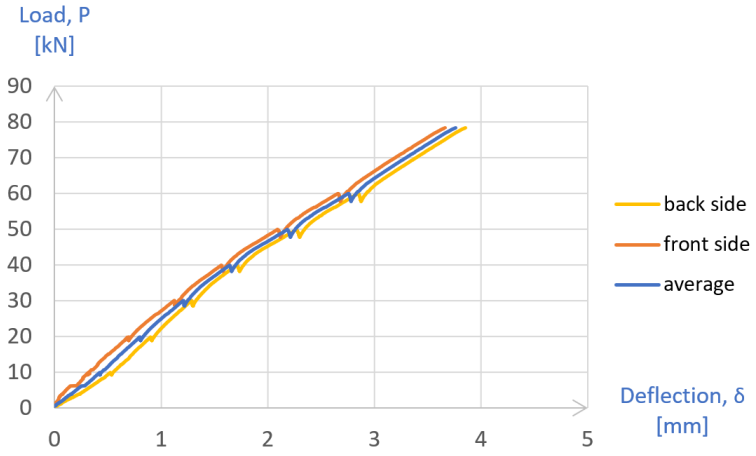

Figure 6.20: Load-deflection of beam B1-6ø10-ALU2

6.2.6 Beam B1-6ø10-ALU3

The final beam to be tested was the last beam from batch 1, beam B1-6ø10-ALU3. This beam was tested the 15.05.18, and had approximately the same compressive strength as the previous beams (25,1 MPa). This beam had the same type of reinforcement as the rest of the beams from batch 1, but it had one less transversal rod in each end. The test setup was modified one last time for the final beam test, as shown in Figure 6.21.

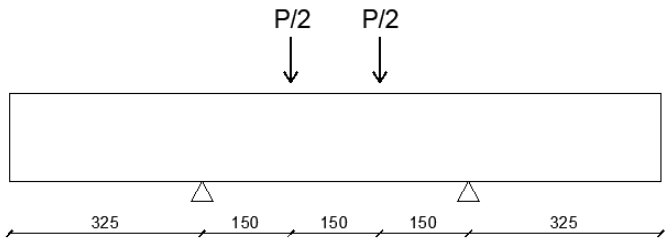

Figure 6.21: Setup for beam B1-6ø10-ALU3

This setup was chosen to obtain a larger anchoring length. The distance between the supports, L_m, was limited by the height ($L_m \geq$ 3h), giving a distance of 450 mm. The distance between the point loads was set to 150 mm. As for beam B2-3T-ALU1, the feeding rate was adjusted several times. It started at a new calculated value of 0,06 mm/min, which was increased to 0,2 mm/min at the load of 3,5 kN. Further on, the feeding rate was increased twice. First, at the point load of 20 kN it was increased to 0,3 mm/min. Finally, it was increased to 0,6 mm/min at the point load of 100 kN.

The first crack was observed at the load of 23,4 kN, and was a bending crack. The bending cracks continued developing along the beam as the load application continued. When the load reached 71,2 kN the first shear crack was noticed. However, anchoring still caused the failure of the beam. The machine was stopped at 113,66 kN, a while after failure had occurred. It can be seen in Figure 6.23 that the actual failure load was 74 kN. Figure 6.22 shows the crack development where the numbers correspond to the load steps in Table 6.11. After load step 5 the loading continued without any stops (except for brief stops when the loading rate was changed), and the test ran until the final load of 113,66 kN. The maximum crack spacing was measured to 101 mm, under the right point load.

Figure 6.22: Crack development of beam B1-6ø10-ALU3

Table 6.11: Load steps for beam B1-6ø10-ALU3

Step	1	2	3	4	5
Load [kN]	20	40	60	80	100

When the beam setup changed, the calculated failure load increased. Load steps of 20 kN was more suitable than load steps of 10 kN, thus, load steps of 20 kN as shown in Table 6.11 was applied.

In the laboratory, the LVDTs for the strains did not work for this beam. Since the relation betweeen the loading and the compression zone height is calculated based on the strain values, it could not be found for this beam.

The graph in Figure 6.23 illustrates the relation between load and deflection. The graph shows that failure occurred at 74 kN, which is where the reinforcement started to slip. The deflection at this point was 0,67 mm. The first crack was observed at 23,4 kN when the deflection was 0,13 mm.

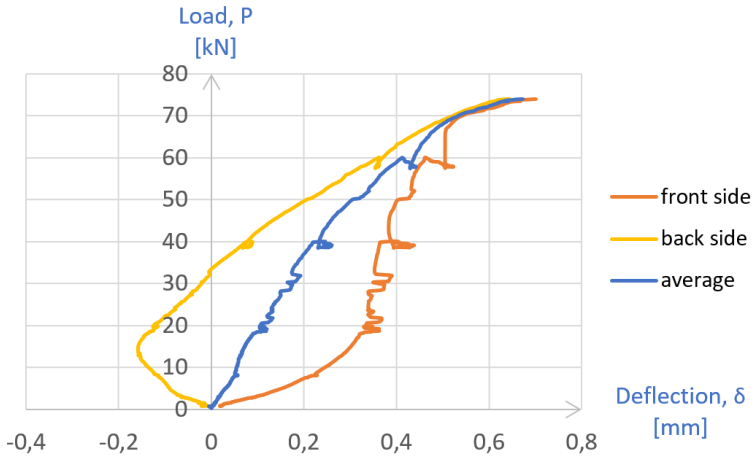

Figure 6.23: Load-deflection of beam B1-6ø10-ALU3

Chapter 7

Discussion

The main purpose of this master thesis is to research whether aluminium alloyed reinforcement bars could be used in concrete structures. Beam results are collected from the laboratory, and this chapter contains analyses of these results. There are several ways of categorizing the beams. Throughout the thesis the beams are divided based on their batch number and reinforcement type. In Table 7.1, all the beams are presented with parameters from their laboratory test setup.

Table 7.1: Overview test setup parameters for each beam

Identification	Distance between			Test date
	Loads [mm]	Supports [mm]	Loads and supports [mm]	
B2-2ø12-STEEL	200	1000	400	08.05.18
B2-3T-ALU1	200	1000	400	08.05.18
B2-3T-ALU2	555	1000	222,5	09.05.18
B1-6ø10-ALU1	555	1000	222,5	14.05.18
B1-6ø10-ALU2	700	1000	150	14.05.18
B1-6ø10-ALU3	150	450	150	15.05.18

In the initial phase of the thesis the content was prepared, assembled and organized based on different aims. These aims described expectations of what to gain from this laboratory study. One of the main purposes was to compare calculated values with laboratory results. On the other hand, it was interesting to compare beams with different reinforcement material and different cross section. Therefore, in this chapter the beams are compared both individually and with each other.

Individually, calculated values are compared with laboratory results.

It was desirable to find out whether the regulations from EC2 gave similar outcomes when using aluminium as reinforcement instead of steel. Traditionally, these regulations are based upon steel reinforced concrete structures, so it was not obvious that the aluminium reinforcement would act similar to steel. Unfortunately, due to poor bond conditions for the beams with aluminium reinforcement, the comparison with the Eurocode became more complicated. Along the way, as mentioned earlier, the test setup was modified in an attempt to improve the bond, but without any luck. However, there are several other opportunities for comparisons of this thesis and they are presented in this chapter.

In retrospect, the use of the Eurocode is questioned, considering the large amount of clay used in the concrete. By comparing the Youngs Modulus of the used concrete with the Youngs Modulus given EC2, Table 3.1 for corresponding compressive strength, it's lower. The used concrete may therefore have a higher strain at its maximal stress than given in EC2, figure 3.4, and calculations in conjunction with this might be wrong. Additionally, some material properties of the used concrete may deviate from ordinary concrete. However, this isn't further discussed.

7.1 Failure load

Expected failure loads from beforehand calculations and actual failure loads from laboratory results are presented in Table 7.2, alongside with expected and actual failure types.

Table 7.2: Failure loads and types

Identification	$P_{cr,calc}$ [kN]	$P_{cr,lab}$ [kN]	Failure type$_{calc}$	Failure type$_{lab}$
B2-2ø12-STEEL	56,1	56,2	Shear	Shear
B2-3T-ALU1	66,8	26,0	Moment	Anchorage
B2-3T-ALU2	72,2	45,0	Shear	Anchorage
B1-6ø10-ALU1	79,3	45,6	Shear	Anchorage
B1-6ø10-ALU2	117,6	78,2	Shear	Anchorage
B1-6ø10-ALU3	117,6	74,0	Shear	Anchorage

The table shows that almost none of the calculated failure loads reached their potential capacity except from the beam with steel reinforcement. This beam failed

approximately in accordance to calculations from the current Eurocode 2, with a failure load of 56,1 kN and the shear failure type. The shear capacity formula in the new Eurocode, which is under development, gave a less accurate value of 65,9 kN.

Comparison of the five remaining aluminium reinforced beams were more complicated, due to modification of the test setup. Table 7.1 presents an overview of the differences in the test setup for all the beams. Common for all of them is that they all failed according to anchorage based on the poor bond conditions.

Originally, the beams with T-shaped reinforcement were equally designed, but as shown in Table 7.2, the design failure loads and failure types are dissimilar. According to the table, beam B2-3T-ALU1 was calculated to obtain a moment failure, while beam B2-3T-ALU2 was supposed to fail according to shear failure. The modifications were executed in conjunction with the development of anchor failure, which occurred when testing the first of the two beams, beam B2-3T-ALU1. Increasing the distance between the failure loads, from 200 mm to 555 mm, resulted in an expansion of the moment zone, which lead to a smaller occurring moment. Thus, greater chance of developing shear failure. The calculated failure load increased slightly after the modification. By decreasing the distance between the external loading and the supports, larger parts of the loading were lead directly to the supports, resulting in higher shear tensile capacity. Failure load results from the beam testing show that beam B2-3T-ALU2 could withstand a much higher failure load (45 kN) than beam B2-3T-ALU1 (26 kN). The reason for this is that the failure loads vary in compliance with failure type and beam setup as explained above. Both of the final failure loads for these beams were much lower than expected values due to the anchorage weakness.

For some of the beams the setups were similar, but the reinforcement material and shapes were different. The two different types of aluminium reinforcement were reinforced with approximately the same total reinforcement area, shown in Table 3.1 from an earlier chapter. The similarity within reinforcement amount together with the equal test setup provided a basis for comparing two beams. Therefore, the last tested aluminium reinforced beam with T-shaped cross section, beam B2-3T-ALU2, were compared with the first tested aluminium reinforced beam with circular cross section, beam B1-6ø10-ALU1. Table 7.2 shows small differences in both calculated values and laboratory results for the two beams, which can indicate that dissimilar reinforcement types could be used to obtain approximately same failure loads. However, several other properties must be investigated to better compare the behaviour.

At last, comparison of the three beams with similar circular aluminium reinforce-

ment were performed. Table 7.2 shows that all of them were calculated to obtain the same failure type, but only beam B1-6ø10-ALU2 and beam B1-6ø10-ALU3 were designed to withstand the same failure load of 117,6 kN. Again, the difference within the failure load calculations are related to the test setup modifications. Table 7.1 shows that the distance between the loads for these beams were modified twice, while the distance between the supports only were changed for the last beam. Thus, none of these beams had the same setup. Comparing the calculated failure loads with the test results, the table shows that when the loads act closer to the supports or the distance between the supports become smaller, higher shear capacities arise. Beam B1-6ø10-ALU2 and beam B1-6ø10-ALU3 developed more similar results even though the test setup was different. The distance between loads and supports were the same, but the distance between the supports were different. This is most likely because the modification of increased anchoring length for the last beam didn't affect the capacity significantly due to the poor bond, hence the equal distance between supports and loading caused approximately the same failure load. The moment zone for beam B1-6ø10-ALU3 is quite small compared to beam B1-6ø10-ALU2, which resulted in fewer and larger cracks. This can be a possible explanation of why this beam failed at a lower load. This is further explained in chapter 7.4.

7.2 Compression zone height

Figure 7.1 - Figure 7.3 show the diagrams of the relation between loading and compression zone height, from both calculations and laboratory results. The graphs are presented in the same figure, overlapping each other for easier comparison. These diagrams are analyzed in this chapter.

To gain a greater understanding of how the loading affects the compression zone height, it's necessary to define some important transitions in the diagrams for the graphs from the calculations. Before reaching the crack load, the concrete is defined as uncracked, stage I. In this stage, the compression zone height is constant and at its greatest. After the applied load exceeds the crack load, the concrete enters stage II, cracked. In the diagrams, where the applied load exceeds the crack load is where the beam transfers from stage I to stage II. The final transition is where either the concrete develops its maximum stress or the reinforcement starts to yield. The transitions on the graphs from laboratory results aren't equally easy to observe since the curvature is more gradually changing. When interpreting the diagrams it's advisable to notice that the compression zone height decreases when the applied load increases, as mentioned earlier. Therefore, the graph should be

read from right to left. As seen on the figures, both the calculated and the laboratory results show that the compression zone height varies based on the applied load.

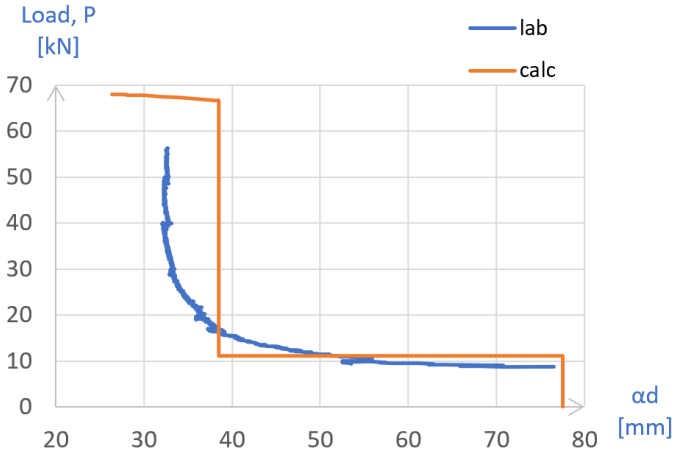

Figure 7.1: Relation between the compression zone height and applied load for beam B2-2ø12-STEEL

Figure 7.1 shows the diagram of the relation between the compression zone height and the applied load for the steel reinforced beam. The graph from the laboratory results, marked in blue, shows a more exponential shaped graph than the calculated one, marked in orange. According to the calculations, it's assumed that the tensile splitting strength was equal to zero in stage II, which isn't in practice the truth. The shape of the calculated graph would, if the actual tensile splitting strength was taken into consideration, be slightly more similar to the one from the laboratory. The calculated graph has a constant compression zone height after exceeding the crack load, compared to the graph from the laboratory results which gradually decreases. Overall, the compression zone height and load relation measured in laboratory for beam B2-2ø12-STEEL has similar values as in the beforehand calculations, even though the shape of the graphs differs.

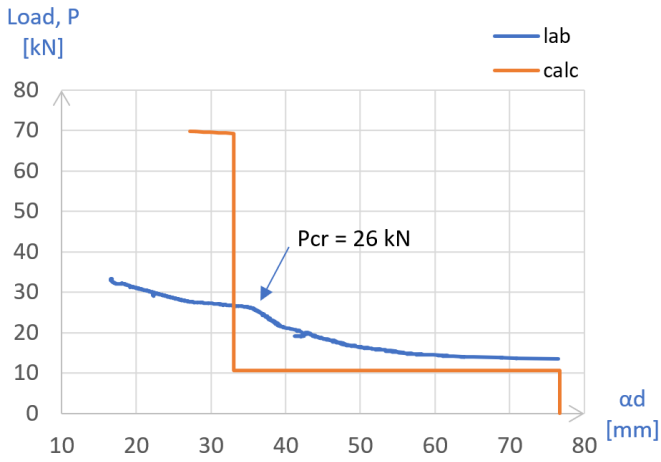

Figure 7.2: Relation between the compression zone height and applied load for beam B2-3T-ALU1

Figure 7.2 shows the diagram of the relation between the compression zone height and the applied load for the aluminium reinforced beam, beam B2-3T-ALU1. The calculated graph has a similar shape as the steel reinforced beam presented above, but with different values. The curvature of the laboratory measurements develops similarly to the steel reinforced beam until the load exceeds the crack load. At the load of 26 kN, the beam reached its failure load. This is easy to observe on the laboratory graph, and is marked with an arrow. The graph changes from a curved shape to a more flatten shape after failure, and the compression zone height decreases while the applied load slightly increases. This early transition was unexpected, and indicates the anchorage failure of the beam. If the beam hadn't failed in accordance to anchorage, it could be assumed that this laboratory graph would look more similar to the one for the steel reinforced beam. Hence, the calculations and laboratory results seem to have achieved similar development if it hadn't failed at such a low load.

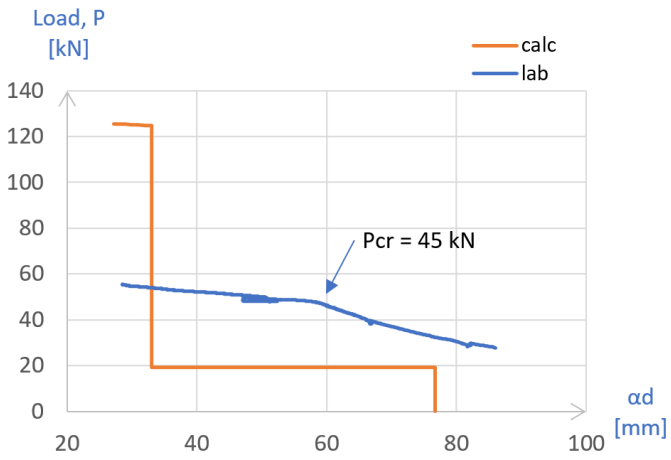

Figure 7.3: Relation between the compression zone height and applied load for beam B2-3T-ALU2

Figure 7.3 shows the diagram of the relation between the compression zone height and applied load of the aluminium reinforced beam, beam B2-3T-ALU2. The development of the relation of both the calculated and the laboratory measurements are similar to the previous graphs of the beam with equal reinforcement. The failure load is higher for this beam because of the modified beam setup with larger spacing between the point loads, as expected.

Unfortunately, the strain output measurements from the three last laboratory tests, beams from batch 1, could not be obtained due to defect equipment. Therefore, the calculations of these beams aren't further discussed since the laboratory results were absent. However, all three beams from batch 1 would probably have had a similar development as the diagrams in Figure 7.2 and Figure 7.3, since they all failed due to poor bond. It could also be assumed that the cross-sectional shape of the reinforcement bareley would affect the outcome values, and therefore the diagrams for the beams with similar beam setup could be expected to look something similar. I.e. the diagram for beam B1-6ø10-ALU1 would probably be similar to the diagram in Figure 7.3.

7.3 Deflection

Figure 7.4 - Figure 7.9 show the relations between load and deflection for all six beams, both from the calculations and the laboratory. The curves from the calculations start off in stage I, uncracked cross section, until the graphs show a break in the curve which is where the first crack appears. At the crack load, the beams enter stage II, cracked cross section, where the beams deflect more per load unit here than in stage I. This is also described in chapter 3.7.

The graphs from the laboratory deviates from the calculated ones, with only a few millimeters. Since the deflection is in such a small scale, this constitutes in fact a large difference. The crack load is not shown as clearly on the graphs from the laboratory as for the graphs from the calculations, but some of the graphs indicate that the first crack appeared earlier than what was observed in the laboratory. This is indicated by a small break in the curve, which is most visible in beam B2-2ø12-STEEL. It appears because the beam goes from stage I to stage II, i.e. from uncracked to cracked cross section. It's not as visible for the aluminium reinforced beams, but it makes sense that the actual crack load is less than the calculated crack load since the beam had larger deflections than anticipated at the crack loads. The crack loads, failure loads and the corresponding deflections at these loads, are presented in Table 7.3 - Table 7.8. These tables are divided into two, showing both the calculated and the laboratory values. The critical load, P_{cr}, in the calculated table is not equal to the calculated failure load, but to the failure load obtained in the laboratory. The reason for this is that the deflection at the failure can be compared more easily.

As mentioned in chapter 4.3, the deflections were measured at both sides of the beam in case the beams deflected asymmetrically. Figure 7.4 - Figure 7.9 show that this is the case for all of the beams.

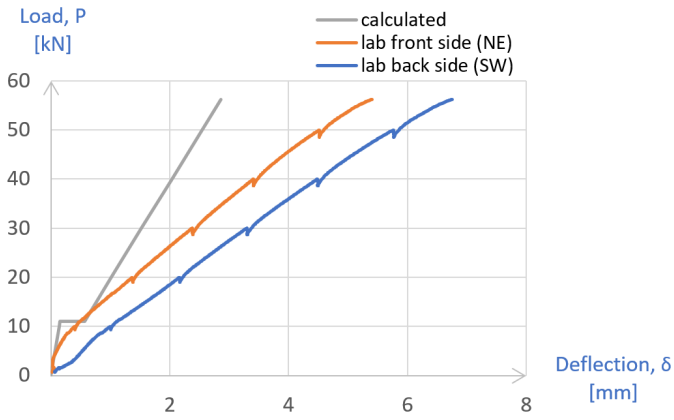

Figure 7.4: Load - deflection relation for beam B2-2ø12-STEEL

P [kN]	P_{crack} 11,1	P_{crack} 11,1	P_{cr} 56,2
δ [mm]	$\delta_{crack,I}$ 0,15	$\delta_{crack,II}$ 0,56	δ_{cr} 2,86

(a) Calculated

P [kN]	$P_{crack,observed}$ 16,4	P_{cr} 56,2
δ [mm]	$\delta_{crack,avg,observed}$ 1,39	$\delta_{cr,avg}$ 6,08

(b) Laboratory results

Table 7.3: Load - deflection relation for beam B2-2ø12-STEEL

As presented in Table 7.3, the calculated crack load for the steel reinforced beam was 11,1 kN, and the crack load observed in the laboratory was 16,4 kN. However, the laboratory curve in Figure 7.4 indicates that the first crack developed at about 8 kN. This is smaller than the calculated crack load, which as mentioned, makes sense considering that the deflections in the laboratory were larger than calculated. It's remarkable that the final deflection of this beam deviates so much from the calculated one, since the bond properties were satisfied and the failure type was as expected. Control calculations are done in accordance to support the results, and are presented in the end of this chapter.

The deflections on each side of the beam deviate from each other. The curve of the deflection on the back of the beam, marked in blue in Figure 7.4, shows that the beam gets a small exponential growth in the very beginning. This indicates that the beam has a larger stiffness at this point, which isn't the case since the stiffness is constant. An explanation of this can be that the supports yielded slightly, or that the load from the loading cylinder didn't get evenly distributed.

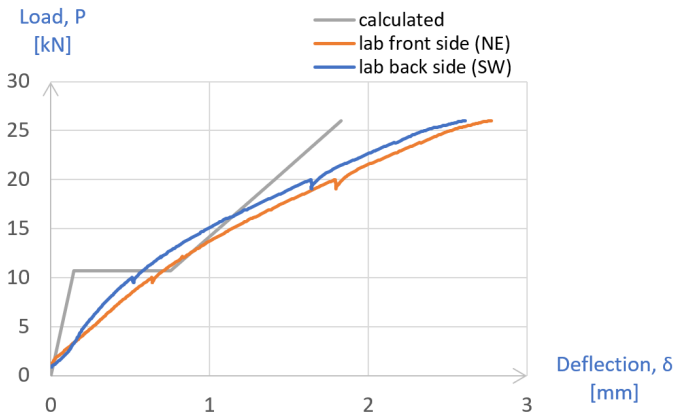

Figure 7.5: Load - deflection relation for beam B2-3T-ALU1

P [kN]	P_{crack} 10,7	P_{crack} 10,7	P_{cr} 26
δ [mm]	$\delta_{crack,I}$ 0,15	$\delta_{crack,II}$ 0,75	δ_{cr} 1,83

(a) Calculated

P [kN]	$P_{crack,observed}$ 11,7	P_{cr} 26
δ [mm]	$\delta_{crack,avg,observed}$ 0,74	$\delta_{cr,avg}$ 2,69

(b) Laboratory results

Table 7.4: Load - deflection relation for beam B2-3T-ALU1

As presented in Table 7.4, the observed crack load for beam B2-3T-ALU1 is 11,7 kN while it's calculated to be 10,7 kN, which is a good estimate. However, it may have occurred earlier than what was observed in the laboratory. This is likely, since the deflection is larger than calculated.

The graphs from Figure 7.5 show that the deflection from the laboratory is larger than from the calculated one. Since the reinforcement slipped in this beam testing, this makes more sense. As for the steel reinforced beam, the graph that shows the deflection of the back of the beam also develop a small exponential growth in the beginning. The explanation of this is the same as for the steel reinforced beam. The deflections on each side of the beam are quite similar.

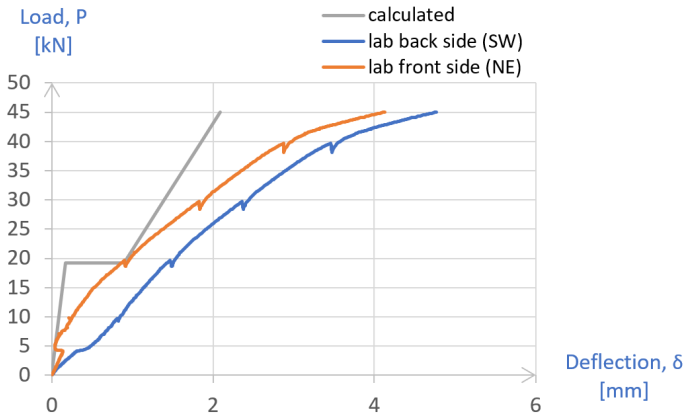

Figure 7.6: Load - deflection relation for beam B2-3T-ALU2

P [kN]	$P_{crack,I}$ 19,3	$P_{crack,II}$ 19,3	P_{cr} 45
δ [mm]	$\delta_{crack,I}$ 0,17	$\delta_{crack,II}$ 0,90	δ_{cr} 2,09

(a) Calculated

P [kN]	$P_{crack,observed}$ 13,9	P_{cr} 45
δ [mm]	$\delta_{crack,avg,observed}$ 0,77	$\delta_{cr,avg}$ 4,43

(b) Laboratory results

Table 7.5: Load - deflection relation for beam B2-3T-ALU2

As presented in Table 7.5 the observed crack load for beam B2-3T-ALU2 is 13,9 kN while it's calculated to be 19,3 kN. This makes sense, since the deflection is larger than calculated.

The graphs from Figure 7.6 show that the deflection from the laboratory is larger than from the calculated one, which makes sense since the reinforcement also slipped in this beam testing. The deflections on each side of the beam deviate more for this beam than for beam B2-3T-ALU1. Both the graphs from laboratory have a peak at around 4 kN, which moves in opposite directions. This can be explained by tilting of the beam, as the deflection on the back of the beam increases while the deflection on the front of the beam decreases.

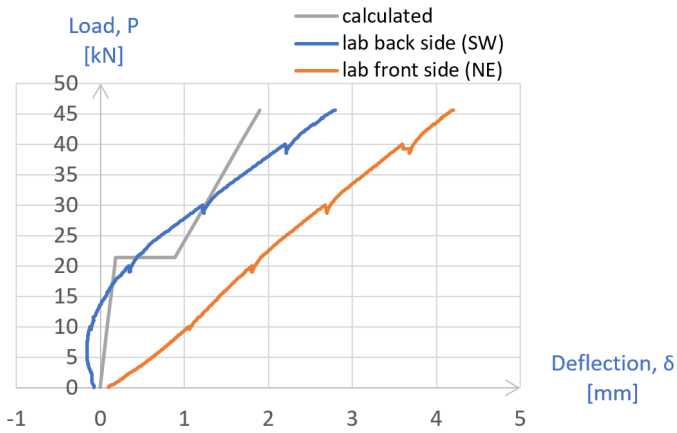

Figure 7.7: Load - deflection relation for beam B1-6ø10-ALU1

P [kN]	P_{crack} 21,4	P_{crack} 21,4	P_{cr} 45,6
δ [mm]	$\delta_{crack,I}$ 0,18	$\delta_{crack,II}$ 0,89	δ_{cr} 1,90

(a) Calculated

P [kN]	$P_{crack,observed}$ 12	P_{cr} 45,6
δ [mm]	$\delta_{crack,avg,observed}$ 0,58	$\delta_{cr,avg}$ 3,50

(b) Laboratory results

Table 7.6: Load - deflection relation for beam B1-6ø10-ALU1

As presented in Table 7.6, the observed crack load for beam B1-6ø10-ALU1 is 12 kN while it's calculated to be 21,4 kN. This makes sense, since the deflection is larger than calculated.

The graphs from Figure 7.7 show that the deflection from the laboratory is larger than from the calculated one, which makes sense since the reinforcement also slipped in this beam testing. The deflections on each side of the beam deviate more for this beam than the previous beams. The back side of the beam is even deflected upwards, shown as negative displacements in the diagram.

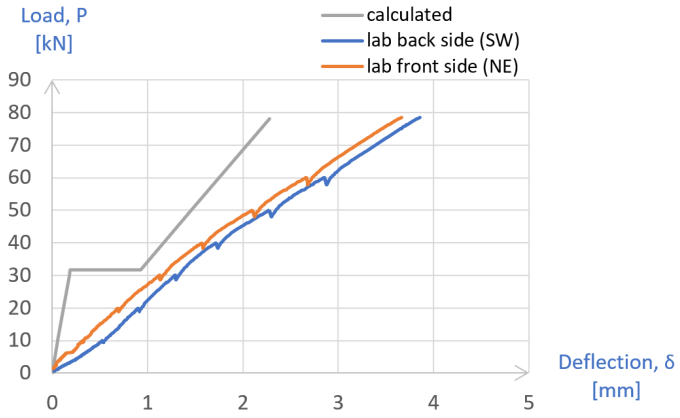

Figure 7.8: Load - deflection relation for beam B1-6ø10-ALU2

P [kN]	P_{crack} 31,8	P_{crack} 31,8	P_{cr} 78,2
δ [mm]	$\delta_{crack,I}$ 0,19	$\delta_{crack,II}$ 0,93	δ_{cr} 2,28

(a) Calculated

P [kN]	$P_{crack,observed}$ 25	P_{cr} 78,2
δ [mm]	$\delta_{crack,avg,observed}$ 1,00	$\delta_{cr,avg}$ 3,75

(b) Laboratory results

Table 7.7: Load - deflection relation for beam B1-6ø10-ALU2

As presented in Table 7.7, the observed crack load for beam B1-6ø10-ALU1 is 25 kN while it's calculated to be 31,8 kN. This makes sense, since the deflection is larger than calculated. However, it may have occurred even earlier than what was observed in the laboratory.

The graphs from Figure 7.8 show that the deflection from the laboratory is larger than from the calculated one. Since the reinforcement slipped in this beam testing, this makes more sense. The deflections on each side of the beam are quite similar.

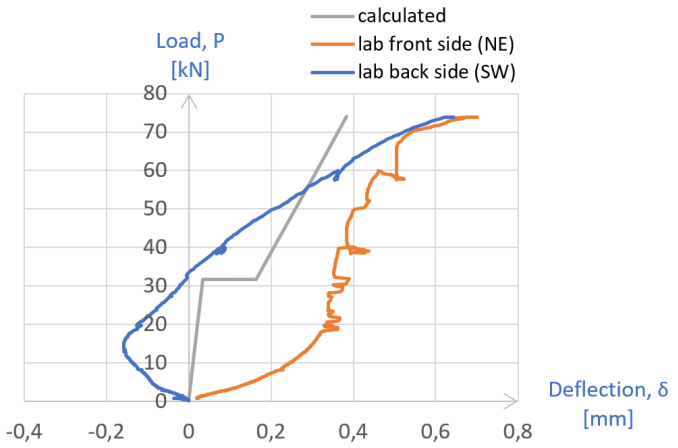

Figure 7.9: Load - deflection relation for beam B1-6ø10-ALU3

P	P_{crack}	P_{crack}	P_{cr}
[kN]	31,8	31,8	74
δ	$\delta_{crack,I}$	$\delta_{crack,II}$	δ_{cr}
[mm]	0,03	0,16	0,38

(a) Calculated

P	$P_{crack,observed}$	P_{cr}
[kN]	23,4	74
δ	$\delta_{crack,avg,observed}$	$\delta_{cr,avg}$
[mm]	0,13	0,67

(b) Laboratory results

Table 7.8: Load - deflection relation for beam B1-6ø10-ALU3

As presented in Table 7.8, the observed crack load for beam B1-6ø10-ALU1 is 23,4 kN while it's calculated to be 31,8 kN. This makes sense, since the deflection is larger than calculated. However, it may have occurred even earlier than what was observed in the laboratory.

The graphs from Figure 7.9 show that the deflection from the laboratory is larger than from the calculated one, which makes sense since the reinforcement also slipped in this beam testing. The deflections on each side of the beam deviate much in the start of the beam testing, but is quite similar at the failure load. As for beam B1-6ø10-ALU1, the back side of the beam is deflected upwards.

For this task, it is also interesting to compare the actual deflections for the beams with the same setup, to see how the reinforcement material and shape affects the deflection.

B2-2ø12-STEEL vs. B2-3T-ALU1

The average deflections from the laboratory for beam B2-2ø12-STEEL and beam B2-3T-ALU1 are plotted in Figure 7.10. The beams have the same setup, but different reinforcement material, shape and amount. The figure shows that the deflections for the two beams are quite similar, but that the steel reinforced beam has a steeper curve in stage II than the aluminium reinforced beam. This indicates that the deflection might have been larger for the aluminium reinforced beam if it had reached the same failure load as the steel reinforced beam, which is also the case for the calculated deflections, plotted in Figure 7.11.

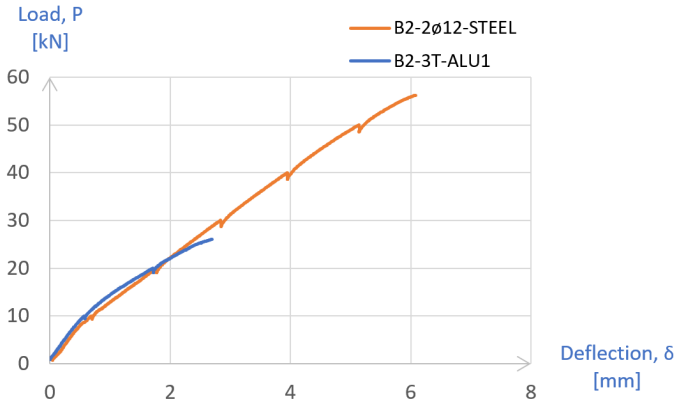

Figure 7.10: Load - deflection relation for beam B2-2ø12-STEEL and beam B2-3T-ALU1 from laboratory

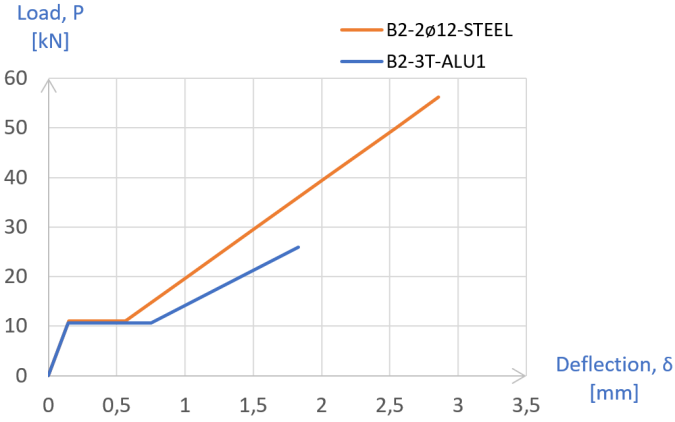

Figure 7.11: Calculated load - deflection relation for beam B2-2ø12-STEEL and beam B2-3T-ALU1

Table 7.9 presents the stiffness of both beams in the two stages, and shows how the steel reinforced beam has larger stiffness in both stages. However, the biggest difference is in stage II, and since the deflection and the stiffness is in inverse ratio, this explains why the curves shows larger deflection in stage II for the aluminium reinforced beam.

Table 7.9: Comparison of values for beam B2-2ø12-STEEL and beam B2-3T-ALU1

Identification	d [mm]	A_r [mm^2]	E_r [MPa]	$(EI)_I$ $\cdot 10^9$ [Nmm^2]	$(EI)_{II}$ $\cdot 10^9$ [Nmm^2]
B2-3T-ALU1	115	468	70000	1434	279,4
B2-2ø12-STEEL	119	226	200000	1466	386,7

Even though there is a difference between the stiffnesses of the beams, this is fairly small, hence, so is the difference of the deflections. As a larger stiffness results in less deflection, the factors affecting the stiffnesses are also the factors affecting the deflections. The reinforcement material, whether it's steel or aluminium, doesn't have a big impact on the deflection as long as the beam stiffness is approximately the same. Table 7.9 presents the factors affecting the stiffness that differs for the two beams. These factors are the effective height, d, the reinforcement area, A_r, and the Young's Modulus of the reinforcement, E_r. Doubling the value of the Young's Modulus has the same impact on the stiffness as doubling the reinforcement area. The reinforcement area is 2,07 times larger for the aluminium reinforced beam, but the Young's Modulus is 2,86 times larger for the steel reinforced beam. This explains why the calculated stiffnesses is higher for the steel reinforced beam. In addition, a larger effective height also contributes to a larger stiffness. However, the difference of the effective heights are fairly small, so the impact isn't as big as for the reinforcement area and the Young's Modulus. All three of these factors, make greater impact on the stiffness in stage II than in stage I. This explains why the differences of the stiffnesses in stage II are larger than in stage I. Since the deflections are directly related to the stiffness, it also explains why the curves in Figure 7.10 and Figure 7.11 are steeper for the steel reinforced beam than the aluminium reinforced beam, in stage II.

The crack load is also based on these factors. The crack load for the steel reinforced beam was calculated to 11,1 kN, as presented in Table 7.3. The aluminium reinforced beam is calculated to crack at 10,7 kN, as presented in Table 7.4, which means it's calculated to crack slightly earlier than the steel reinforced beam. This makes sense since the crack load is based on the factors as mentioned.

B2-3T-ALU2 vs. B1-6ø10-ALU1

The average deflections from the laboratory for beam B2-3T-ALU2 and beam B1-6ø10-ALU1 are plotted in Figure 7.12. The beams have the same setup and reinforcement material, but different reinforcement shape. The figure shows that the deflections for the two beams are quite similar, but that the beam with circular reinforcement has a slightly steeper curve, i.e. slightly less deflection per load unit, than the beam with T-shaped reinforcement. This is also the case for the calculated deflections plotted in Figure 7.13.

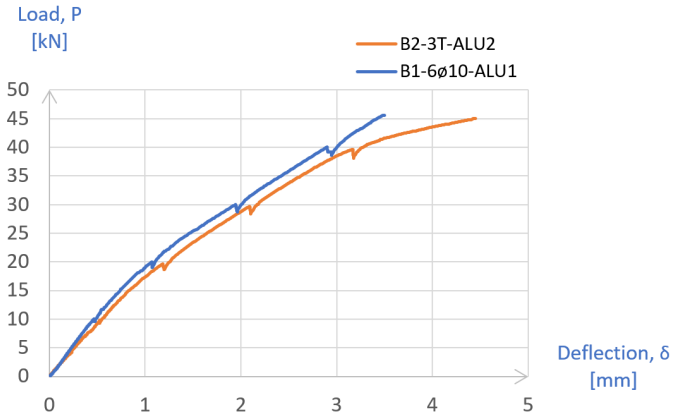

Figure 7.12: Load - deflection relation for beam B2-3T-ALU2 and beam B1-6ø10-ALU1 from laboratory

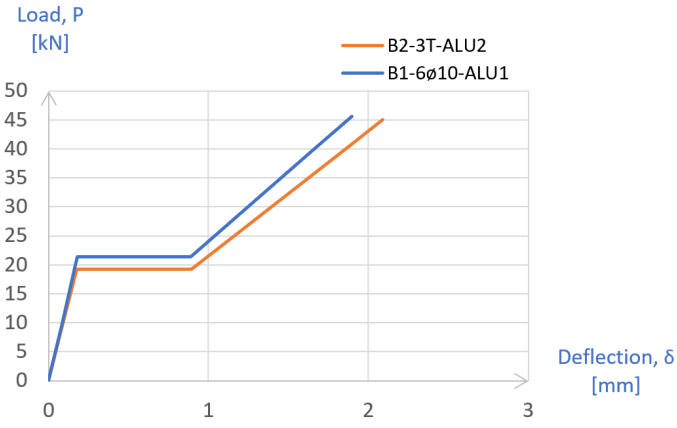

Figure 7.13: Calculated load - deflection relation for beam B2-3T-ALU2 and beam B1-6ø10-ALU1

Based on these comparisons, the reinforcement shape doesn't have a big impact on the deflection as long as the beam stiffness is approximately the same. The T-shaped reinforcement itself has larger stiffness than the circular reinforcement, but since this is in such a small scale, it doesn't affect the total beam stiffness. The stiffness is based on several values, where the ones that differ are the Young's Modulus of the concrete, E_c, the effective height, d, and the reinforcement area, A_r, as presented in Table 7.10. The larger these values are, the larger is the stiffness of the beam. This explains why the stiffness is higher and deflections are smaller for the beam with circular reinforcement than for the beam with T-shaped reinforcement, in both stages. The stiffness in stage I and stage II for the two beams are also presented in the table. However, the biggest difference is in stage I. This makes sense because the the Young's Modulus of the concrete makes a larger impact on the stiffness in stage I than in stage II, and is the value that differs the most.

Table 7.10: Comparison of values for beam B2-3T-ALU2 and beam B1-6ø10-ALU1

Identification	E_c [MPa]	f_{ct} [MPa]	d [mm]	A_r [mm^2]	$(EI)_I$ $\cdot 10^9$ [Nmm^2]	$(EI)_{II}$ $\cdot 10^9$ [Nmm^2]
B2-3T-ALU2	19676	2,16	115	468	1434	279,4
B1-6ø10-ALU1	20868	2,38	120	471	1531	312,2

The crack load for the beam with circular reinforcement was calculated to 21,4 kN, as presented in Table 7.6. The beam with T-shaped reinforcement is calculated to crack at 19,3 kN, as presented in Table 7.5, which means that it's calculated to crack slightly earlier than for the beam with circular reinforcement. The crack load is based on several factors, where the ones that differ are the tensile splitting strength of the concrete, f_{ct}, also presented in Table 7.10, in addition to the effective height and the reinforcement area. The higher these values are, the higher crack load, which explains why the calculated crack load is larger for the beam with circular reinforcement than for the beam with T-shaped reinforcement.

The observed crack load was 13,9 for the beam with T-shaped reinforcement, as presented in Table 7.5b, and 12 kN for the beam with circular reinforcement, as presented in Table 7.6b. This doesn't make sense, since the deflection for the beam with T-shaped reinforcement was larger than for the beam with circular reinforcement from beginning to end. An explanation to this can be that the first cracks occurred before they were observed, and that the first crack for the beam with T-shaped reinforced in reality occurred before the first crack on the beam with circular shaped reinforcement.

There is no clear difference between the beam with T-shaped reinforcement and the beam with circular reinforcement, by looking at the deflections. If the different values in Table 7.10 had been equal, the beams would have had the same deflections in the calculations, and probably also in the laboratory.

Control calculations for beam B2-2ø12-STEEL

As mentioned, the large deflection of the steel beam is remarkable, since the bond properties were satisfied and the failure type was as expected. Therefore, control calculations of the deflection and the strains are performed, at a given load, to find out if the measured values from the LVDTs are correct.

First, the control calculation of the deflection is presented. For this calculation, the curvature of the cross section needs to be defined.

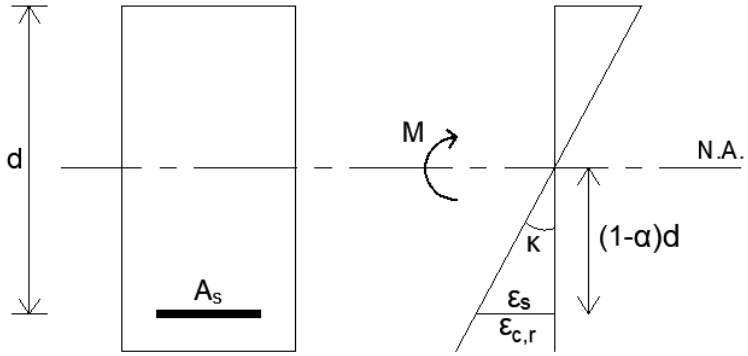

Figure 7.14: Strain distribution of a cross section

This curvature can be found by equation (7.1).

$$\kappa = \frac{\varepsilon_{c,top} + \varepsilon_{c,r}}{d} \tag{7.1}$$

where

$\varepsilon_{c,r}$ is the concrete strain at the height of the reinforcement

The concrete strains in this equation are taken from the horizontal LVDT measurements in the laboratory, at a given load.

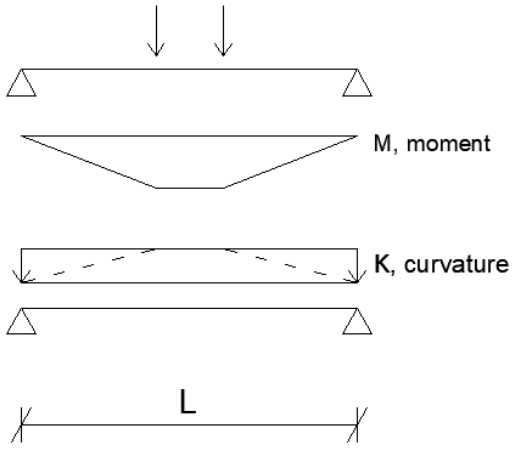

Figure 7.15: Deflection of a beam by applying the curvature as an external load

The curvature can be used to determine the deflection of a beam, by applying the curvature as an external load to the beam, as indicated with the dashed lines in Figure 7.15. For this calculation, the distribution of the curvature is simplified by applying the load evenly distributed along the beam length, as shown in the same figure. The deflection of a beam with evenly distributed load is given in equation (7.2).

$$\delta = \frac{\kappa L^2}{8} \tag{7.2}$$

The calculated deflection is compared to the deflection from the laboratory, at a given load, measured from the vertical LVDTs.

Second, the control calculation of the concrete strains is presented. Here, the laboratory concrete strain at the height of the reinforcement is compared to the theoretical reinforcement strain, given in equation (7.3). It is not completely accurate to compare the concrete strain at the height of the reinforcement with the reinforcement strain, but since the reinforcement strain wasn't measured in the laboratory, this is the closest comparison. However, these strains will not differ much.

$$\varepsilon_s = \frac{M(1-\alpha)\cdot d}{EI} \tag{7.3}$$

The comparison of the control calculations and the laboratory results are shown in Table 7.11. All values are given from a loading of 40 kN.

Table 7.11: Control calculations of beam B2-6ø10-STEEL

Control of deflection		Control of strains	
δ_{calc} [mm]	$\delta_{lab,avg}$ [mm]	$\varepsilon_{s,calc}$ [‰]	$\varepsilon_{c,r,lab}$ [‰]
3,80	3,95	1,92	2,64

As seen in the table, the average deflection measured in the laboratory for the steel reinforcement, at 40 kN, is 3,95 mm. The calculated deflection with the curvature as an external load is almost equal, 3,80 mm. This indicates that the measurements from the vertical LVDTs were correct. When comparing the strains, the difference is somewhat larger. The measured concrete strain at the height of the reinforcement is 2,64 ‰, while the calculated reinforcement strain is 1,92 ‰. This difference may be due to the fact that the strain isn't measured on the reinforcement in the laboratory, and/or because of inaccurate measures from the horizontal LVDTs.

Overall, the control calculations show that the measured deflection for the steel reinforced beam seems valid. The full calculations are shown in Appendix L.

7.4 Crack spacing

The maximal final crack spacing calculated in chapter 5.2.6 is only calculated for the beams with circular rods. A comparison of these values and the actual maximal final crack spacing from the laboratory is shown in Table 7.12. The average of the crack spacings between the point loads is also shown in the table.

Table 7.12: Comparison of crack spacings

Identification	$S_{r,max,calc}$ [mm]	$S_{r,max,lab}$ [mm]	$S_{r,avg,lab}$ [mm]
B2-2ø12-STEEL	161	161	123
B2-3T-ALU1	not calculated	126	98
B2-3T-ALU2	not calculated	125	100
B1-6ø10-ALU1	122	199	84
B1-6ø10-ALU2	122	148	80
B1-6ø10-ALU3	122	101	80

As the table shows, the calculated value for $S_{r,max}$ is equal to the crack spacing measured in laboratory for the steel reinforced beam. For the aluminium reinforced beams with circular rods, the calculated values for $S_{r,max}$ are equal, while the measured values in the laboratory change due to different setups. By looking at the average values of the crack spaces, these are quite similar for the beams with same reinforcement.

The crack pattern for each beam is shown in Figure 7.16, with measurements on the crack spaces.

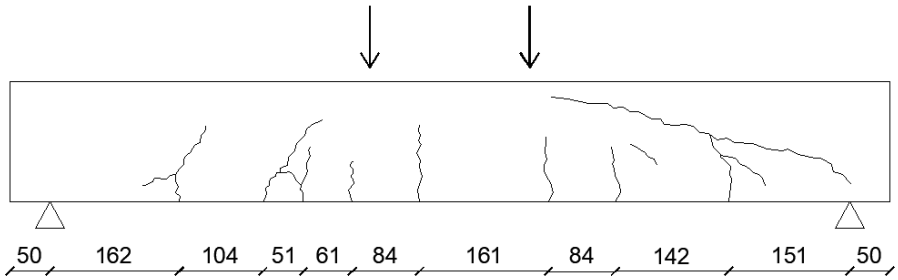

(a) B2-2ø12-STEEL

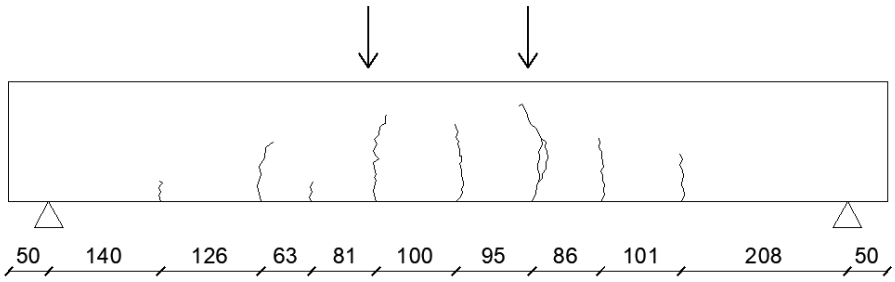

(b) B2-3T-ALU1

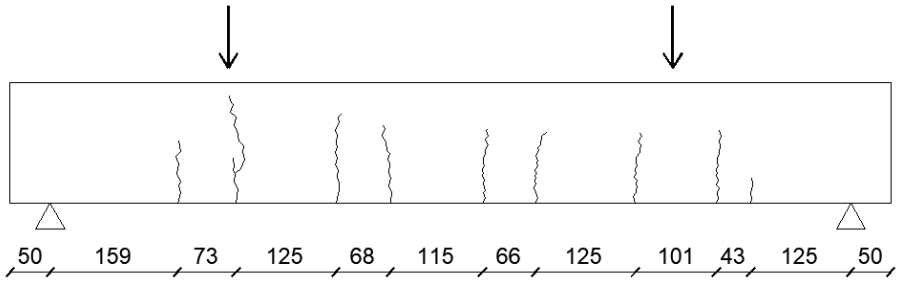

(c) B2-3T-ALU2

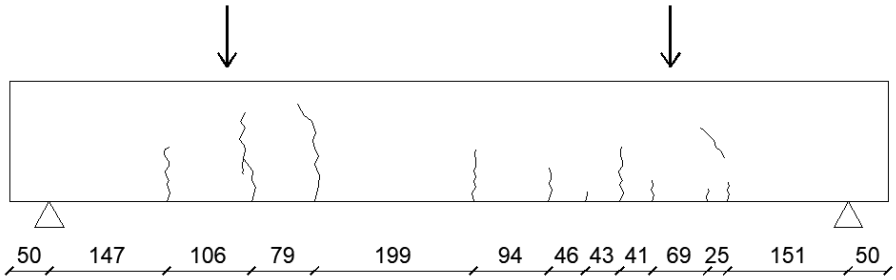

(d) B1-6ø10-ALU1

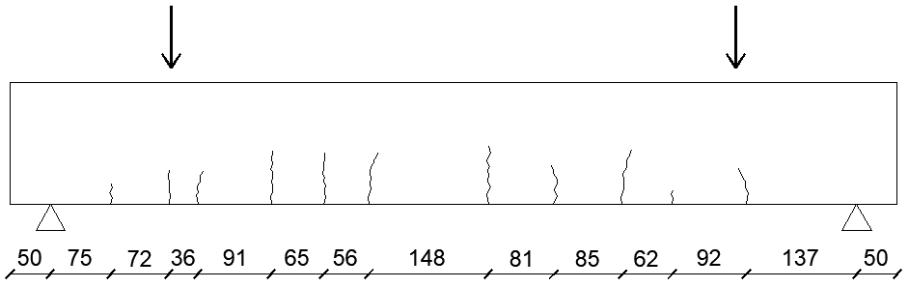

(e) B1-6ø10-ALU2

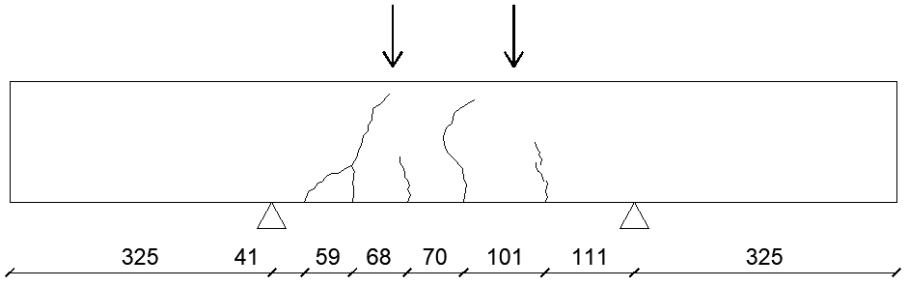

(f) B1-6ø10-ALU3

Figure 7.16: Crack pattern for the beams

For this task, it's interesting to compare the actual crack spaces for each beam with each other, and see how the reinforcement material, reinforcement shape and beam setup affect the crack pattern.

B2-2ø12-STEEL vs. B2-3T-ALU1

These beams are compared because they have the same beam setup with a distance of 200 mm between the point loads, but different reinforcement material. The maximal final crack spacing measured for beam B2-2ø12-STEEL (161 mm)

is larger than for beam B2-3T-ALU1 (126 mm). The average crack spacing measured in the laboratory is also larger for the steel reinforced beam compared to the beam with aluminium reinforcement (123 mm vs. 98 mm). This deviates from the expectations of the crack spaces, as ribbed reinforcement normally distributes the cracks better than reinforcement with smooth surface. The first crack occurs when the concrete tensile stress exceeds the tensile strength of the concrete, as a result of increased reinforcement stress. By further loading, the concrete stress increases along the reinforcement, from zero at the crack, until it exceeds the tensile strength of the concrete again, and forms a new crack. Because the transition of stresses between the concrete and the reinforcement with smooth surface isn't as good as for ribbed reinforcement, it takes longer time before the reinforcement stress is large enough to form new cracks. The crack spaces are therefore normally larger for rebars with smooth surfaces.

Beyond that, one can see that the size of the bending cracks are more even for the beam with steel reinforcement. For the aluminium reinforced beam, the cracks in the middle region of the beam are quite large while the cracks near the supports are smaller. This is expected since the lack of bond between the concrete and the smooth reinforcement results in larger cracks in the middle region, as explained in chapter 2.4.

B2-3T-ALU1 vs. B2-3T-ALU2

These beams are compared because they have the same reinforcement material and reinforcement shape, but different beam setup. Beam B2-3T-ALU1 has its point loads placed with a distance of 200 mm, while the distance for beam B2-3T-ALU2 is increased to 555 mm.

The maximal final crack spacings measured for the beams are almost equal (126 mm vs. 125 mm). The average crack spacings for the beams are also quite similar (98 mm vs. 100 mm), however, the crack development is somewhat different. Beam B2-3T-ALU2 with larger distance between the point loads has more even crack sizes along the beam length than beam B2-3T-ALU1, which has larger cracks in the middle of the beam. This is related to the size of the occurring bending moment and the moment zone. Smaller distance between the point loads gives a larger moment, resulting in large and concentrated cracks. Correspondingly, a larger distance between the point loads gives smaller moment, resulting in smaller and more even crack sizes along the beam length. The similarity of both of the beams is that the crack sizes are largest and most even in the moment zone, and decreases towards the supports.

B2-3T-ALU2 vs. B1-6ø10-ALU1

These beams are compared because they have the same beam setup with a distance of 555 mm between the point loads, same reinforcement material, but different reinforcement shape.

The maximal final crack spacing measured for beam B1-6ø10-ALU1 is larger than for beam B2-3T-ALU2 (199 mm vs. 125 mm). The average crack spacing on the other hand, is larger for beam B2-3T-ALU2 than for beam B1-6ø10-ALU1 (98 mm vs. 84 mm), but with less difference. The cracks are distributed within the same area for both of the beams, but are more even in size for the beam with T-profiles. For the beam with circular profiles, the cracks are longer on the left front side of the beam than on the right front side. This is most likely because of inaccuracy of the beam setup, resulting in asymmetrical load distribution and differences in the crack spaces on the left and right side of the beam.

B1-6ø10-ALU1 vs. B1-6ø10-ALU2 vs. B1-6ø10-ALU3

These beams are compared because they have the same reinforcement material and reinforcement shape, but different beam setup. Beam B1-6ø10-ALU1 has a distance of 555 mm between the point loads, while the distance for beam B1-6ø10-ALU2 is increased to 700 mm. The distance between the point loads is just 150 mm for beam B1-6ø10-ALU3. In difference to all of the other beams, where the distance between the supports is 1000 mm, the distance between the supports for beam B1-6ø10-ALU3 is 450 mm.

The maximal final crack spacing measured for beam B1-6ø10-ALU1 is quite big compared to beam B1-6ø10-ALU2 (199 mm vs. 148 mm). The reason for the big value for beam B1-6ø10-ALU1 is, as mentioned, most likely because of inaccuracy of the beam setup. If both of the beam setups for these beams had been accurate, it had been likely to obtain more similar values for the maximal final crack spacing (as for the beams with aluminium T-profiles). Comparison of the average crack spacing for these two beams is more similar, and is also quite similar to the last beam, beam B1-6ø10-ALU3, even though the distance between the supports is decreased to 450 mm for this beam. Similar to the comparison of the T-profiles, the cracks are most even in size for the beam with largest distance between the point loads, beam B2-6ø10-ALU2. Beam B1-6ø10-ALU3 on the other hand, is the beam with the largest and most uneven crack sizes because of the small distance between the point loads.

A similarity for all the aluminium reinforced beams is that the largest cracks develop within the moment zone, which is where the greatest moment occurs. Fur-

thermore, it can be seen that the cracks become more even in size as the distance between the point loads increases. Comparison of the average crack spacing values between the aluminium reinforced beams with T-shaped profiles and circular profiles, shows that the values for the beams with T-shaped profiles are slightly higher than for the ones with circular profiles. An explanation of this may be that the concrete doesn't have full contact with the reinforcement around the entire surface of the T-profile, resulting in poorer bond compared to the circular reinforcement. The transmission of tensile stresses from the reinforcement to the concrete will then be less for the T-shaped reinforcement. Therefore, it takes longer time before the concrete tensile stress along the reinforcement exceeds the concrete's tensile strength, giving a larger spacing between the cracks. A modification that could improve the contact between the T-profile and the concrete is to round the corners of the profiles.

7.5 Bond between concrete and reinforcement

The differences among the three reinforcement types, disregarding the material they are made of, are the surfaces and cross-sectional shapes.

The steel reinforcement bars differ from the other rebars based on their ribbed surface, which improves the interaction with the concrete. This interaction, traditionally called bond strength, was very poor for the beams with aluminium reinforcement because of the smooth surface. As an attempt to improve the anchoring, as mentioned in chapter 3.5, all the longitudinal reinforcement were connected to transversal bars at each end. This might have made a small difference, but not enough to avoid anchorage failure. Since the transversal bars were tied to the longitudinal reinforcement, the anchoring might have been somewhat better if they had been welded instead. However, it's likely that this wouldn't have had a great influence, and that anchorage failure would still occur. Another attempt was then initiated, which involved changing the distance between the applied loads to minimize the chance of anchorage failure, but this was unsuccessful. As a final attempt, the distance between the supports were decreased to increase the anchoring length. Still, anchorage failure was obtained.

All of the aluminium beams failed according to anchorage, based on bond issues. The beam with steel reinforcement rods, on the other hand, didn't show any sign of having anchorage problems. It's therefore interesting to investigate the bond between the concrete and the reinforcement to get a greater understanding. According to this, two different sets of calculations are performed.

First, the bond factor k_1 is investigated for the aluminium reinforced beam, B1-6ø10-ALU3, by rearranging the three equations below with regard to k_1. These equations are all collected from chapter 3.5, where the different factors are explained.

(I) $$l_{b.rqd} = \frac{A_{al} \cdot \sigma_{sd}}{O_r \cdot f_{bd}}$$

(II) $$f_{bd} = k_1 \cdot f_{td}$$

(III) $$\sigma_{sd} = \frac{V_{cr}}{A_{al} \cdot n}$$

After rearranging and assembling the equations above, and using the anchor length from the laboratory, $l_{b,lab}$, equation (7.4) ended up representing the bond factor.

$$k_{1.lab} = \frac{V_{cr}}{l_{bd.lab} \cdot f_{td} \cdot n \cdot O_r} \tag{7.4}$$

Calculation of the bond factor was only calculated for the last tested beam, B1-6ø10-ALU3, where the anchoring length of the reinforcement was modified from 25 mm to 300 mm.

Second, the ultimate bond stress was calculated for the steel reinforced beam by comparing laboratory result with a calculated value. Equation (7.5) and equation (7.6), given from EC2 were used.

$$f_{bd.lab} = \frac{V_{cr}}{l_{bd.lab} \cdot n \cdot O_s} \tag{7.5}$$

$$f_{bd.calc} = 2,25 \cdot f_{td} \tag{7.6}$$

The results from the bond calculations are presented in Table 7.13, and the full calculations are shown in Appendix M.

Table 7.13: Bond of reinforcement

Identification	$l_{bd.lab}$ [mm]	$k_{1.lab}$	$k_{1.rqd}$	f_{td} [MPa]	$f_{bd.lab}$ [MPa]	$f_{bd.calc}$ [MPa]
B2-2ø12-STEEL	25	-	-	2,16	14,9	4,9
B1-6ø10-ALU3	300	0,27	0,9	2,38	0,65	2,14

Results from Table 7.13 show that the bond factor, k_1, calculated from the laboratory results differs from the bond factor given in the previous concrete standard, NS-EN 3473. Further, this k_1 factor affects the results of the ultimate bond strength since it's included in this formula shown in equation (II) above.

By comparing the results from bond calculations with the beam test results, it clarifies why the aluminium reinforced beams failed according to anchorage. Apparently, the transversal anchorage at the ends weren't enough. Even the last beam tested, with a modified anchor length of 300 mm, failed according anchorage. This indicates that lack of bond, due to the smooth surface, occurred along the entire reinforcement length, and wasn't just caused by slipping at the ends.

On the other hand, the anchorage for the steel reinforced beam showed no sign of weakness. This is reflected in the results presented in Table 7.13, which shows that the ultimate bond strength is more than good enough.

The results indicate that ribbed bars provide a much better bond since the steel reinforced beam didn't fail according to anchorage, although it was anchored at the ends as the other beams, and had an anchoring length of 25 mm. In difference to the aluminium reinforced beams, the anchorage of the steel reinforced beam was welded. However, as mentioned, welding probably wouldn't have had a big impact on the aluminium reinforced beams, and was therefore not the decisive factor.

Chapter 8

Conclusion

In connection with this master thesis, alloyed aluminium reinforcement was used in five of six beams, while ordinary steel reinforcement was used in the last one as a reference beam. The machine used to extrude the aluminium reinforcement couldn't produce ribbed rods, hence the aluminium reinforcement had smooth surface, while the steel reinforcement was ribbed. All the beams were tested in a 4-point bending test. To obtain the correct material properties of the concrete, cylinders were tested. The mean compression strength from the laboratory tests was 25,1 MPa for batch 1 and 23,6 MPa for batch 2. These compression strengths were lower than expected, based on the prescription.

The steel reinforced beam failed due to shear at the calculated failure load, while all the aluminium reinforced beams obtained anchorage failure due to poor bond between the concrete and the smooth surfaces of the aluminium bars. To avoid the anchorage failure, modifications of the test setups were made during testing, without success. Because of anchorage failure for the aluminium reinforced beams, the capacities differed from the corresponding calculated failure loads.

The deflections for all beams were larger than calculated. This can be explained due to poor bond for the aluminium reinforced beams. The steel reinforced beam had good bond conditions, and the large deflections are therefore remarkable. After the laboratory testing, control calculations of the deflection and strains were performed for the steel reinforced beam. The beam stiffness is the only factor based on the cross section affecting the deflection. The reinforcement material and shape can be designed to give a desired total beam stiffness. Thus, the reinforcement material and shape dont directly impact the deflection, as long as the bond requirements are satisfied. Inaccuracies in the laboratory constitute the result a lot when the deflection is in such a small scale.

Calculations of the bond properties, for the steel reinforced beam and one of the

aluminium reinforced beams, were carried out to find the actual bond strength. These calculations show that the bond strength of the aluminium reinforced beam was lower than the given requirements, while it was within the requirements for the steel reinforced beam. Since the aluminium reinforced beams obtained anchorage failure, a final conclusion of whether regulations for steel reinforced concrete could be used for aluminium reinforcement, can not be drawn. However, the mechanical behaviour of the aluminium reinforced beams were similar to the steel reinforced beam, until the reinforcement slipped.

The thesis has shown that it's possible to provide a concrete that chemically function together with alloyed aluminium reinforcement. Further studies with ribbed aluminium reinforcement needs to be carried out to conclude if aluminium can be used as reinforcement in concrete structures.

Chapter 9

Sources of error

There are several sources of error that can influence the outcome of this master thesis, from simple assumptions in calculations to accuracy in laboratory work.

The background theory approaches and calculation assumptions are both basic human errors. It is important to be critical to the choice of sources and read the textbook approaches, to reduce the probability of errors. Underneath, some of the possible errors in conjunction with theory and assumptions are presented:

- It was assumed that requirements in the Eurocode could be used for aluminium reinforcement.
- It was assumed that requirements in the Eurocode could be used for concrete with a large amount of clay.
- Self-weight of the beams are not included in the calculations.
- Assumptions of full bond between reinforcement and concrete.
- The tensile strength of the concrete is ignored for some of the calculations
- The anchorage is assumed to be sufficient because of the transversal rods in each end.

The most common errors in conjunction with laboratory studies are human or machine made. It is important to be concentrated and accurate while executing projects in the laboratory to accomplish the best outcomes and prevent as many errors as possible, and therefore laboratory work demand thoroughly beforehand planning and knowledge within special field.

The level of accuracy that the laboratory equipment/instrument can provide is often

described in an instruction manual or testing manual. On the other hand there could occur sources of error committed to laboratory performance in conjunction with preparation, execution or testing. The sources of error that can develop from instruments and laboratory performance are:

- Nonconformity or error of an instrument
- Nonconformity from placing/using the instrument
- Inaccurate reading of the instrument
- Human preparation of a test
- The casting quality and uneven surfaces
- Various time of hardening
- Anchorage: welded or tied connection
- Spacing in conjunction with concrete cover

Chapter 10

Further Studies

This master thesis constitutes only a part of the development of the DARE2C project, but is an important study which declares that the physical work is feasible. Because this thesis was performed at such an early stage and since it was the first time this aluminium reinforced concrete was used, simple beams and cylinders were produced, tested and analyzed to confirm that the project was heading in the right direction. The concrete with alloyed aluminium reinforcement showed no sign of developing hydrogen gas, which indicates that the chemical part of this project is satisfied.

There are several possibilities for improvements of this small scaled laboratory study. Further studies can be based on different usage of reinforcement, adjustment of the beam dimensions or investigation of the anchoring opportunities. Since the aluminium reinforced beams obtained anchorage failure, the last-mentioned theme is of most interest. First of all, ribbed reinforcement rods should be used in order to improve the bond between the concrete and the reinforcement. Further, the anchorage at the ends can be done in different ways. Increasing the anchoring areas, in an attempt to achieve enough anchoring space, could be one solution. On the other hand there are many improvement possibilities for the anchoring connections, such as welding, tying or additional support of a plate. Further laboratory studies must also establish whether the current Eurocode is valid for aluminium reinforced concrete, or if it's necessary to develop new requirements and regulations.

The DARE2C project aims for larger inventions in the long run, which hopefully could be an environmental door opener for the aluminium industry. The next big step for Hydro, together with the rest of their partners in the DARE2C project, is

to figure out how to use the contaminated sediment red-mud from the aluminium industry in concrete structures, to erase an environmental issue. As mentioned earlier, this isn't possible yet based on stability requirements.

Based on some of the results from this thesis and results from future studies, it can be decided which structure types this low pH concrete with aluminium reinforcement suits the most. The product can be improved by supplying and changing it until the ultimate combination develops.

Bibliography

Connectivity, T., 2017. Linear Variable Differential Transformer - LVDT.

Gjerp, P., Opsahl, M., Smeplass, S., 2014. Betongkompetanse, Grunnleggende betongteknologi. Vol. 2. Byggenæringens forlag.

Justnes, H., 2017. Durable Aluminum Reinforced Environmentally-friendly Concrete Construction - DARE2C, 71–82.

Karlsson, J., 2014. Alternative Reinforcement Approaches - Extended service life of exposed concrete structures, 1–44.

Muttoni, A., Ruiz, M. F., Cavagnis, F., 2017. Background document to subsection 8.2.1 and 8.2.2. Shear in members without shear reinforcement. In: Eurocode 2: Design of concrete structures - Part 1-1: General rules, rules for buildings, bridges and civil engineering structures. Background documents to the second interim draft prEN 1992-1-1:2017-10. EPFL.

SNL, 2018. Betong, Available from: https://snl.no/betong.

Sørensen, S. I., 2013. Betongkonstruksjoner, Beregning og dimensjonering etter Eurokode 2. Vol. 2. Fagbokforlaget.

Standard, N., 1992. Eurocode 2: Design of concrete structures - Part 1-1: General rules and rules for buildings. Standard Norge.

Standard, N., 2009. NS-EN12390: Testing hardened concrete - Part 3: Compressive strength of test specimens. Standard Norge.

Xing, G., Ozbulut, O., 2016. Flexural performance of concrete beams with aluminum alloy bars, 53–65.

Appendix

Appendix list

Appendix A: Total mixing form and grading curves

Proporsjonering av betong

SKANSKA

Prosjekt	102015640 DARE2C
Reseptnummer	Blanding 1 Norcem Anl + kalsinert leire Masseforhold 0,70
Tilsiktet kvalitet	B30 M60
Utført av	Kari Aarstad, SINTEF Byggforsk
Dato	16.02.2018

Initialparametre	**Verdi**
m = v/(c+Σkp)	0,70
Luftinnhold	2,0 %

Sementtype	**Andel**	**Andel klinker**	**Andel FA**	**Andel slagg**	**[kg/m^3]**	**Alkalier**	**Klorider**
Norcem Anlegg	100,0 %	100,0 %	0,0 %	0,0 %	3140	0,6 %	0,0 %
	0,0 %	100,0 %	0,0 %	0,0 %	1000	0,0 %	0,0 %
	0,0 %	100,0 %	0,0 %	0,0 %	1000	0,0 %	0,0 %

Tilsetningsmaterialer	**Type**	**Andel (av b)**	**k**	**[kg/m^3]**	**Alkalier**	**Klorider**
Kalsinet leire, A-5011	Silika	55,0 %	1,0	2660	0,0 %	0,0 %
	FA	0,0 %	1,0	2310	2,1 %	0,0 %
	Slagg	0,0 %	0,6	1000	1,0 %	0,3 %

Tilsetningsstoff	**% av b**	**[kg/m^3]**	**Tørrstoff**	**[kg/m^3] TS**	**Alkalier**	**Klorider**
Sika Viscocrete RMC-315 A-4871	0,6 %	1040	18,0 %	1272	0,6 %	0,0 %
Løselig magnesiumsalt	6,0 %	1000	100,0 %	1000	0,0 %	0,0 %
	0,0 %	1000	100,0 %	1000	0,0 %	0,0 %
	0,0 %	1000	100,0 %	1000	0,0 %	0,0 %

Fiber	**Vol %**	**[kg/m3]**
	0,0 %	7800
	0,0 %	1050

Matriks	**Verdi**
Ønsket matriksvolum [l/m^3]	380
Oppnådd matriksvolum [l/m^3]	382
Klinkerandel i bindemiddel	45,0 %
Total FA- andel av bindemiddel	0,0 %
Total slaggandel av bindemiddel	0,0 %
Volum sementlim [l/m^3]	355,3
Effektivt vanninnhold [l/m^3]	223,9
v/p	0,57
Effektivt bindemiddel [kg/m^3]	320
Totalt bindemiddel [kg/m^3]	320

Beregn

Kommentarer:
Gule felt fylles ut, grønne beregnes.
Rød bakgrunn i cellen for oppnådd matriksvolum indikerer at beregningsmakroen ikke er kjørt, og at det derfor ikke er samsvar mellom ønsket og oppnådd matriksvolum. Dette vil også gi blanke felt i reseptskjemaet.

Blandeskjema Batch 7 SKANSKA

Prosjekt	102015640 DARE2C
Reseptnummer	Blanding 1 Norcem Anl + kalsinert leire Masseforhold 0,70
Tilsiktet kvalitet	B30 M60

Blandevolum	158 liter
Dato:	
Tidspunkt for vanntilsetning:	
Ansvarlig:	
Utført av:	

Materialer	**Resept** kg/m³	**Sats** kg	**Fukt*** %	**Korr.** kg	**Oppveid**** kg	
Norcem Anlegg	143,9	22,738			22,738	22,74
	0,0	0,000			0,000	
	0,0	0,000			0,000	
Kalsinet leire, A-5011	175,9	27,790	0,0	0,000	27,790	27,78
0	0,0	0,000			0,000	
	0,0	0,000			0,000	
Fritt vann	223,9	35,370		-4,821	30,549	31,453 31,46
Absorbert vann	5,7	0,904			0,904	
0-8 Årdal A-4751	0,0	0,000	0,0	0,000	0,000	
8-16 Årdal A-4223	0,0	0,000	0,0	0,000	0,000	
Ardal0-8mm 08-16	970,9	153,400	2,4	3,700	157,100	157,1
Årdal 8-16 02-18	702,4	110,972	0,8	0,872	111,844	111,85
	0,0	0,000	0,0	0,000	0,000	
	0,0	0,000	0,0	0,000	0,000	
	0,0	0,000	0,0	0,000	0,000	
	0,0	0,000	0,0	0,000	0,000	
	0,0	0,000	0,0	0,000	0,000	
	0,0	0,000	0,0	0,000	0,000	
Sika Viscocrete RMC-315 A-4871	1,9	0,303	82	0,249	0,303	0,205
Løselig magnesium salt	19,2	3,032	0	0,000	3,032	3,032
	0,0	0,000	0	0,000	0,000	
	0,0	0,000	0	0,000	0,000	
	0,0	0,000			0,000	
	0,0	0,000			0,000	

*Se fotnote på delark "Resept" ** NB! Våte mengder, også for silikaslurry

Fersk betong					
Tid etter vanntilsetning					
Synkmål					
Utbredelsesmål					
Luft					
Densitet					

Prøvestykker (antall)					
Utstøpningstidspunkt					
Terninger					
150x300 sylindre					
100x200 sylindre					

Blandeskjema Batch 2 SKANSKA

Prosjekt	102015640 DARE2C
Reseptnummer	Blanding 1 Norcem Anl + kalsinert leire Masseforhold 0,70
Tilsiktet kvalitet	B30 M60

Blandevolum	158 liter
Dato:	
Tidspunkt for vanntilsetning:	
Ansvarlig:	
Utført av:	

Materialer	**Resept** kg/m³	**Sats** kg	**Fukt*** %	**Korr.** kg	**Oppveid**** kg	
Norcem Anlegg	143,9	22,738			22,738	22,74
	0,0	0,000			0,000	
	0,0	0,000			0,000	
Kalsinet leire, A-5011	175,9	27,790	0,0	0,000	27,790	27,78
0	0,0	0,000			0,000	
	0,0	0,000			0,000	
Fritt vann	223,9	35,370		-4,821	30,549	31,453 31,46
Absorbert vann	5,7	0,904			0,904	
0-8 Årdal A-4751	0,0	0,000	0,0	0,000	0,000	
8-16 Årdal A-4223	0,0	0,000	0,0	0,000	0,000	
Ardal0-8mm 08-16	970,9	153,400	2,4	3,700	157,100	157,1
Årdal 8-16 02-18	702,4	110,972	0,8	0,872	111,844	111,85
	0,0	0,000	0,0	0,000	0,000	
	0,0	0,000	0,0	0,000	0,000	
	0,0	0,000	0,0	0,000	0,000	
	0,0	0,000	0,0	0,000	0,000	
	0,0	0,000	0,0	0,000	0,000	
	0,0	0,000	0,0	0,000	0,000	
Sika Viscocrete RMC-315 A-4871	1,9	0,303	82	0,249	0,303	0,171
Løselig magnesium salt	19,2	3,032	0	0,000	3,032	3,032
	0,0	0,000	0	0,000	0,000	
	0,0	0,000	0	0,000	0,000	
	0,0	0,000			0,000	
	0,0	0,000			0,000	

*Se fotnote på delark "Resept" ** NB! Våte mengder, også for silikaslurry

Fersk betong					
Tid etter vanntilsetning					
Synkmål					
Utbredelsesmål					
Luft					
Densitet					

Prøvestykker (antall)					
Utstøpningstidspunkt					
Terninger					
150x300 sylindre					
100x200 sylindre					

Sammensatt tilslag

Fraksjon	Navn	Densitet [kg/m^3]	Abs. fukt [%]	Alk. reakt. Sv[%]	Klorider [%]	Andel volum	Andel vekt	Bruk
I	0-8 Årdal A-4751	2670	0.3	0.0	0.00	0.000	0.000	
II	8-16 Årdal A-4223	2690	0.4	0.0	0.00	0.000	0.000	
III	Ardal0-8mm 08-16	2670	0.3	0.0	0.00	0.582	0.580	ok
IV	Årdal 8-16 02-18	2690	0.4	0.0	0.00	0.418	0.420	ok
V		2700	0.0	0.0	0.00	0.000	0.000	
VI		2700	0.0	0.0	0.00	0.000	0.000	
VII		2700	0.0	0.0	0.00	0.000	0.000	
VIII		2700	0.0	0.0	0.00	0.000	0.000	
IX		2700	0.0	0.0	0.00	0.000	0.000	
X		2700	0.0	0.0	0.00	0.000	0.000	
Sammensatt		2678		0.0	0.00	1.000	1.000	

Finhetsmoduler	
FM_{vekt} =	4.58
FM_{vol} =	4.57
FM_{ref} =	8.50
FMg =	5.55

Tilpass til ref. gradering, Ctrl T

Sett ref. gradering, Ctrl R

Tilpass til FMg, Ctrl F

Sikterest vol.[%]	Sikterest vekt [%]	Gjennomgang vol.[%]	Gjennomgang vekt [%]	Ref. SR [vol. %]	Ref. grad. [vol. %]	Vekt ved tilpasning
0.0	0.0	100.0	100.0	100.0		1
0.0	0.0	100.0	100.0	100.0		1
6.1	6.1	93.9	93.9	100.0		1
26.3	26.4	73.7	73.6	100.0		1
39.8	40.0	60.2	60.0	100.0		1
53.1	53.3	46.9	46.7	100.0		1
63.5	63.6	36.5	36.4	100.0		1
73.7	73.8	26.3	26.2	100.0		2
83.0	83.0	17.0	17.0	100.0		2
90.4	90.4	9.6	9.6	100.0		2
95.7	95.7	4.3	4.3	100.0		2
98.4	98.4	1.6	1.6	100.0		2

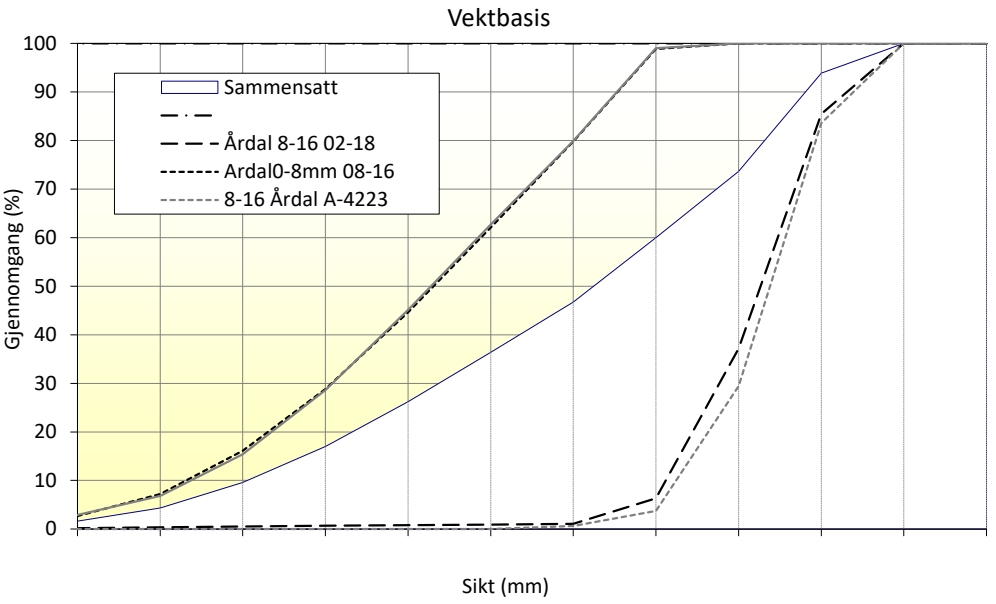
Vektbasis
100
90
80
70
60
50
40
30
20
10
0
Gjennomgang (%)
Sammensatt
Årdal 8-16 02-18
Ardal0-8mm 08-16
8-16 Årdal A-4223
Sikt (mm)

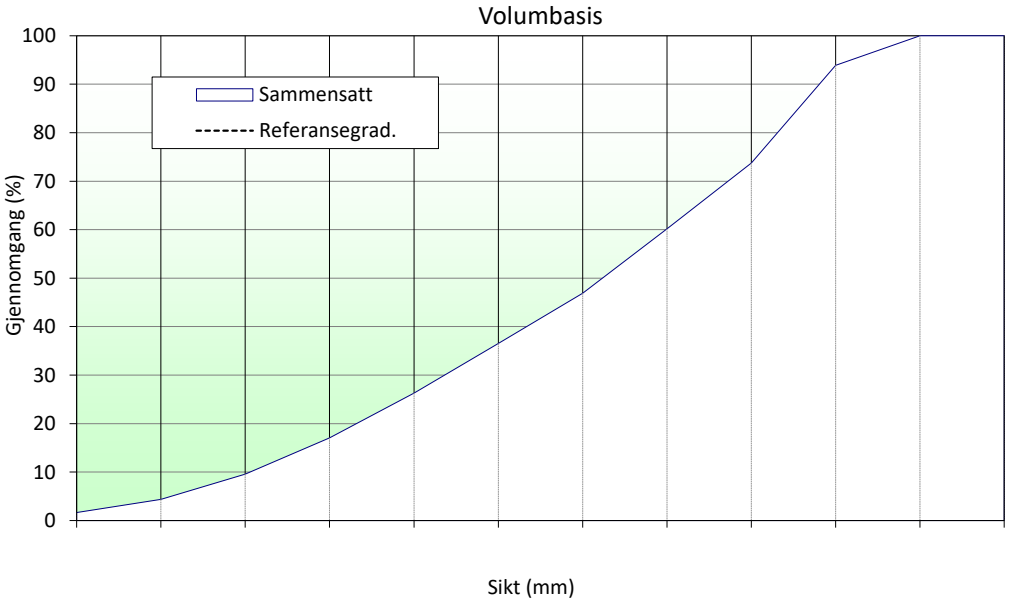
Volumbasis
100
90
80
70
60
50
40
30
20
10
0
Gjennomgang (%)
Sammensatt
Referansegrad.
Sikt (mm)

Fraksjon III

Type:	Ardal0-8mm 08-16
Dato:	8/12/2016
FM =	3.16

Åpning	Sikterest (g)		Sikterest (%)	Gjennom-gang (%)
	1	2		
32	0	0	0.0	100.0
22.4	0	0	0.0	100.0
16	0	0	0.0	100.0
11.2	0	0	0.0	100.0
8	9.8	9.8	1.1	98.9
4	175	175	20.2	79.8
2	329	329	37.9	62.1
1	480	480	55.4	44.6
0.5	617	617	71.2	28.8
0.25	727	727	83.9	16.1
0.125	805	805	92.8	7.2
0.063	844	844	97.3	2.7
Bunn	867	867		

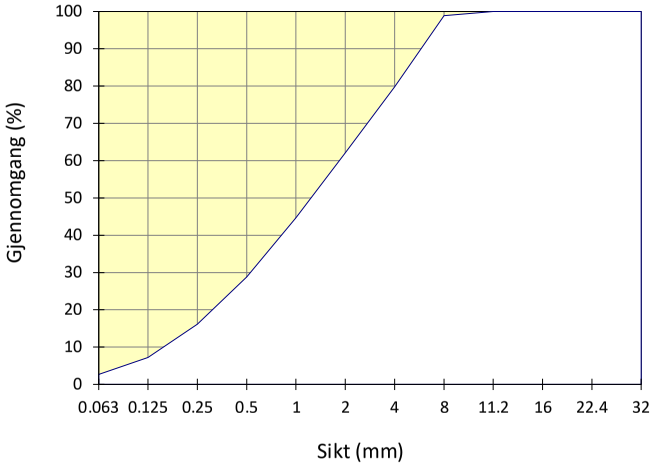

Fraksjon IV

Type:	Årdal 8-16 02-18
Dato:	09.02.2018
FM =	6,54

Åpning	Sikterest (g)		Sikterest (%)	Gjennom-gang (%)
	1	2		
32	0	0	0,0	100,0
22,4	0	0	0,0	100,0
16	278,5	278,5	14,5	85,5
11,2	1204,2	1204,2	62,8	37,2
8	1795,7	1795,7	93,7	6,3
4	1897	1897	98,9	1,1
2	1900	1900	99,1	0,9
1	1902	1902	99,2	0,8
0,5	1904	1904	99,3	0,7
0,25	1908	1908	99,5	0,5
0,125	1911	1911	99,7	0,3
0,063	1914	1914	99,8	0,2
Bunn	1917	1917		

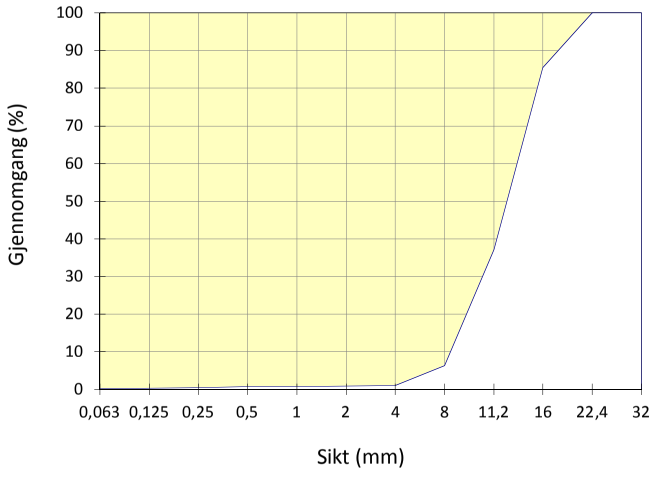

Appendix B: Beam design

B2-2Ø12-STEEL

Beam design

h [mm]	b [mm]	f_{cm} [MPa]	f_{ct} [MPa]	E_c [MPa]	Rod diameter [mm^2]
150	250	30	2.9	33000	12

number of rods	A_r [mm^2]	f_{ym} [MPa]	E_r [MPa]	A_{rb} [mm^2]
2	226	550	200000	535

α	under-/ over reinforced	ε_r	d [mm]	αd [mm]	M_{Rd} [kNm]
0.174	under	0.017	119	20.7	13.8

$V_{Rd,current}$ [kN]	V_{Ed} [kN]	$V_{Rd,new}$ [kN]	$V_{Rd,max}$ [mm]	P_M [kN]	P_V [kN]
30.4	30.4	35.9	235.6	68.9	60.7

Deflelctions and crack load

ρ_l	η	$(\alpha d)_I$ [mm]	α_{II}	I_{rI} x10^6 [mm^4]	I_{cI} x10^6 [mm^4]
0.008	6.06	76.6	0.261	0.4	70.4

$(EI)_I$ x10^9 [Nmm^2]	I_c x10^6 [mm^4]	$(EI)_{II}$ x10^9 [Nmm^2]	$(\alpha d)_{II}$ [mm]	M_{crack} [kNm]	P_{crack} [kN]
2405	13.1	432.3	31.1	2.88	14.4

δ_I [mm]	δ_{II} [mm]	$\delta_{failure}$ [mm]	L_s [mm]	L [mm]	L_m [mm]
0.12	0.65	2.76	400	1000	200

B2-3T-ALU1 and B2-3T-ALU2

Beam design

h [mm]	b [mm]	f_{cm} [MPa]	f_{ct} [MPa]	E_c [MPa]	Rod area [mm^2]
150	250	30	2.9	33000	156

number of rods	A_r [mm^2]	Rod neutral axis, $z_{T.P.}$ [mm]	f_{ym} [MPa]	E_r [MPa]	A_{rb} [mm^2]
3	468	9.96	250	70000	1367

α	under-/ over reinforced	ε_r	d [mm]	αd [mm]	M_{Rd} [kNm]
0.170	under	0.017	115	19.5	12.5

$V_{Rd,current}$ [kN]	V_{Ed} [kN]	$V_{Rd,new}$ [kN]	$V_{Rd,max}$ [mm]	P_M [kN]	P_V [kN]
37.8	31.4	29.9	227.8	62.7	75.7

Deflelctions and crack load

ρ_I	η	$(\alpha d)_I$ [mm]	α_{II}	I_{rI} x10^6 [mm^4]	I_{cI} x10^6 [mm^4]
0.016	2.12	76.0	0.230	0.7	70.4

$(EI)_I$ x10^9 [Nmm^2]	I_c x10^6 [mm^4]	$(EI)_{II}$ x10^9 [Nmm^2]	$(\alpha d)_{II}$ [mm]	M_{crack} [kNm]	P_{crack} [kN]
2371	9.33	308.0	26.5	2.82	14.1

δ_I [mm]	δ_{II} [mm]	$\delta_{failure}$ [mm]	L_s [mm]	L [mm]	L_m [mm]
0.12	0.90	4.01	400	1000	200

B1-6Ø10-ALU1, B1-6Ø10-ALU2 and B1-6Ø10-ALU3

Beam design

h [mm]	b [mm]	f_{cm} [MPa]	f_{ct} [MPa]	E_c [MPa]	Rod diameter [mm^2]
150	250	30	2.9	33000	10

number of rods	A_r [mm^2]	f_{ym} [MPa]	E_r [MPa]	A_{rb} [mm^2]
6	471	250	70000	1186

α	under-/ over reinforced	ε_r	d [mm]	αd [mm]	M_{Rd} [kNm]
0.164	under	0.018	120	19.6	13.2

$V_{Rd,current}$ [kN]	V_{Ed} [kN]	$V_{Rd,new}$ [kN]	$V_{Rd,max}$ [mm]	P_M [kN]	P_V [kN]
39.0	33.0	32.6	237.6	66.1	78.0

Deflelctions and crack load

ρ_l	η	$(\alpha d)_I$ [mm]	α_{II}	I_{rI} x10^6 [mm^4]	I_{cI} x10^6 [mm^4]
0.016	2.12	76.2	0.227	0.9	70.4

$(EI)_I$ x10^9 [Nmm^2]	I_c x10^6 [mm^4]	$(EI)_{II}$ x10^9 [Nmm^2]	$(\alpha d)_{II}$ [mm]	M_{crack} [kNm]	P_{crack} [kN]
2385	10.3	339.4	27.2	2.84	14.2

δ_I [mm]	δ_{II} [mm]	$\delta_{failure}$ [mm]	L_s [mm]	L [mm]	L_m [mm]
0.12	0.82	3.83	400	1000	200

Appendix C: Anchorage

Anchor of reinforcement- ahead of laboratory testing

Calculations below are performed according to Eurocode 2: NS-EN 1992 -1-1:
Design of concrete structures (EC2) and the previous used standard NS-EN 3473.

B2-2ø12-STEEL

$\phi := 12mm$ — *Rod diameter*

$A_s := \frac{\pi \cdot \phi^2}{4} = 113 \cdot mm^2$ — *Area of a steel reinforcement rod*

$O_s := \pi \cdot \phi = 38 \cdot mm$ — *Circumference*

$l_{bd.lab} := 25mm \quad c := 25mm \quad s := 176mm$ — *Anchor length, concrete cover and spacing between reinforcement*

$n := 2$ — *Number of reinforcement bars*

Stress in reinforcement with given anchor length:

$f_{td} := 2.9MPa$ — *Tensile strength of the concrete*

$f_{bd} := 2.25 \cdot f_{td} = 6.5 \cdot MPa$ — eq (8.2) in EC2

$\sigma_{sd.max} := \frac{l_{bd.lab} \cdot f_{bd} \cdot O_s}{A_s} = 54.4 \cdot MPa$ — eq (8.3) in EC2

Anchor length required, based on the stress at beam failure:

$P_{cr} := 60.7kN$ — *Failure load from calculations*

$V_{cr} := \frac{P_{cr}}{2} = 30 \cdot kN$ — *Total shear load in the reinforcement*

$\sigma_{sd} := \frac{V_{cr}}{A_s \cdot n} = 134.2 \cdot MPa$ — *Stress in each reinforcement rod*

$l_{b.rqd..} := \frac{\sigma_{sd} \cdot A_s}{f_{bd} \cdot O_s} = 62 \cdot mm$ — eq (8.3) in EC2

B2-3T-ALU1 and B2-3T-ALU2

$A_{al} := 156mm^2$ — *Area of an aluminium reinforcement rod*

$O_{al} := 76mm$ — *Circumference*

$l_{bd.lab} := 25mm \quad c := 25mm \quad s := 66mm$ — *Anchor length, concrete cover and spacing between reinforcement*

$n := 3$ — *Number of reinforcement rods*

Stress in reinforcement with given anchor length:

$k_1 := 0.9 \quad f_{td} := 2.9MPa$ — *Factor based on reinf. surface and tensile strength of the concrete*

$f_{bd} := k_1 \cdot f_{td} = 2.6 \cdot MPa$ — pt [12.8.5.] in NS-EN3473

$$\sigma_{sd.max} := \frac{l_{bd.lab} \cdot f_{bd} \cdot O_{al}}{A_{al}} = 31.8 \cdot MPa$$ — eq (8.3) in EC2

Anchor length required, based on the stress at beam failure:

$P_{cr} := 62.7kN$ — *Failure load from calculations*

$V_{cr} := \frac{P_{cr}}{2} = 31 \cdot kN$ — *Total shear load in the reinforcement*

$$\sigma_{sd.} := \frac{V_{cr}}{A_{al} \cdot n} = 67 \cdot MPa$$ — *Stress in each reinforcement rod*

$$l_{b.rqd.} := \frac{\sigma_{sd.} \cdot A_{al}}{f_{bd} \cdot O_{al}} = 53 \cdot mm$$ — eq (8.3) in EC2

B1-6ø10-ALU1, B1-6ø10-ALU2 and B1-6ø10-ALU3

$\phi := 10mm$ — *Rod diameter*

$A_{al} := \frac{\pi \cdot \phi^2}{4} = 79 \cdot mm^2$ — *Area of an aluminium reinforcement rod*

$O_{al} := \pi \cdot \phi = 31 \cdot mm$ — *Circumference*

$l_{bd.lab} := 25mm \quad c := 25mm \quad s := 28mm$ — *Anchor length, concrete cover and spacing between reinforcement*

$n := 6$ — *Number of reinforcement rods*

Stress in reinforcement with given anchor length:

$k_{1.} := 0.9 \quad f_{td} := 2.9MPa$ — *Factor based on reinf. surface and tensile strength of the concrete*

$f_{bd} := k_{1.} \cdot f_{td} = 2.6 \cdot MPa$ — pt [12.8.5.] in NS-EN3473

$\sigma_{sd.max} := \frac{l_{bd.lab} \cdot f_{bd} \cdot O_{al}}{A_{al}} = 26.1 \cdot MPa$ — eq (8.3) in EC2

Anchor length required, based on the stress at beam failure:

$P_{cr} := 66.1kN$ — *Failure load from calculations*

$V_{cr} := \frac{P_{cr}}{2} = 33.05 \cdot kN$ — *Total shear load in the reinforcement*

$\sigma_{sd} := \frac{V_{cr}}{A_{al} \cdot n} = 70.1 \cdot MPa$ — *Stress in each reinforcement rod*

$l_{b.req} := \frac{\sigma_{sd} \cdot A_{al}}{f_{bd} \cdot O_{al}} = 67 \cdot mm$ — eq (8.3) in EC2

Appendix D: Compression zone height

B2-2Ø12-STEEL

Load - compressive zone height

h [mm]	b [mm]	f_c [MPa]	f_{ym} [MPa]	A_r [mm2]	E_r [N/mm2]
150	250	30	550	226	200000

f_c/ε_{c3} [MPa]	$(\alpha d)_{failure}$ [mm]	$(\alpha d)_{II}$ [mm]	ε_{cu2}	ε_y	L_s [mm]
17143	20.7	31.1	0.00350	0.00275	400

αd [mm]	$\varepsilon_{c,top}$	T_c [N]	S [N]	ε_r	z [mm]
20.7	0.00440	124407	124407	0.02113	111.5
22	0.00356	124407	124407	0.01584	111.4
22.1	0.00350	124407	124407	0.01549	111.4
24	0.00283	124407	124407	0.01133	111.2
26	0.00242	124407	124407	0.00874	110.8
28	0.00215	124407	124407	0.00705	110.4
30	0.00196	124407	124407	0.00587	109.9
31.1	0.00188	124407	124407	0.00536	109.6

M [kNm]	P [kN]	Pcrack [kN]
13.9	69.4	14.4
13.9	69.3	
13.9	69.3	
13.8	69.1	
13.8	68.9	
13.7	68.7	
13.7	68.4	
13.6	68.2	

B2-3T-ALU1 and B2-3T-ALU2

Load - compressive zone height

h [mm]	b [mm]	f_c [MPa]	f_{ym} [MPa]	A_r [mm2]	E_r [N/mm2]
150	250	30	250	468	70000

f_c/ε_{c3} [MPa]	$(\alpha d)_{failure}$ [mm]	$(\alpha d)_{II}$ [mm]	ε_{cu2}	ε_y	L_s [mm]
17143	19.5	26.5	0.00350	0.00357	400

αd [mm]	$\varepsilon_{c,top}$	T_c [N]	S [N]	ε_r	z [mm]
19.5	0.00438	117000	117000	0.02255	112.0
20	0.00398	117000	117000	0.01989	112.0
20.8000008	0.00350	117000	117000	0.01669	111.9
21	0.00340	117000	117000	0.01604	111.9
22	0.00301	117000	117000	0.01340	111.8
23	0.00272	117000	117000	0.01147	111.6
24	0.00250	117000	117000	0.01000	111.4
25	0.00233	117000	117000	0.00884	111.3
26	0.00219	117000	117000	0.00791	111.0
26.5	0.00213	117000	117000	0.00751	110.9

M [kNm]	P [kN]	Pcrack [kN]
13.1	65.5	14.1
13.1	65.5	
13.1	65.5	
13.1	65.5	
13.1	65.4	
13.1	65.3	
13.0	65.2	
13.0	65.1	
13.0	65.0	
13.0	64.9	

B1-6Ø10-ALU1, B1-6Ø10-ALU2 and B1-6Ø10-ALU3

Load - compressive zone height

h [mm]	b [mm]	f_c [MPa]	f_{ym} [MPa]	A_r [mm2]	E_r [N/mm2]
150	250	30	250	471	70000

f_c/ε_{c3} [MPa]	$(\alpha d)_{failure}$ [mm]	$(\alpha d)_{II}$ [mm]	ε_{cu2}	ε_y	L_s [mm]
17143	19.6	27.2	0.00350	0.00357	400

αd [mm]	$\varepsilon_{c,top}$	T_c [N]	S [N]	ε_r	z [mm]
19.6	0.00441	117810	117810	0.02257	112.0
20	0.00408	117810	117810	0.02039	112.0
20.9	0.00350	117810	117810	0.01655	111.9
21	0.00347	117810	117810	0.01637	111.8
22	0.00306	117810	117810	0.01363	111.7
23	0.00276	117810	117810	0.01164	111.6
24	0.00253	117810	117810	0.01013	111.4
25	0.00235	117810	117810	0.00895	111.2
26	0.00221	117810	117810	0.00799	111.0
27	0.00209	117810	117810	0.00721	110.8
27.2	0.00207	117810	117810	0.00707	110.7

M [kNm]	P [kN]	Pcrack [kN]
13.2	66.0	14.2
13.2	65.9	
13.2	65.9	
13.2	65.9	
13.2	65.8	
13.1	65.7	
13.1	65.6	
13.1	65.5	
13.1	65.4	
13.1	65.3	
13.0	65.2	

Appendix E: Crack spacing

Crack spacing- ahead of laboratory testing

Calculations below are based on Eurocode 2: NS-EN 1992-1-1:
Design of concrete structures (EC2)

$h := 150mm$

$b := 250mm$

$c = 25 \cdot mm$

B2-2ø12-STEEL

$\phi := 12mm$	*Rod diameter*
$s = 176 \cdot mm$	*Reinforcement spacing*
$n := 6$	*Number of rods*
$\alpha d := 20.7mm$	*Compressive zone height*
$A_r := \pi \cdot \left(\frac{\phi}{2}\right)^2 \cdot n = 679 \cdot mm^2$	*Reinforcement area*
$5\left(c + \frac{\phi}{2}\right) = 155 \cdot mm$	< 176 mm, eq (7.14) in EC2 can be used to calculate the maximum final crack spacing
$S_{r.max} := 1.3(h - \alpha d) = 168 \cdot mm$	eq (7.14) in EC2

B1-6ø10-ALU1, B1-6ø10-ALU2 and B1-6ø10-ALU3

$\phi := 10mm$ *Rod diameter*

$s = 28 \cdot mm$ *Reinforcement spacing*

$n := 6$ *Number of rods*

$\alpha d := 19.6mm$ *Compressive zone height*

$A_r := \pi \cdot \left(\frac{\phi}{2}\right)^2 \cdot n = 471 \cdot mm^2$ *Reinforcement area*

$5\left(c + \frac{\phi}{2}\right) = 150 \cdot mm$ < 28 mm, eq (7.11) in EC2 can be used to calculate the maximum final crack spacing

$k_1 := 0.8$ because of high bond bars

$k_2 := 0.5$ because of bending

$k_3 := 3.4$ given in NA.7.3.4(3)

$k_4 := 0.425$ given in NA.7.3.4(3)

$h_{c.eff} := \min\left[2.5(h - \alpha d), \frac{h - \alpha d}{3}, \frac{h}{2}\right] = 43 \cdot mm$

$A_{c.eff} := b \cdot h_{c.eff} = 10867 \cdot mm^2$

$\rho_{p.eff} := \frac{A_r}{A_{c.eff}} = 0.043$

$S_{r.max} := k_3 \cdot c + k_1 \cdot k_2 \cdot k_4 \cdot \frac{\phi}{\rho_{p.eff}} = 124 \cdot mm$ eq (7.11) in EC2

Appendix F: Beam design- modification

B2-2Ø12-STEEL

Beam design

h [mm]	b [mm]	f_c [MPa]	f_{ct} [MPa]	E_c [MPa]	Rod diameter [mm^2]
150	250	23.6	2.155	19676	12

number of rods	A_r [mm^2]	f_{ym} [MPa]	E_r [MPa]	A_{rb} [mm^2]
2	226	550	200000	421

α	under-/ over reinforced	ε_r	d [mm]	αd [mm]	M_{Rd} [kNm]
0.221	under	0.012	119	26.4	13.5

$V_{Rd,current}$ [kN]	V_{Ed} [kN]	$V_{Rd,new}$ [kN]	$V_{Rd,max}$ [mm]	P_M [kN]	P_V [kN]
28.0	28.0	32.9	190.7	67.5	56.1

Deflelctions and crack load

ρ	η	$(\alpha d)_I$ [mm]	α_{II}	I_{rI} $x10^6$ [mm^4]	I_{cI} $x10^6$ [mm^4]
0.008	10.16	77.5	0.323	0.4	70.6

$(EI)_I$ $x10^9$ [Nmm^2]	I_c $x10^6$ [mm^4]	$(EI)_{II}$ $x10^9$ [Nmm^2]	$(\alpha d)_{II}$ [mm]	M_{crack} [kNm]	P_{crack} [kN]
1466	19.7	386.7	38.5	2.22	11.1

δ_I [mm]	δ_{II} [mm]	$\delta_{failure}$ [mm]	L_s [mm]	L [mm]	L_m [mm]
0.15	0.56	2.85	400	1000	200

B2-3T-ALU1

Beam design

h [mm]	b [mm]	f_c [MPa]	f_{ct} [MPa]	E_c [MPa]	Rod area [mm^2]
150	250	23.6	2.155	19676	156

number of rods	A_r [mm^2]	Rod neutral axis, $z_{C.G.}$ [mm]	f_{ym} [MPa]	E_r [MPa]	A_{rb} [mm^2]
3	468	9.96	274	70000	935

α	under-/ over reinforced	ε_r	d [mm]	αd [mm]	M_{Rd} [kNm]
0.236	under	0.011	115	27.2	13.4

$V_{Rd,current}$ [kN]	V_{Ed} [kN]	$V_{Rd,new}$ [kN]	$V_{Rd,max}$ [mm]	P_M [kN]	P_V [kN]
34.9	33.4	27.3	184.4	66.8	69.9

Deflelctions and crack load

ρ	η	$(\alpha d)_I$ [mm]	α_{II}	I_{rI} $x10^6$ [mm^4]	I_{cI} $x10^6$ [mm^4]
0.016	3.56	76.7	0.287	0.7	70.4

$(EI)_I$ $x10^9$ [Nmm^2]	I_c $x10^6$ [mm^4]	$(EI)_{II}$ $x10^9$ [Nmm^2]	$(\alpha d)_{II}$ [mm]	M_{crack} [kNm]	P_{crack} [kN]
1434	14.2	279.4	33.0	2.14	10.7

δ_I [mm]	δ_{II} [mm]	$\delta_{failure}$ [mm]	L_s [mm]	L [mm]	L_m [mm]
0.15	0.75	4.70	400	1000	200

B2-3T-ALU2

Beam design

h [mm]	b [mm]	f_c [MPa]	f_{ct} [MPa]	E_c [MPa]	Rod area [mm^2]
150	250	23.6	2.155	19676	156

number of rods	A_r [mm^2]	Rod neutral axis, $z_{C.G.}$ [mm]	f_{ym} [MPa]	E_r [MPa]	A_{rb} [mm^2]
3	468	9.96	274	70000	935

α	under-/ over reinforced	ε_r	d [mm]	αd [mm]	M_{Rd} [kNm]
0.236	under	0.011	115	27.2	13.4

$V_{Rd,current}$ [kN]	V_{Ed} [kN]	$V_{Rd,new}$ [kN]	$V_{Rd,max}$ [mm]	P_M [kN]	P_V [kN]
36.1	36.1	34.4	184.4	120.1	72.2

Deflelctions and crack load

ρ	η	$(\alpha d)_I$ [mm]	α_{II}	I_{rI} x10^6 [mm^4]	I_{cI} x10^6 [mm^4]
0.016	3.56	76.7	0.287	0.7	70.4

$(EI)_I$ x10^9 [Nmm^2]	I_c x10^6 [mm^4]	$(EI)_{II}$ x10^9 [Nmm^2]	$(\alpha d)_{II}$ [mm]	M_{crack} [kNm]	P_{crack} [kN]
1434	14.2	279.4	33.0	2.14	19.3

δ_I [mm]	δ_{II} [mm]	$\delta_{failure}$ [mm]	L_s [mm]	L [mm]	L_m [mm]
0.17	0.90	3.36	222.5	1000	555

B1-6Ø10-ALU1

Beam design

h [mm]	b [mm]	f_c [MPa]	f_{ct} [MPa]	E_c [MPa]	Rod diameter [mm^2]
150	250	25.1	2.375	20868	10

number of rods	A_r [mm^2]	f_{ym} [MPa]	E_r [MPa]	A_{rb} [mm^2]
6	471	274	70000	1038

α	under-/ over reinforced	ε_r	d [mm]	αd [mm]	M_{Rd} [kNm]
0.214	under	0.013	120	25.72	14.2

$V_{Rd,current}$ [kN]	V_{Ed} [kN]	$V_{Rd,new}$ [kN]	$V_{Rd,max}$ [mm]	P_M [kN]	P_V [kN]
39.6	39.6	37.9	203.2	127.3	79.3

Deflelctions and crack load

ρ	η	$(\alpha d)_I$ [mm]	α_{II}	I_{rI} x10^6 [mm^4]	I_{cI} x10^6 [mm^4]
0.016	3.354	76.8	0.276	0.9	70.4

$(EI)_I$ x10^9 [Nmm^2]	I_c x10^6 [mm^4]	$(EI)_{II}$ x10^9 [Nmm^2]	$(\alpha d)_{II}$ [mm]	M_{crack} [kNm]	P_{crack} [kN]
1531	15.0	312.2	33.1	2.382	21.4

δ_I [mm]	δ_{II} [mm]	$\delta_{failure}$ [mm]	L_s [mm]	L [mm]	L_m [mm]
0.18	0.89	3.30	222.5	1000	555

B1-6Ø10-ALU2

Beam design

h [mm]	b [mm]	f_c [MPa]	f_{ct} [MPa]	E_c [MPa]	Rod diameter [mm^2]
150	250	25.1	2.375	20868	10

number of rods	A_r [mm^2]	f_{ym} [MPa]	E_r [MPa]	A_{rb} [mm^2]
6	471	274	70000	1038

α	under-/ over reinforced	ε_r	d [mm]	αd [mm]	M_{Rd} [kNm]
0.214	under	0.013	120	25.72	14.2

$V_{Rd,current}$ [kN]	V_{Ed} [kN]	$V_{Rd,new}$ [kN]	$V_{Rd,max}$ [mm]	P_M [kN]	P_V [kN]
58.8	58.8	64.0	203.2	188.9	117.6

Deflelctions and crack load

ρ	η	$(\alpha d)_I$ [mm]	α_{II}	I_{rI} x10^6 [mm^4]	I_{cI} x10^6 [mm^4]
0.016	3.354	76.8	0.276	0.9	70.4

$(EI)_I$ x10^9 [Nmm^2]	I_c x10^6 [mm^4]	$(EI)_{II}$ x10^9 [Nmm^2]	$(\alpha d)_{II}$ [mm]	M_{crack} [kNm]	P_{crack} [kN]
1531	15.0	312.2	33.1	2.382	31.8

δ_I [mm]	δ_{II} [mm]	$\delta_{failure}$ [mm]	L_s [mm]	L [mm]	L_m [mm]
0.19	0.93	3.43	150	1000	700

B1-6Ø10-ALU3

Beam design

h [mm]	b [mm]	f_c [MPa]	f_{ct} [MPa]	E_c [MPa]	Rod diameter [mm^2]
150	250	25.1	2.375	20868	10

number of rods	A_r [mm^2]	f_{ym} [MPa]	E_r [MPa]	A_{rb} [mm^2]
6	471	274	70000	1038

α	under-/ over reinforced	ε_r	d [mm]	αd [mm]	M_{Rd} [kNm]
0.214	under	0.013	120	25.7	14.2

$V_{Rd,current}$ [kN]	V_{Ed} [kN]	$V_{Rd,new}$ [kN]	$V_{Rd,max}$ [mm]	P_M [kN]	P_V [kN]
58.8	58.8	64.0	203.2	188.9	117.6

Deflelctions and crack load

ρ	η	$(\alpha d)_I$ [mm]	α_{II}	I_{rI} x10^6 [mm^4]	I_{cI} x10^6 [mm^4]
0.016	3.354	76.8	0.276	0.9	70.4

$(EI)_I$ x10^9 [Nmm^2]	I_c x10^6 [mm^4]	$(EI)_{II}$ x10^9 [Nmm^2]	$(\alpha d)_{II}$ [mm]	M_{crack} [kNm]	P_{crack} [kN]
1531	15.0	312.2	33.1	2.382	31.8

δ_I [mm]	δ_{II} [mm]	$\delta_{failure}$ [mm]	L_s [mm]	L [mm]	L_m [mm]
0.03	0.16	0.61	150	450	150

Appendix G: Anchorage - modification

Anchor of reinforcement- modification after laboratory testing

Calculations below are performed according to Eurocode 2: NS-EN 1992 -1-1:
Design of concrete structures (EC2) and the previous used standard NS-EN 3473.

B2-2ø12-STEEL

$\phi := 12mm \quad n := 2$

Rod diameter and number of reinforcement rods

$A_s := \frac{\pi \cdot \phi^2}{4} = 113 \cdot mm^2$

Area of a steel reinforcement rod

$O_s := \pi \cdot \phi = 38 \cdot mm$

Circumference

$l_{bd.lab} := 25mm \quad c := 25mm \quad s := 176mm$

Anchor length, concrete cover and spacing between reinforcement

Stress in reinforcement with given anchor length:

$f_{td} := 2.16MPa$

Tensile strength of the concrete

$f_{bd} := 2.25 \cdot f_{td} = 4.9 \cdot MPa$

eq (8.2) in EC2

$\sigma_{sd.max} := \frac{l_{bd.lab} \cdot f_{bd} \cdot O_s}{A_s} = 40.5 \cdot MPa$

eq (8.3) in EC2

Anchor length required, based on the stress at beam failure:

$P_{cr} := 56.1kN$

Failure load from calculations

$V_{cr} := \frac{P_{cr}}{2} = 28 \cdot kN$

Total shear load in the reinforcement

$\sigma_{sd} := \frac{V_{cr}}{A_s \cdot n} = 124 \cdot MPa$

Stress in each reinforcement rod

$l_{b.rqd..} := \frac{\sigma_{sd} \cdot A_s}{f_{bd} \cdot O_s} = 77 \cdot mm$

eq (8.3) in EC2

B2-3T-ALU1

$A_{Al} := 156mm^2$ *Area of an aluminium reinforcement rod*

$O_{Al} := 76mm$ *Circumference*

$l_{bd.lab} := 25mm \quad c := 25mm \quad s := 66mm$ *Anchor length, concrete cover and spacing between reinforcement*

Stress in reinforcement with given anchor length:

$k_1 := 0.9 \quad f_{td} := 2.16MPa$ *Factor based on reinf. shape and tensile strength of the concrete*

$f_{bd} := k_1 \cdot f_{td} = 1.9 \cdot MPa$ pt [12.8.5.] in NS-EN3474

$$\sigma_{sd.max} := \frac{l_{bd.lab} \cdot f_{bd} \cdot O_{Al}}{A_{Al}} = 23.7 \cdot MPa$$ eq (8.3) in EC2

Anchor length required, based on the stress at beam failure:

$P_{cr} := 66.8kN$ *Failure load from calculations*

$$V_{cr} := \frac{P_{cr}}{2} = 33 \cdot kN$$ *Total shear load in the reinforcement*

$$\sigma_{sd.} := \frac{V_{cr}}{A_{Al} \cdot 3} = 71.4 \cdot MPa$$ *Stress in each reinforcement rod*

$$l_{b.rqd.} := \frac{\sigma_{sd.} \cdot A_{Al}}{f_{bd} \cdot O_{Al}} = 75 \cdot mm$$ eq (8.3) in EC2

B2-3T-ALU2

$A_{Al} := 156mm^2$ *Area of an aluminium reinforcement rod*

$O_{Al} := 76mm$ *Circumference*

$l_{bd.lab} := 25mm$ $c := 25mm$ $s := 66mm$ *Anchor length, concrete cover and spacing between reinforcement*

Stress in reinforcement with given anchor length:

$k_1 := 0.9$ $f_{td} := 2.16MPa$ *Factor based on reinf. shape and tensile strength of the concrete*

$f_{bd} := k_1 \cdot f_{td} = 1.9 \cdot MPa$ pt [12.8.5.] in NS-EN3474

$$\sigma_{sd.max} := \frac{l_{bd.lab} \cdot f_{bd} \cdot O_{Al}}{A_{Al}} = 23.7 \cdot MPa$$ eq (8.3) in EC2

Anchor length required, based on the stress at beam failure:

$P_{cr} := 72.2kN$ *Failure load from calculations*

$$V_{cr} := \frac{P_{cr}}{2} = 36 \cdot kN$$ *Total shear load in the reinforcement*

$$\sigma_{sd.} := \frac{V_{cr}}{A_{Al} \cdot 3} = 77.1 \cdot MPa$$ *Stress in each reinforcement rod*

$$l_{b.rqd.} := \frac{\sigma_{sd.} \cdot A_{Al}}{f_{bd} \cdot O_{Al}} = 81 \cdot mm$$ eq (8.3) in EC2

B1-6ø10-ALU1

$\phi := 10mm$ — *Rod diameter*

$A_{Al} := \frac{\pi \cdot \phi^2}{4} = 79 \cdot mm^2$ — *Area of an aluminium reinforcement rod*

$O_{Al} := \pi \cdot \phi = 31 \cdot mm$ — *Circumference*

$l_{bd.lab} := 25mm \quad c := 25mm \quad s := 28mm$ — *Anchor length, concrete cover and spacing between reinforcement*

Stress in reinforcement with given anchor length:

$k_{1.} := 0.9 \quad f_{td} := 2.38MPa$ — *Factor based on reinf. shape and tensile strength of the concrete*

$f_{bd} := k_{1.} \cdot f_{td} = 2.1 \cdot MPa$ — pt [12.8.5.] in NS-EN3473

$\sigma_{sd.max} := \frac{l_{bd.lab} \cdot f_{bd} \cdot O_{Al}}{A_{Al}} = 21.4MPa$ — eq (8.3) in EC2

Anchor length required, based on the stress at beam failure:

$P_{cr} := 79.3kN$ — *Failure load from calculations*

$V_{cr} := \frac{P_{cr}}{2} = 39.65kN$ — *Total shear load in the reinforcement*

$\sigma_{sd} := \frac{V_{cr}}{A_{Al} \cdot 6} = 84.1 \cdot MPa$ — *Stress in each reinforcement rod*

$l_{b.req} := \frac{\sigma_{sd} \cdot A_{Al}}{f_{bd} \cdot O_{Al}} = 98 \cdot mm$ — eq (8.3) in EC2

B1-6ø10-ALU2

$\phi := 10mm$ — *Rod diameter*

$A_{Al} := \frac{\pi \cdot \phi^2}{4} = 79 \cdot mm^2$ — *Area of an aluminium reinforcement rod*

$O_{Al} := \pi \cdot \phi = 31 \cdot mm$ — *Circumference*

$l_{bd.lab} := 25mm \quad c := 25mm \quad s := 28mm$ — *Anchor length, concrete cover and spacing between reinforcement*

Stress in reinforcement with given anchor length:

$k_{1.} := 0.9 \quad f_{td} := 2.38MPa$ — *Factor based on reinf. shape and tensile strength of the concrete*

$f_{bd} := k_{1.} \cdot f_{td} = 2.1 \cdot MPa$ — pt [12.8.5.] in NS-EN3473

$\sigma_{sd.max} := \frac{l_{bd.lab} \cdot f_{bd} \cdot O_{Al}}{A_{Al}} = 21.4 \cdot MPa$ — eq (8.3) in EC2

Anchor length required, based on the stress at beam failure:

$P_{cr} := 117.6kN$ — *Failure load from calculations*

$V_{cr} := \frac{P_{cr}}{2} = 58.8 \cdot kN$ — *Total shear load in the reinforcement*

$\sigma_{sd} := \frac{V_{cr}}{A_{Al} \cdot 6} = 124.8 \cdot MPa$ — *Stress in each reinforcement rod*

$l_{b.req} := \frac{\sigma_{sd} \cdot A_{Al}}{f_{bd} \cdot O_{Al}} = 146 \cdot mm$ — eq (8.3) in EC2

B1-6ø10-ALU3

$\phi := 10mm$

Rod diameter

$A_{Al} := \frac{\pi \cdot \phi^2}{4} = 79 \cdot mm^2$

Area of an aluminium reinforcement rod

$O_{Al} := \pi \cdot \phi = 31 \cdot mm$

Circumference

$l_{bd.lab} := 300mm \quad c := 25mm \quad s := 28mm$

Anchor length, concrete cover and spacing between reinforcement

Stress in reinforcement with given anchor length:

$k_{1.} := 0.9 \quad f_{td} := 2.38MPa$

Factor based on reinf. shape and tensile strength of the concrete

$f_{bd} := k_{1.} \cdot f_{td} = 2.1 \cdot MPa$

pt [12.8.5.] in NS-EN3473

$\sigma_{sd.max} := \frac{l_{bd.lab} \cdot f_{bd} \cdot O_{Al}}{A_{Al}} = 257 \cdot MPa$

eq (8.3) in EC2

Anchor length required, based on the stress at beam failure:

$P_{cr} := 117.6kN$

Failure load from calculations

$V_{cr} := \frac{P_{cr}}{2} = 58.8 \cdot kN$

Total shear load in the reinforcement

$\sigma_{.sd} := \frac{V_{.cr}}{A_{.Al} \cdot 6} = 124.8 \cdot MPa$

Stress in each reinforcement rod

$l_{b.req} := \frac{\sigma_{sd} \cdot A_{Al}}{f_{bd} \cdot O_{Al}} = 146 \cdot mm$

eq (8.3) in EC2

Appendix H: Compression zone height- modification

B2-2Ø12-STEEL

Load - compressive zone height

h [mm]	b [mm]	f_c [MPa]	f_{ym} [MPa]	A_r [mm2]	E_r [N/mm2]
150	250	23,6	550	226	200000

f_c/ε_{c3} [MPa]	$(\alpha d)_{failure}$ [mm]	$(\alpha d)_{II}$ [mm]	ε_{cu2}	ε_y	L_s [mm]
13486	26,4	38,5	0,00350	0,00275	400

αd [mm]	$\varepsilon_{c,top}$	T_c [N]	S [N]	ε_r	z [mm]
26,4	0,00435	124407	124407	0,01541	109,2
28	0,00354	124407	124407	0,01164	109,1
28,1	0,00350	124407	124407	0,01144	109,1
30	0,00294	124407	124407	0,00883	108,8
32	0,00257	124407	124407	0,00706	108,5
34	0,00230	124407	124407	0,00583	108,1
36	0,00211	124407	124407	0,00493	107,7
38	0,00197	124407	124407	0,00424	107,2
38,5	0,00193	124407	124407	0,00410	107,1

M [kNm]	P [kN]	P_{crack} [kN]
13,6	67,9	11,1
13,6	67,9	
13,6	67,8	
13,5	67,7	
13,5	67,5	
13,5	67,3	
13,4	67,0	
13,3	66,7	
13,3	66,6	

B2-3T-ALU1

Load - compressive zone height

h [mm]	b [mm]	f_c [MPa]	f_{ym} [MPa]	A_r [mm2]	E_r [N/mm2]
150	250	23,6	274	468	70000

f_c/ε_{c3} [MPa]	$(\alpha d)_{failure}$ [mm]	$(\alpha d)_{II}$ [mm]	ε_{cu2}	ε_y	L_s [mm]
13486	27,2	33,0	0,00350	0,00391	400

αd [mm]	$\varepsilon_{c,top}$	T_c [N]	S [N]	ε_r	z [mm]
27,2	0,00435	128232	128232	0,01486	108,9
28	0,00391	128232	128232	0,01285	108,8
29	0,00349	128232	128232	0,01096	108,7
30	0,00318	128232	128232	0,00953	108,6
31	0,00293	128232	128232	0,00840	108,5
32	0,00273	128232	128232	0,00750	108,3
33,0	0,00256	128232	128232	0,00676	108,2

M [kNm]	P [kN]	P_{crack} [kN]
14,0	69,8	10,7
14,0	69,8	
13,9	69,7	
13,9	69,6	
13,9	69,5	
13,9	69,5	
13,9	69,3	

B2-3T-ALU2

Load - compressive zone height

h [mm]	b [mm]	f_c [MPa]	f_{ym} [MPa]	A_r [mm2]	E_r [N/mm2]
150	250	23,6	274	468	70000

f_c/ε_{c3} [MPa]	$(\alpha d)_{failure}$ [mm]	$(\alpha d)_{II}$ [mm]	ε_{cu2}	ε_y	L_s [mm]
13486	27,2	33,0	0,00350	0,00391	222,5

αd [mm]	$\varepsilon_{c,top}$	T_c [N]	S [N]	ε_r	z [mm]
27,2	0,00435	128232	128232	0,015	108,9
28	0,00391	128232	128232	0,013	108,8
28,98	0,00350	128232	128232	0,011	108,7
29	0,00349	128232	128232	0,011	108,7
30	0,00318	128232	128232	0,010	108,6
31	0,00293	128232	128232	0,008	108,5
32	0,00273	128232	128232	0,008	108,3
33,0	0,00256	128232	128232	0,007	108,2

M [kNm]	P [kN]	P_{crack} [kN]
14,0	125,5	19,3
14,0	125,4	
13,9	125,3	
13,9	125,3	
13,9	125,2	
13,9	125,0	
13,9	124,9	
13,9	124,7	

B1-6Ø10-ALU1

Load - compressive zone height

h [mm]	b [mm]	f_c [MPa]	f_{ym} [MPa]	A_r [mm2]	E_r [N/mm2]
150	250	25,1	274	471	70000

f_c/ε_{c3} [MPa]	$(\alpha d)_{failure}$ [mm]	$(\alpha d)_{II}$ [mm]	ε_{cu2}	ε_y	L_s [mm]
14343	25,7	33,1	0,00350	0,00391	222,5

αd [mm]	$\varepsilon_{c,top}$	T_c [N]	S [N]	ε_r	z [mm]
25,7	0,00439	129119	129119	0,01611	109,5
26	0,00419	129119	129119	0,01517	109,5
27	0,00368	129119	129119	0,01267	109,4
27,4	0,00350	129119	129119	0,01181	109,3
28	0,00330	129119	129119	0,01084	109,3
29	0,00301	129119	129119	0,00945	109,1
30	0,00279	129119	129119	0,00836	109,0
31	0,00260	129119	129119	0,00747	108,8
32	0,00245	129119	129119	0,00674	108,7
33	0,00232	129119	129119	0,00613	108,5
33,1	0,00231	129119	129119	0,00607	108,4

M [kNm]	P [kN]	P_{crack} [kN]
14,1	127,1	21,4
14,1	127,1	
14,1	126,9	
14,1	126,9	
14,1	126,8	
14,1	126,7	
14,1	126,5	
14,1	126,3	
14,0	126,1	
14,0	125,9	
14,0	125,9	

B1-6Ø10-ALU2

Load - compressive zone height

h [mm]	b [mm]	f_c [MPa]	f_{ym} [MPa]	A_r [mm2]	E_r [N/mm2]
150	250	25,1	274	471	70000

f_c/ε_{c3} [MPa]	$(\alpha d)_{failure}$ [mm]	$(\alpha d)_{II}$ [mm]	ε_{cu2}	ε_y	L_s [mm]
14343	25,7	33,1	0,00350	0,00391	150

αd [mm]	$\varepsilon_{c,top}$	T_c [N]	S [N]	ε_r	z [mm]
25,7	0,00439	129119	129119	0,01611	109,5
26	0,00419	129119	129119	0,01517	109,5
27	0,00368	129119	129119	0,01267	109,4
27,4	0,00350	129119	129119	0,01181	109,3
28	0,00330	129119	129119	0,01084	109,3
29	0,00301	129119	129119	0,00945	109,1
30	0,00279	129119	129119	0,00836	109,0
31	0,00260	129119	129119	0,00747	108,8
32	0,00245	129119	129119	0,00674	108,7
33	0,00232	129119	129119	0,00613	108,5
33,1	0,00231	129119	129119	0,00607	108,4

M [kNm]	P [kN]	P_{crack} [kN]
14,1	188,5	31,8
14,1	188,5	
14,1	188,3	
14,1	188,2	
14,1	188,1	
14,1	187,9	
14,1	187,6	
14,1	187,4	
14,0	187,1	
14,0	186,7	
14,0	186,7	

B1-6Ø10-ALU3

Load - compressive zone height

h [mm]	b [mm]	f_c [MPa]	f_{ym} [MPa]	A_r [mm2]	E_r [N/mm2]
150	250	25,1	274	471	70000

f_c/ε_{c3} [MPa]	$(\alpha d)_{failure}$ [mm]	$(\alpha d)_{II}$ [mm]	ε_{cu2}	ε_y	L_s [mm]
14343	25,7	33,1	0,00350	0,00391	150

αd [mm]	$\varepsilon_{c,top}$	T_c [N]	S [N]	ε_r	z [mm]
25,7	0,00439	129119	129119	0,01611	109,5
26	0,00419	129119	129119	0,01517	109,5
27	0,00368	129119	129119	0,01267	109,4
27,4	0,00350	129119	129119	0,01181	109,3
28	0,00330	129119	129119	0,01084	109,3
29	0,00301	129119	129119	0,00945	109,1
30	0,00279	129119	129119	0,00836	109,0
31	0,00260	129119	129119	0,00747	108,8
32	0,00245	129119	129119	0,00674	108,7
33	0,00232	129119	129119	0,00613	108,5
33,1	0,00231	129119	129119	0,00607	108,4

M [kNm]	P [kN]	P_{crack} [kN]
14,1	188,5	31,8
14,1	188,5	
14,1	188,3	
14,1	188,2	
14,1	188,1	
14,1	187,9	
14,1	187,6	
14,1	187,4	
14,0	187,1	
14,0	186,7	
14,0	186,7	

Appendix I: Crack spacing - modification

Crack spacing- modification after laboratory testing

Calculations below are based on Eurocode 2: NS-EN 1992-1-1:
Design of concrete structures (EC2)

$h := 150mm$

$b := 250mm$

$c = 25 \cdot mm$

B2-2ø12-STEEL

$\phi := 12mm$	*Rod diameter*
$s = 176 \cdot mm$	*Reinforcement spacing*
$n := 6$	*Number of rods*
$\alpha d := 26.4mm$	*Compressive zone height*
$A_r := \pi \cdot \left(\frac{\phi}{2}\right)^2 \cdot n = 679 \cdot mm^2$	*Reinforcement area*
$5\left(c + \frac{\phi}{2}\right) = 155 \cdot mm$	< 176 mm, eq (7.14) in EC2 can be used to calculate the maximum final crack spacing
$S_{r.max} := 1.3(h - \alpha d) = 161 \cdot mm$	eq (7.14) in EC2

B1-6ø10-ALU1, B1-6ø10-ALU2 and B1-6ø10-ALU3

$\phi := 10mm$ *Rod diameter*

$s = 28 \cdot mm$ *Reinforcement spacing*

$n := 6$ *Number of rods*

$\alpha d := 25.7mm$ *Compressive zone height*

$A_r := \pi \cdot \left(\frac{\phi}{2}\right)^2 \cdot n = 471 \cdot mm^2$ *Reinforcement area*

$5\left(c + \frac{\phi}{2}\right) = 150 \cdot mm$ < 28 mm, eq (7.11) in EC2 can be used to calculate the maximum final crack spacing

$k_1 := 0.8$ because of high bond bars

$k_2 := 0.5$ because of bending

$k_3 := 3.4$ given in NA.7.3.4(3)

$k_4 := 0.425$ given in NA.7.3.4(3)

$h_{c.eff} := \min\left[2.5(h - \alpha d), \frac{h - \alpha d}{3}, \frac{h}{2}\right] = 41 \cdot mm$

$A_{c.eff} := b \cdot h_{c.eff} = 10358mm^2$

$\rho_{p.eff} := \frac{A_r}{A_{c.eff}} = 0.045$

$S_{r.max} := k_3 \cdot c + k_1 \cdot k_2 \cdot k_4 \cdot \frac{\phi}{\rho_{p.eff}} = 122 \cdot mm$ eq (7.11) in EC2

Appendix J: Small specimen tests

Test Method: Tensile test 25mm_round,msm

Sample I, D,	Spcmn No,	Diameter [mm]	Area [mm^2]	Modulus [GPa]	Stress At Offset Yield [MPa]
120418,mss	1,00	3,96	01,12,1932	2,41	145,00
120418,mss	2,00	3,97	01,12,1938	2,66	146,80
120418,mss	3,00	3,94	01,12,2019	3,14	144,70
Average				2,74	145,50

Sample I, D,	Peak Load [kN]	Peak Stress [MPa]	Strain At Break [%]	Strain At Offset Yield [mm/mm]
120418,mss	3,33	270,00	****	0,03
120418,mss	3,40	274,90	38,90	0,03
120418,mss	3,38	277,00	36,80	0,02
Average	3,37	273,97		

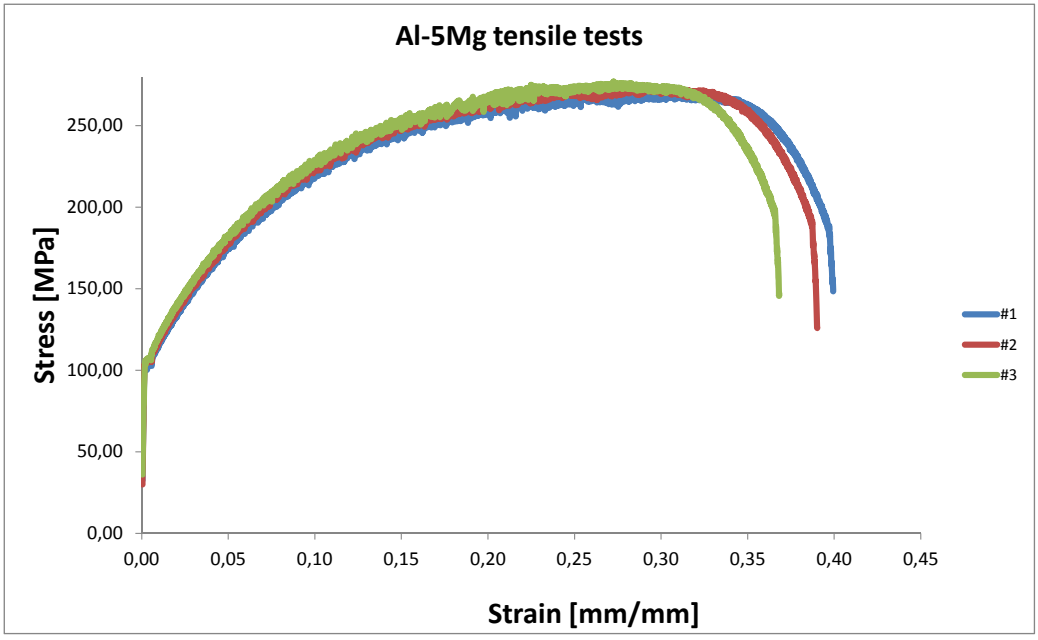

NS-EN 12390-3:2009 PRØVELEGEMERS TRYKKFASTHET SYLINDRE

SINTEF

Oppdragsgiver: DARE2C

Prosjektnr: 102015640

Reg.nr. vekt: B-181

Støpedato 20/3-18

Journalnummer:

Prøve nr.	Høyde etter planslip	Diam.	Trykk-flate	Vekt i vann	Vekt i luft	Vekt av jern i vann	Vekt av jern i luft	Netto volum	Netto densitet	Middel densitet	Brudd-last*	Trykk-fasthet	h/d	Omregn.-faktor	Omregn. trykk-fasthet	Middel trykk-fasthet
	mm	mm	mm²	g	g	g	g	dm³	kg/m³	kg/m³	kN	MPa			MPa	MPa
1-1	197,1	100,1	7869,7	2030,9	3567,0			1,539	2318	2320	175,8	22,3	1,971	1	22,3	23,0
1-2	197,4	100,0	7854,0	2041,6	3583,0			1,544	2321		186,1	23,7	1,974	1	23,7	
2-1	195,5	100,3	7901,2	2019,0	3545,0			1,529	2319	2322	170,9	21,6	1,949	1	21,6	21,4
2-2	195,6	100,7	7964,3	2044,5	3582,6			1,541	2325		170,4	21,2	1,942	0,99	21,2	

Prøvene ble lagt i ~~vann~~: under våte sekker og plast

Trykkprøvd den 17/4-18 i Form Test B-62 ved innstilling 2000kN

Dato/sign: 17/4-18 EZ

Dato/sign daglig lab.leder:

* Ved **utilfredsstillende** bruddform (se s. 2) anmerkes dette med **kode** i kommentarfeltet.

Kommentarer:

NS-EN 12390-3:2009 PRØVELEGEMERS TRYKKFASTHET SYLINDRE

SINTEF

Oppdragsgiver: DARE2C Prosjektnr: 102015640

Reg.nr. vekt: B-181 Støpedato 20/3-18 Journalnummer:

Prøve nr.	Høyde etter planslip	Diam.	Trykk-flate	Vekt i vann	Vekt i luft	Vekt av jern i vann	Vekt av jern i luft	Netto volum	Netto densitet	Middel densitet	Brudd-last*	Trykk-fasthet	h/d	Omregn.-faktor	Omregn. trykk-fasthet	Middel trykk-fasthet
	mm	mm	mm²	g	g	g	g	dm³	kg/m³	kg/m³	kN	MPa			MPa	MPa
2-5	195	100	7854	2030	3558			1,531	2324	2320	191,2	24,3	1,95	1	24,3	23,6
2-6	195	100	7854	2013	3539			1,529	2315		179,5	22,9	1,95	1	22,9	

Prøvene ble lagt i ~~vann~~: under våte sekker og plast Dato/sign: 9/5-18 E. Johansen

Trykkprøvd den 9/5-18 i Form Test B-62 ved innstilling 2000 kN Dato/sign daglig lab.leder:

* Ved **utilfredsstillende** bruddform (se s. 2) anmerkes dette med **kode** i kommentarfeltet.

Kommentarer:

NS-EN 12390-3:2009 PRØVELEGEMERS TRYKKFASTHET SYLINDRE

SINTEF

Oppdragsgiver: DAREC

Prosjektnr: 102015640

Reg.nr. vekt: B-181 Støpedato 20/3-18

Journalnummer:

Prøve nr.	Høyde etter planslip	Diam.	Trykk-flate	Vekt i vann	Vekt i luft	Vekt av jern i vann	Vekt av jern i luft	Netto volum	Netto densitet	Middel densitet	Brudd-last*	Trykk-fasthet	h/d	Omregn.-faktor	Omregn. trykk-fasthet	Middel trykk-fasthet
	mm	mm	mm²	g	g	g	g	dm³	kg/m³	kg/m³	kN	MPa			MPa	MPa
1-5	196	100	7854	2038	3567			1,532	2328	2329	194,8	24,8	1,96	1	24,8	25,1
1-6	196	100	7854	2034	3559			1,528	2329		200,0	25,4	1,96	1	25,4	

Prøvene ble lagt i ~~vann~~: under våte sekker og plast

Dato/sign: 14/5-18 E. Tolvsrud

Trykkprøvd den 14/5-18 i B-62 ved innstilling 2000 kN

Dato/sign daglig lab.leder:

* Ved **utilfredsstillende** bruddform (se s. 2) anmerkes dette med **kode** i kommentarfeltet.

Kommentarer:

NS-EN 12390-6:2009 PRØVELEGEMERS SPALTESTREKKFASTHET

SINTEF

Oppdragsgiver: DARE2C

Prosjektnr: 102015640

Reg.nr. vekt: B-181 Støredato 20/3-18

Journalnummer:

Prøvestykke nr.	Vekt i vann	Vekt i luft	Volum	Densitet	Lengde, *L*	Diameter, *d*	Bruddlast, *F*	Merknad	Spaltestrekk-fasthet, f_{ct}
	kg	kg	dm^3	kg/dm^3	mm	mm	kN		MPa
1-7	2,0865	3,6490	1,566	2,330	201,4	99,9	71,3		(2,2) 2,26
1-8	2,0754	3,6415	1,569	2,321	201,9	100,0	79,1		(2,4) 2,49
2-7	2,0752	3,6419	1,570	2,320	200,7	99,7	61,3		(1,9) 1,95
2-8	2,0433	3,6038	1,564	2,304	200,5	100,0	74,4		(2,3) 2,36

Spaltestrekkfasthet

$$f_{ct} = \frac{2 \cdot F}{\pi \cdot L \cdot d}$$

Prøvene ble lagt i ~~vann~~: under våte sekker og plast

Trykkprøvd den 17/4-18 i B-62

Dato/sign: 17/4-18 EF.

Største nominelle steinstørrelse i prøve: 16 mm

Dato/sign daglig lab.leder:

Beskrivelse av evtuell utilfredsstillende bruddform:

Kommentarer:

NS 3676 E-MODUL VED TRYKKPRØVING

SINTEF

Oppdragsgiver: DARE2C

Prosjektnr: 102015640

Reg.nr. vekt: B-181 Støpedato 2013-18

Journalnummer:

Prøve nr.	Høyde etter planslip	Diam.	Trykk-flate	Vekt i vann	Vekt i luft	Volum	Rom-densitet	Brudd-last	E_0	E_c	Trykk-fasthet	Høyde/ diameter-forhold	Omregn.-faktor	Omregn. trykk-fasthet
	mm	mm	mm²	g	g	dm³	kg/m3	kN	GPa	GPa	MPa			MPa
1-3	195,7	99,9	7838,3	2034,9	3562,7	1,531	2327	181,3	20,24	21,34	23,1	1,959	1	23,1
1-4	196,5	100,0	7854,0	2032,2	3566,8	1,538	2319	179,4	19,54	20,40	22,8	1,965	1	22,8
2-3	195,4	100,1	7869,7	2029,7	3559,6	1,533	2322	170,4	19,36	20,21	21,7	1,952	1	21,7
2-4	195,8	99,9	7838,3	2009,7	3537,2	1,531	2310	167,4	18,25	19,15	21,4	1,960	1	21,4

Prøvene ble lagt i ~~vann~~: under våte sekker og plast Dato/sign: 17/4-18 EZ

Trykkprøvd den 17/4-18 i B-62 ved innstilling 2000 kN Dato/sign daglig lab.leder:

Kommentarer:

SINTEF

Betonglaboratoriet

Prøvingsrapport

Prøve ID: 1

Dato 17.04.2018

Funksjonstest e-modul **NS 3676** **Prøvestykke : Cylinder** **100x200**

Prøveseriens betegnelse	Stålsyl	Operatør	EJ
Produksjonsdato	17.04.2018	Alder	0
Prøvingsdato	17.04.2018		

Designation	Dimensions [mm]		Mass	Bulk	Strain [‰]		E-Modulus [MPa]		Strength	Remarks
	d	h	[g]	[kg/m³]	e01	e02	E0	Ec	MPa	
1	100,0	200,0			1,15	-0,01	32681	32592	.... *	

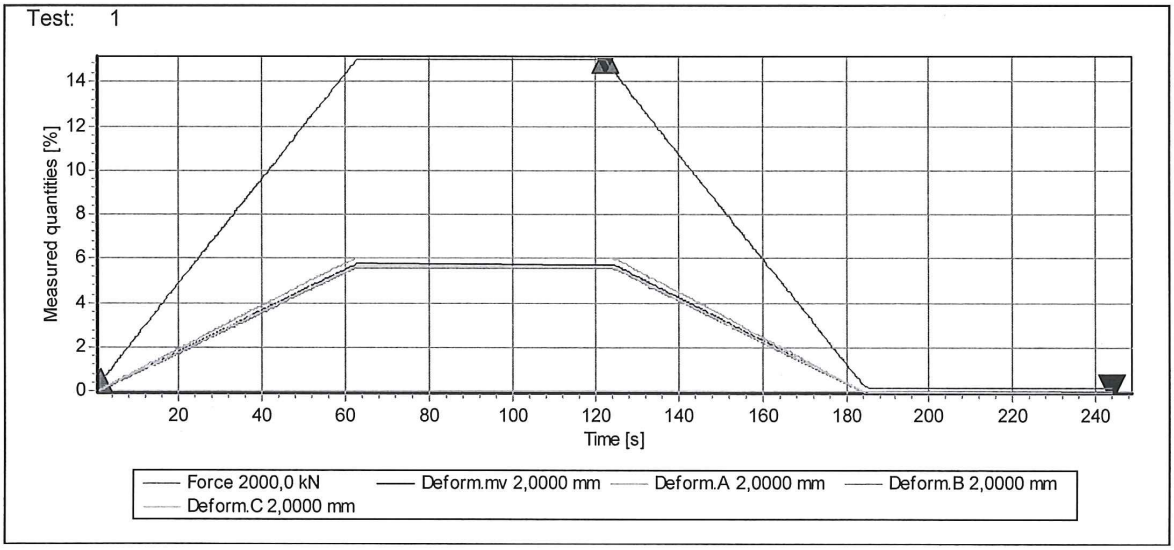

E-Modulus test **NS 3676** **Prøvestykke : Cylinder** **100x200**

Prøveseriens betegnelse	Mix 2	Operatør	FD
Produksjonsdato	20.03.2018	Alder	28
Prøvingsdato	17.04.2018		

Designation	Dimensions [mm]		Mass	Bulk	Strain [‰]		E-Modulus [MPa]		Strength	Remarks
	d	h	[g]	[kg/m³]	e01	e02	E0	Ec	MPa	
2-3	100,1	195,4	3559,6	2314,8	0,50	0,02	19356	20206	22	
2-4	99,9	195,8	3537,2	2304,8	0,53	0,03	18252	19145	21	
Average				2309,8	0,5	....	18804,4	19675,5	21,5	
Standard Deviation				7,1	....	....	780,8	750,5	0,2	

* : Single values rejected

Quality control passed

Test: 2-3

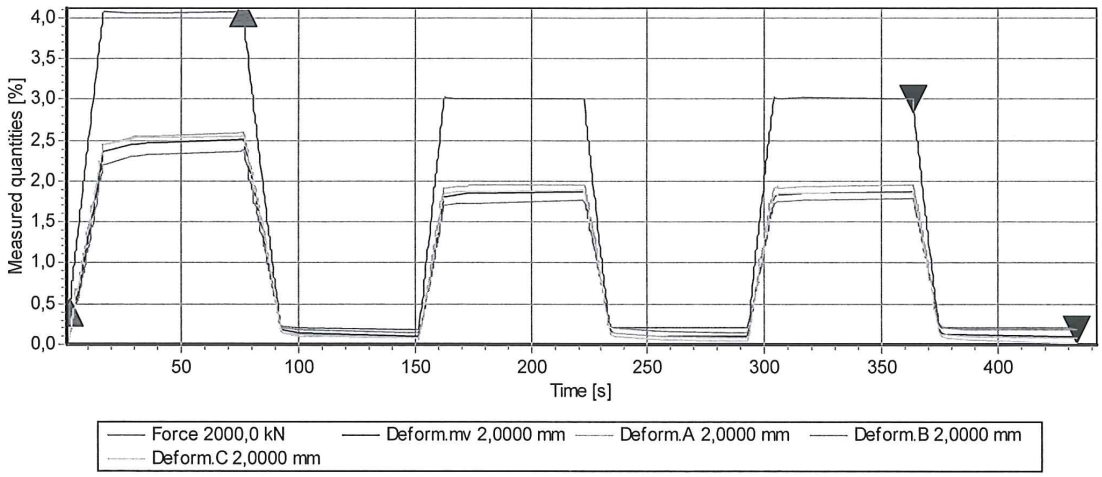

Test: 2-4

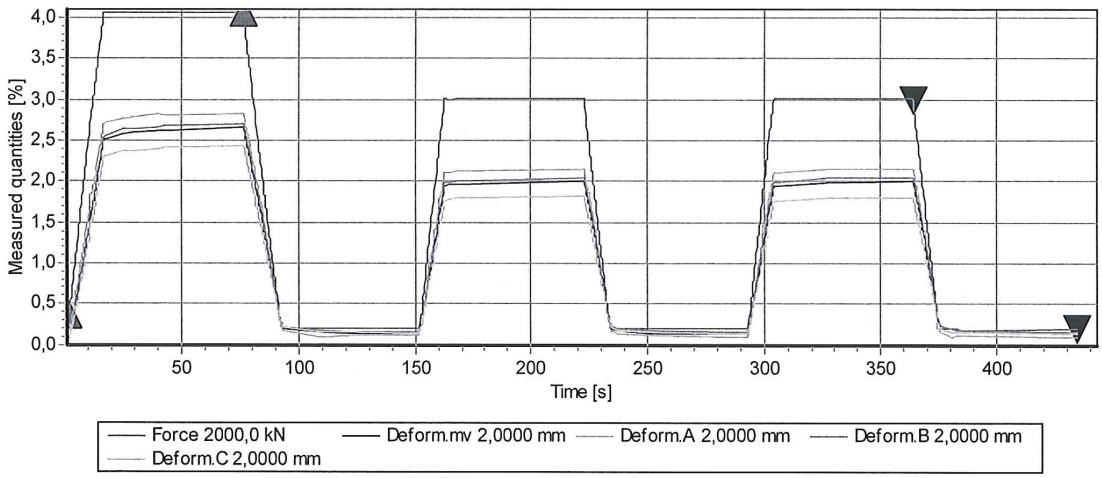

E-Modulus test **NS 3676** **Prøvestykke : Cylinder** **100x200**

Prøveseriens betegnelse	Mix 1	Operatør	EJ
Produksjonsdato	20.03.2018	Alder	28
Prøvingsdato	17.04.2018		

Designation	Dimensions [mm]		Mass	Bulk	Strain [‰]		E-Modulus [MPa]		Strength	Remarks
	d	h	[g]	[kg/m³]	e01	e02	E0	Ec	MPa	
1-3	100,0	196,0	3563,0	2314,6	0,50	0,03	20237	21337	23	
1-4	100,0	196,5	3566,8	2311,1	0,52	0,03	19536	20399	23	
Average				2312,9	0,5	....	19886,7	20867,9	23,0	
Standard Deviation				2,4	....	....	495,3	663,0	0,2	

* : Single values rejected

Quality control passed

Test: 1-3

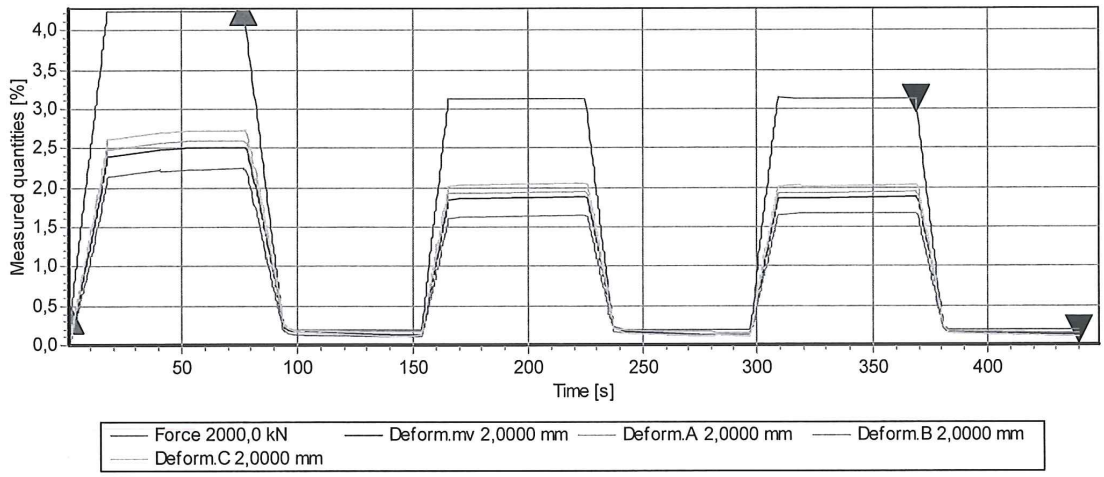

Test: 1-4

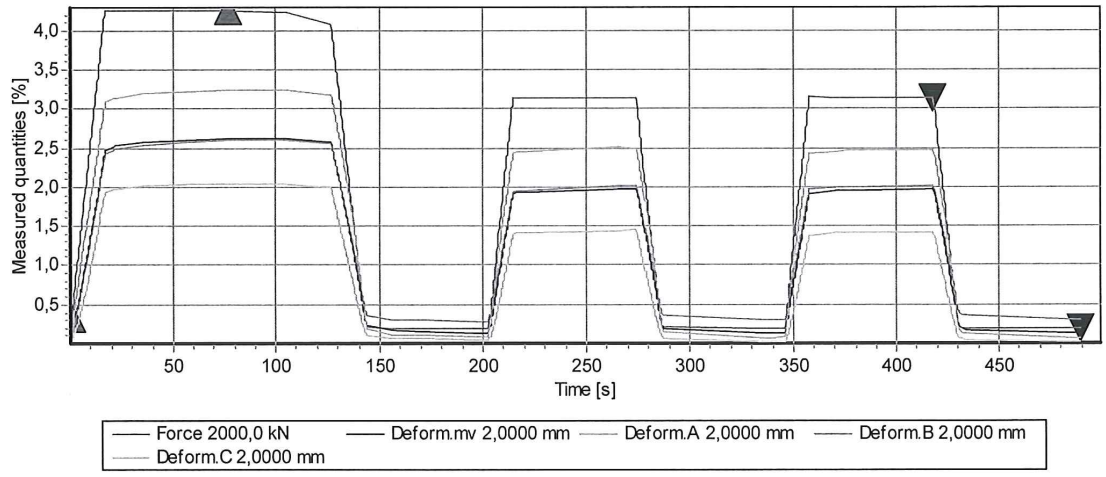

Merknader:

Signatur:_____

Appendix K: Pictures of the crack development

B2-2ø12-STEEL

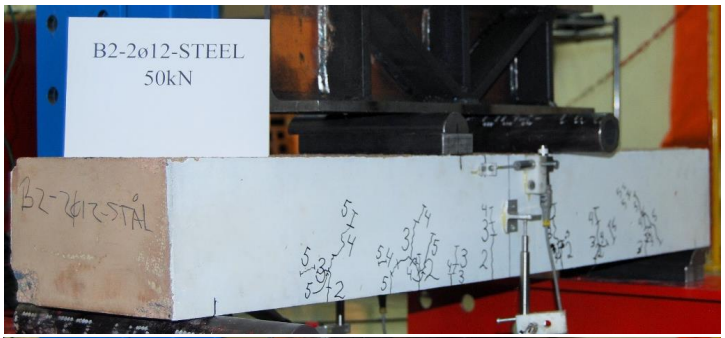
B2-2ø12-STEEL
50kN


B2-2ø12-STEEL
~~60kN~~
56 kN
Shear failure

B2-3T-ALU1

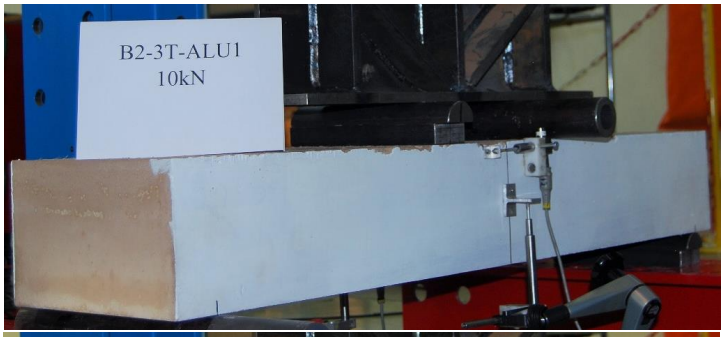
B2-3T-ALU1
10kN

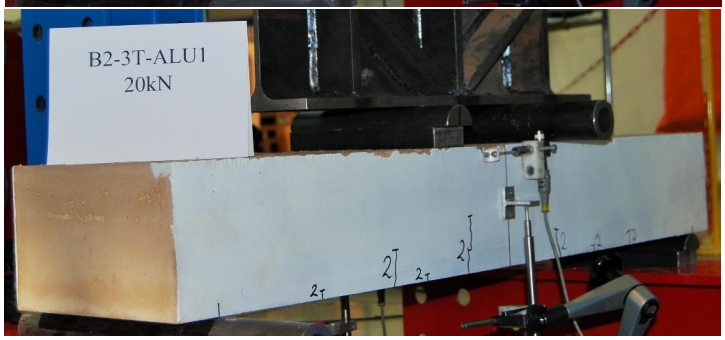
B2-3T-ALU1
20kN


B2-3T-ALU1
30kN


B2-3T-ALU1
39,52 kN
failure

B2-3T-ALU2

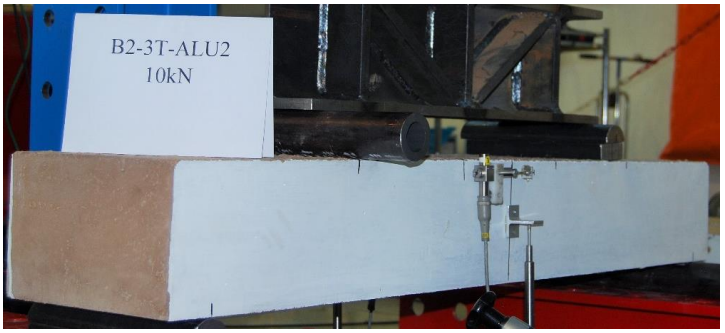
B2-3T-ALU2
10kN

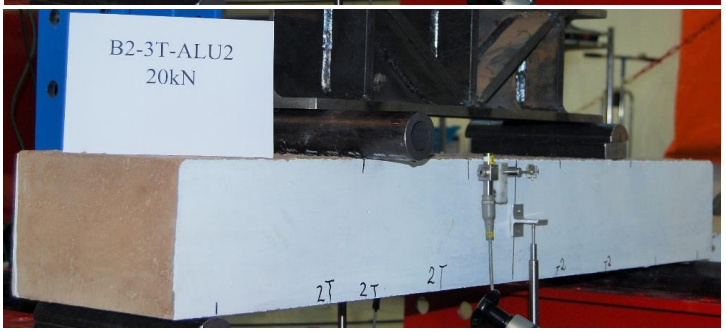
B2-3T-ALU2
20kN

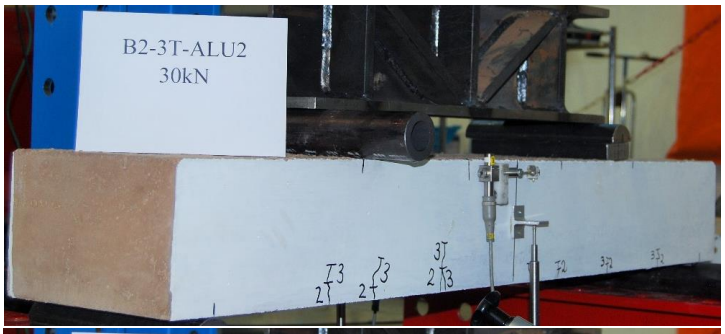
B2-3T-ALU2
30kN

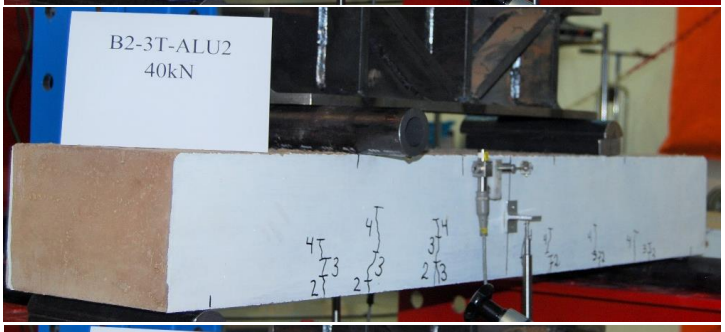
B2-3T-ALU2
40kN

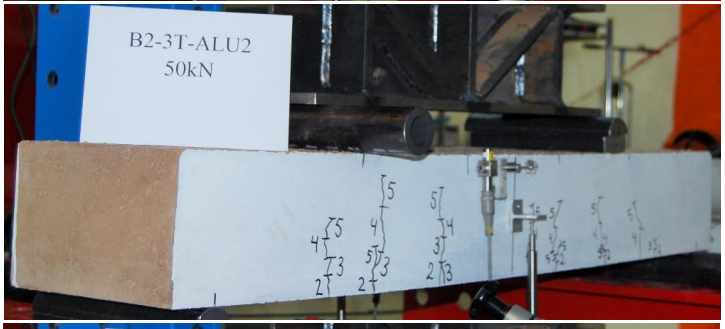
B2-3T-ALU2
50kN

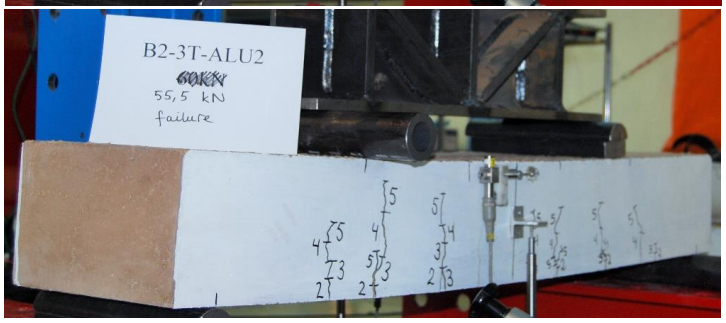
B2-3T-ALU2
55,5 kN
failure

B1-6ø10-ALU1

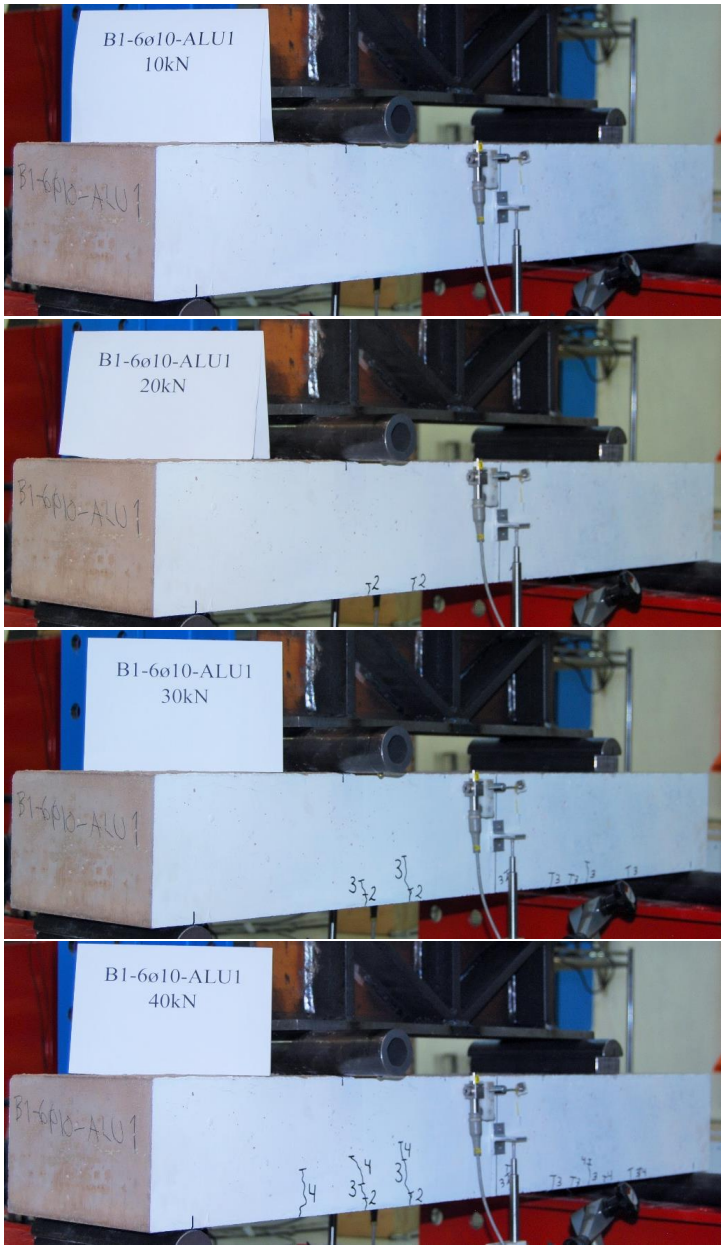
B1-6ø10-ALU1
10kN
B1-6ø10-ALU1
20kN
B1-6ø10-ALU1
30kN
B1-6ø10-ALU1
40kN

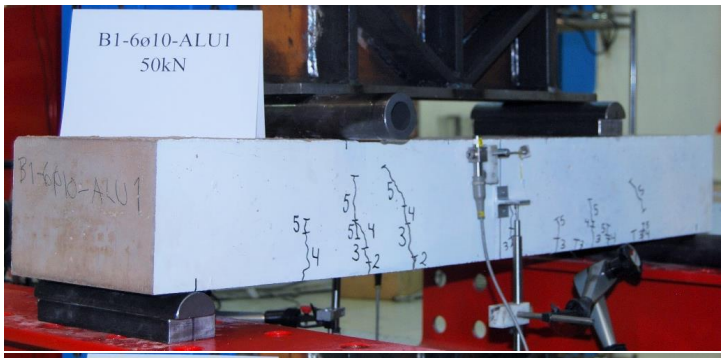
B1-6ø10-ALU1
50kN

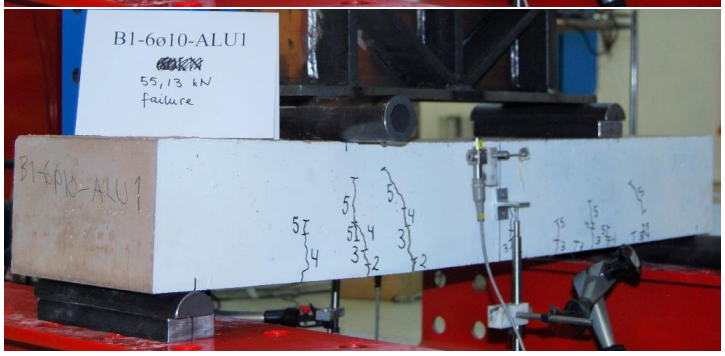
B1-6ø10-ALU1
55,13 kN
failure

B1-6ø10-ALU2

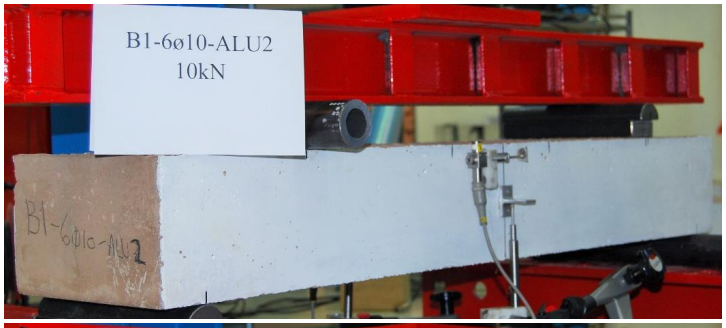
B1-6ø10-ALU2
10kN


B1-6ø10-ALU2
20kN

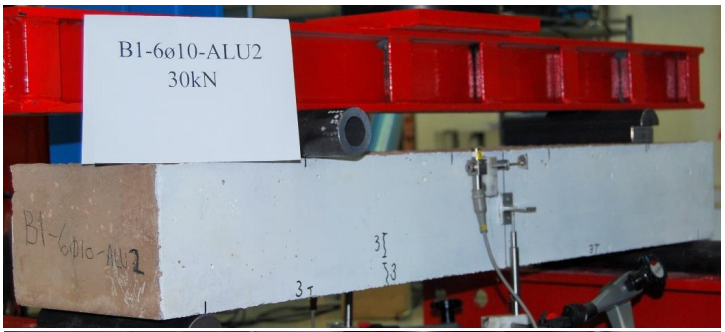
B1-6ø10-ALU2
30kN

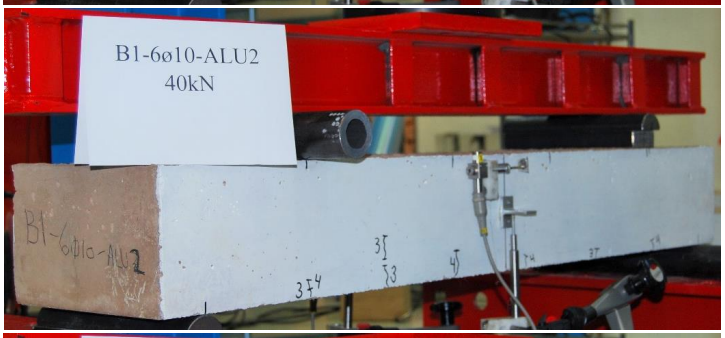
B1-6ø10-ALU2
40kN

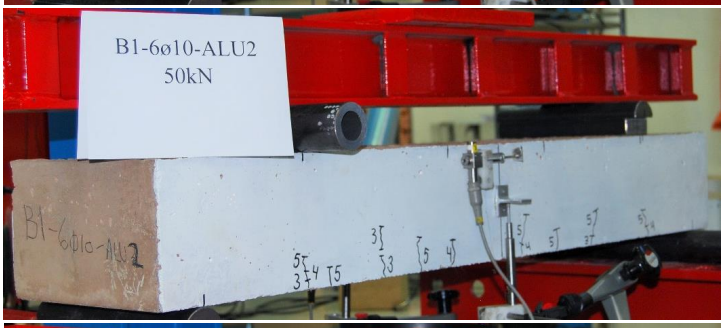
B1-6ø10-ALU2
50kN

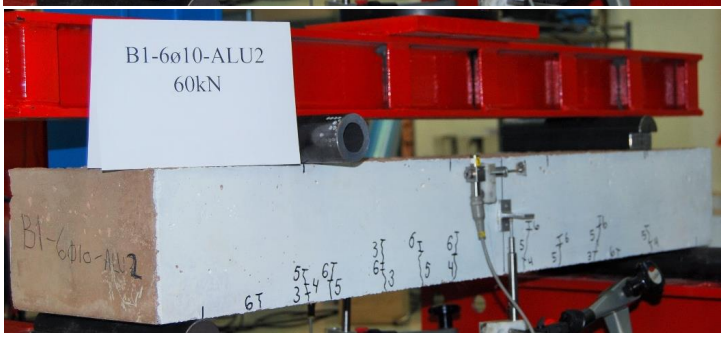
B1-6ø10-ALU2
60kN

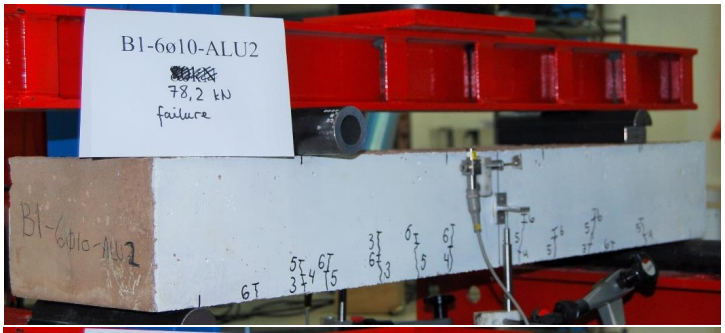
B1-6ø10-ALU2
78,2 kN
failure

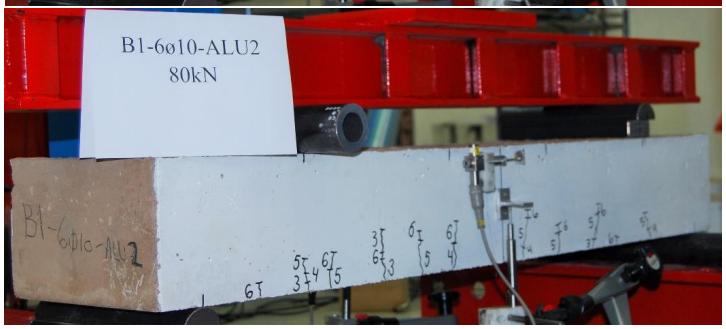
B1-6ø10-ALU2
80kN

B1-6ø10-ALU3

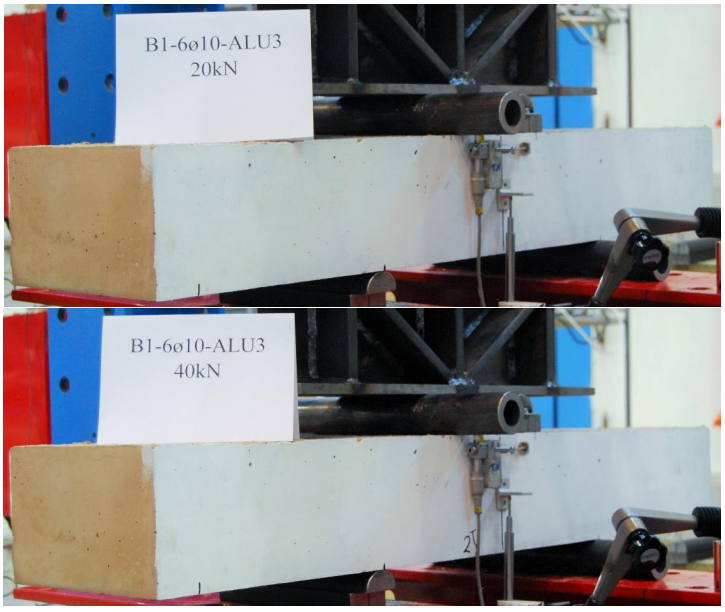
B1-6ø10-ALU3
20kN
B1-6ø10-ALU3
40kN

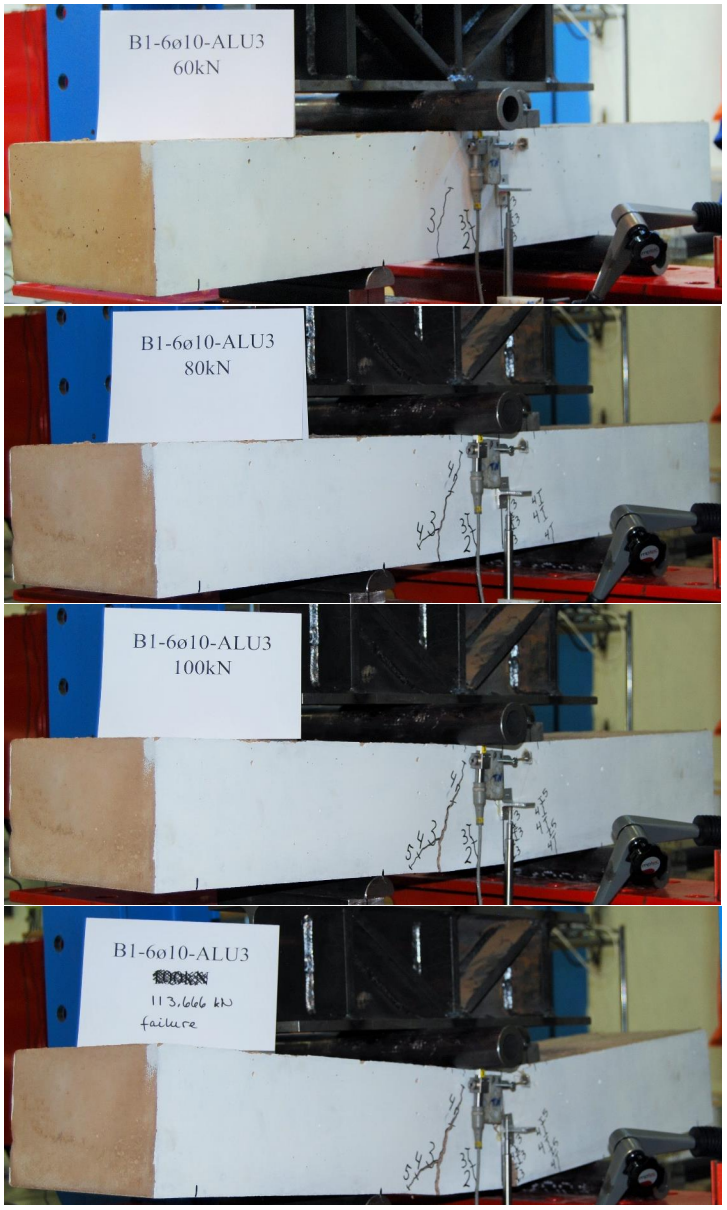
B1-6ø10-ALU3
60kN
B1-6ø10-ALU3
80kN
B1-6ø10-ALU3
100kN
B1-6ø10-ALU3
[redacted]
113,666 kN
failure

Appendix L: Control calculations of deflection and strain

Control of laboratory results for B2-2ø12-STEEL

The concrete strains and deflection from the laboratory testing are collected from the LVDT measurements, at a point load of 40 kN.

Control of deflection

$\varepsilon_{c.top} := 0.00098$ *Concrete strain at the top*

$\varepsilon_{c.r} := 0.00264$ *Concrete strain at the height of the reinforcement*

$d = 119 \cdot mm$ *Effective height of the beam*

$L = 1 \times 10^{3} \cdot mm$ *Distance between the supports*

$\kappa := \frac{\varepsilon_{c.top} + \varepsilon_{c.r}}{d} = 0.03 \frac{1}{m}$ *Curvature*

$\delta := \frac{\kappa \cdot L^{2}}{8} = 3.8 \cdot mm$ *Deflection at the middle of the beam*

Control of concrete strain

$P := 40kN$ *Loading from the cylinder*

$\alpha := 0.221$ *Compression zone factor*

$L_s := 0.4m$ *Distance between support and point load*

$M := \frac{P}{2} \cdot L_s = 8 \cdot kN \cdot m$ *Bending moment*

$EI := 386.7 \cdot 10^{9} N \cdot mm^{2}$ *Bending stiffness for cracked cross section*

$\varepsilon_s := \frac{M \cdot (1 - \alpha) \cdot d}{EI} = 1.918 \times 10^{-3}$ *Reinforcement strain*

Appendix M: Control calculations of bond stress

Control of reinforcement bond - after laboratory testing

Calculations below are performed according to Eurocode 2: NS-EN 1992-1-1 Design of concrete structures (EC2) and the previous concrete standard NS-EN 3473.

B2-2ø12-STEEL

$\phi := 12mm$ — *Rod diameter*

$A_s := \frac{\pi \cdot \phi^2}{4} = 113 \cdot mm^2$ — *Area of a steel reinforcement rod*

$O_s := \pi \cdot \phi = 37.7 \cdot mm$ — *Circumference*

$l_{bd.lab} := 25mm$ $c := 25mm$ $s := 176mm$ — *Anchor length, concrete cover and spacing between reinforcement*

$n := 2$ — *Number of reinforcement bars*

$P_{cr} := 56.2kN$ — *Failure load from laboratory*

$V_{cr} := \frac{P_{cr}}{2} = 28.1 \cdot kN$ — *Total shear load in the reinforcement*

$\sigma_{sd} := \frac{V_{cr}}{A_s \cdot n}$ — *Stress in each reinforcement rod*

Bond

$f_{td} := 2.16MPa$ — *Tensile strength of the concrete*

$l_{b.rqd.} := \frac{\sigma_{sd} \cdot A_s}{f_{bd} \cdot O_s}$ I — eq (8.3) in EC2

$\sigma_{sd.} := \frac{V_{cr}}{A_s \cdot n}$ II

Rearrganging the equations above (marked in pink) on behalf of f_{bd}, gives the equation:

$f_{bd.lab} := \frac{V_{cr}}{l_{bd.lab} \cdot O_s \cdot n} = 14.9 \cdot MPa$

$f_{bd.calc} := 2.25 \cdot f_{td} = 4.9 \cdot MPa$ — eq (8.2) in EC2

B1-6ø10-ALU3

$\phi := 10mm$ — *Rod diameter*

$A_{al} := \frac{\pi \cdot \phi^2}{4} = 78.5 \cdot mm^2$ — *Area of an aluminium reinforcement rod*

$O_{al} := \pi \cdot \phi = 31.4 \cdot mm$ — *Circumference*

$l_{bd.lab} := 300mm$ $c := 25mm$ $s := 28mm$ — *Anchor length, concrete cover and spacing between reinforcement*

$f_{td} := 2.38MPa$ — *Tensile strength of the concrete*

$P_{cr} := 74kN$ — *Failure load from laboratory testing*

$V_{cr} := \frac{P_{cr}}{2} = 37 \cdot kN$ — *Total shear load in the reinforcement*

$n := 6$ $k_{1.} := 0.9$

Bond factor

$f_{bd} := k_{1.} \cdot f_{td}$	I	[12.8.5.] in NS-EN3473
$l_{b.rqd.} := \frac{\sigma_{sd} \cdot A_{al}}{f_{bd} \cdot O_{al}}$	II	eq (8.3) in EC2
$\sigma_{sd.} := \frac{V_{cr}}{A_{al} \cdot n}$	III	

Rearrganging the equations above (marked in pink) on behalf of k_1, gives the equation:

$k_{.1} := \frac{V_{cr}}{O_{al} \cdot f_{td} \cdot n \cdot l_{bd.lab}} = 0.275$ $0.275 < 0.9$ not ok

$f_{bd.lab} := \frac{V_{cr}}{O_{al} \cdot n \cdot l_{bd.lab}} = 0.654MPa$

$f_{bd.calc} := 0.9 \cdot f_{td} = 2.14MPa$